# Entropic transport in confined media

**Dissertation**

zur Erlangung des akademischen Grades eines
Doktors der Naturwissenschaften,
der Mathematisch–Naturwissenschaftlichen Fakultät
der Universität Augsburg vorgelegt


von

**Poornachandra Sekhar Burada**

Lehrstuhl für Theoretische Physik I
Universität Augsburg

Augsburg, im Mai 2008

Betreuer:

Prof. Dr. Peter Hänggi
Theoretical Physics I
University of Augsburg, Germany

Dr. Eric Lutz
Assistant Professor (Emmy Noether Fellow)
University of Augsburg, Germany

| | |
|---|---|
| Erstgutachter: | Prof. Dr. Peter Hänggi |
| Zweitgutachter: | Dr. Eric Lutz |
| Tag der münlichen Prüfung: | 11 Juli 2008 |

*Dedicated to my parents*

# Contents

# 1

# Introduction

The Brownian particle, named after the Scottish botanist Robert Brown, diffuses freely in the host medium and the root mean square distance traveled by it, subjected to random collisions, is proportional to the square root of time [1, 2]. The diffusion coefficient is proportional to thermal noise which is present in the surrounding fluid of the Brownian particle. This theory of Brownian motion based on the molecular-kinetic theory of heat was proposed by Albert Einstein [1, 2] in 1905. Around the same time, other theoretical proposals made by William Sutherland [3], Marian Smoluchowski [4], and Paul Langevin [5] with different approaches confirmed the same relation. After a couple of years an experimental confirmation was made by Jean Perrin [6]. In the theoretical description of the Brownian motion, the particles are free and do not experience any geometrical constraints during their movements. If we consider a Brownian particle which is moving in a potential energy landscape or in a confined geometry where the geometrical confinements may regulate or control the diffusion process, then diffusion may vary significantly from the free case, bulk diffusion. Depending on the conditions imposed, the diffusion coefficient can be larger or smaller than the bulk diffusion coefficient.

Brownian particles, when moving in a confined geometry, instead of diffusing freely in the host liquid phase, undergo a constrained motion, where their kinetic behavior could exhibit peculiar behavior. This feature of constrained motion is ubiquitous in ion channels, nanopores, zeolites, and generally for processes occurring at sub-cellular level [7–28]. The uneven shape of these structures regulates the transport of particles yielding important effects exhibiting peculiar properties [23–28]. The results have implications in processes such as catalysis, osmosis and particle separation [7–12, 14, 16–19], and on the noise-induced transport in periodic potential landscapes that lack reflection symmetry, such as ratchet systems [29–37].

The understanding of the novel properties of these confined geometries, zeolites, biological channels, nanoporous materials, and microfluidic devices, as well as the transport behavior of species in these systems is of primary importance. In recent decades, there has been an increasing interest in using these fascinating systems for chemical processing, separation techniques, petrochemical cracking, ion-exchange, detergents, and catalysis process [7–19, 38, 39]. In the following, we address a few of these systems and their

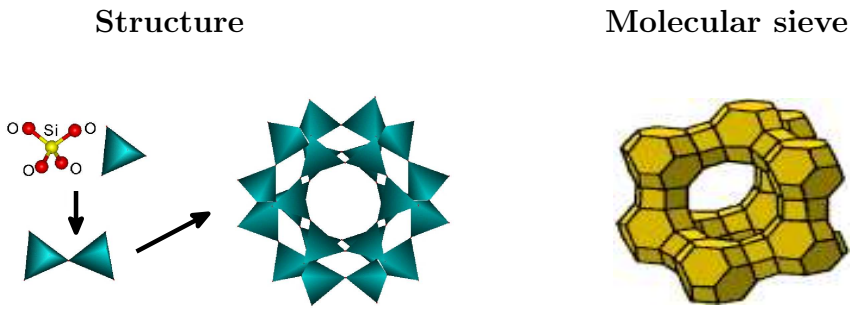


**Figure 1.1:** The formation and structure of a molecular sieve.

applications in various fields.

### Zeolites

Zeolites are nanoporous crystalline solids with well-defined structures [8–10, 34]. They naturally occur as minerals and can be synthesized commercially, for specific uses. More than 150 zeolite types have been synthesized and 48 naturally occurring zeolites are known. In general, zeolites consist of silicon, aluminum and oxygen in their framework and of cations, water and/or other molecules within their pore structure [8–10]. They often also referred as molecular sieves. In these structures, silicon forms tetrahedra subunits with oxygen. These small subunits will form a cavity (cage) and finally, in a bulk, they form long structures with small openings or, in other words, vacant spaces (see Fig. 1.1) [1]. The vacant spaces are interconnected and form long wide channels of varying sizes depending on the mineral. These long channels allow for the easy movement of resident ions and molecules into and out of the structure. Sometimes these tiny openings can trap molecules which are passing through them. Therefore, these materials could lead to new technologies with regard to energy storage and nanodevices [39–43].

#### *Catalysis and Ion exchange*

Since cations are free to migrate in and out of zeolite structures, zeolites are often used for catalysis processes (see top panel in Fig. 1.2) [2] which take place in the internal cavities [39–43]. During the catalysis process, there will be an exchange of ions between the molecules of the cavity walls and the foreign molecules. An important catalysis reaction is hydrogen exchange. Therefore, during a chemical reaction the *p*H level could increase drastically. In fact, changing the *p*H level helps a lot in these reactions, including petro-

[1] http://www.bza.org/zeolites.html
[2] http://www.che.caltech.edu/groups/med/catmat.html

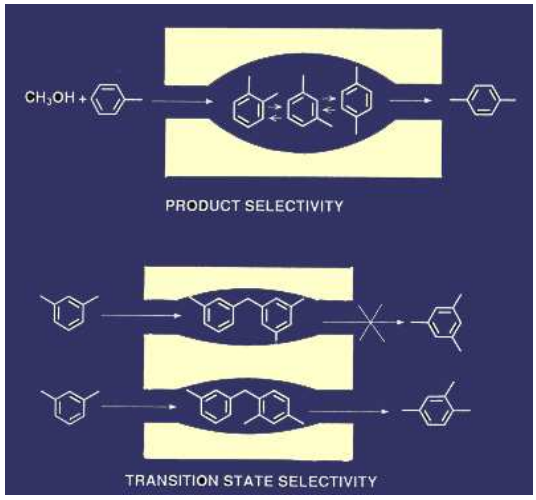


**Figure 1.2:** Application of zeolites: Catalysis and ion exchange process.

chemical cracking, purification, and isomerisation. Some classes of Zeolites can be used in water purification by replacing the hard ions in the water with their own lighter ones via ion exchange. For example, during the softening process, the hard ions like Calcium and Magnesium in un-purified water can be replaced by lighter ones, like as Sodium or Potassium.

*Filtering and Separation*

Zeolites have large vacant spaces or cages in their structures. Depending on the respective size of the pore openings and the entering species, Zeolites can act like filters [34, 39]. When molecules with different sizes enter into a Zeolite, some get stuck in the cavities, and others pass through the bottleneck openings freely. It can allow the large cations such as sodium, potassium and calcium, and even relatively large molecules and cation groups such as water, ammonia, carbonate ions and nitrate ions [8–10, 39]. It can block the species which are relatively bigger than the bottleneck openings of the sieve. This property can be used to filter the molecules and indeed separate other molecular mixtures. This feature has potential applications in industry, and in various fields [8–10, 34, 39–43]. Therefore, it is interesting and necessary to study the interactions, and transport properties in these irregular geometries.

### Nanopores

Nanopores are highly confined structures with small openings [13–15, 44–56]. Charged molecule or ions passing through these confined structures, exhibit different ionic signatures due to the electrostatic interaction between the ions transversing the nanopore, and the surface charge at the small opening (bottleneck) of the pore [13–15, 44, 47–49, 55, 56]. Here, the degree of confinement of the bottleneck opening also plays an important role due to its impact on the behavior of the molecular or ionic current [49, 56]. In some situations, these openings act like gates, and regulate the transport of ions or molecules [7]. Nanopores are available in nature, called biological nanopores, and can also be fabricated, called synthetic nanopores [13, 44–46].

*Biological nanopores*

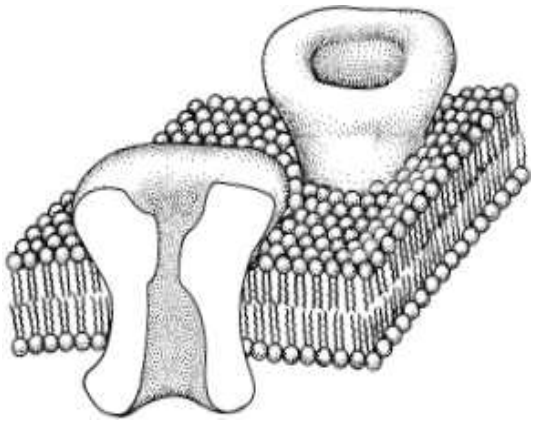

**Figure 1.3:** Biological nanopores, Ion channels [7], with irregular geometric structure which control and regulate the ionic transport in the cell membrane.

The biological nanopores (ion channels) are transmembrane pores, which control and regulate the ionic transport in all living cells in the presence of an electro-chemical gradient. The ion channel is an integral membrane protein or in other words, an assembly of several protein subunits (see Fig. 1.3) [3]. Identical or homologous protein subunits assemble in a circular arrangement closely packed around a water-filled pore going through the plane of the membrane or lipid bilayer [7]. In fact, the subunits are not visible in Fig. 1.3. In general, there are different kinds of ion channels, and they can be distinguished on the basis of their ion selectivity, gating mechanism, and sequence similarity [7]. Apart from the voltage gradient, charge, and ion selectivity, the geometrical confinement also plays a significant role in the ionic transport.

[3] B. Hille, *Ion Channels of Excitable Membranes* (Sinauer, Sunderland, 2001)

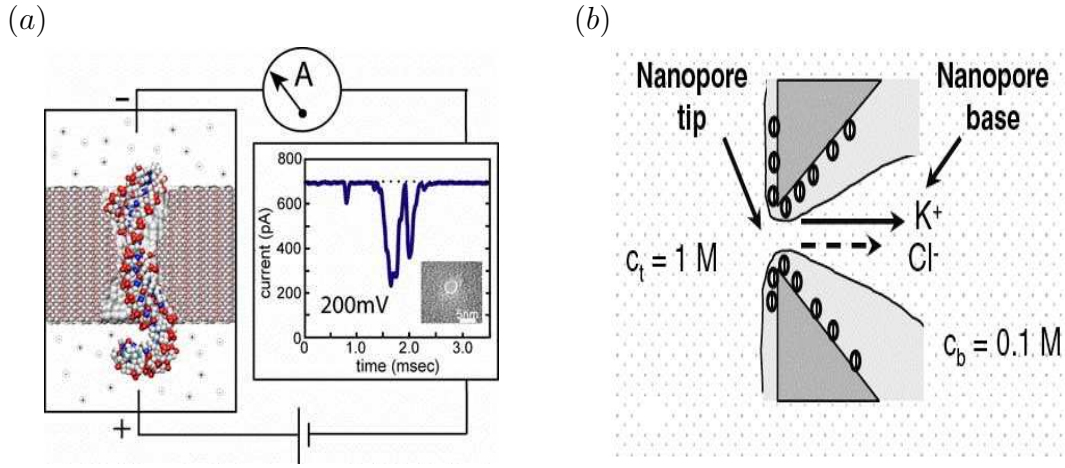


**Figure 1.4:** Experimental setup for measuring electrical signatures (a) of double-stranded DNA [49], passing trough a synthetic nanopore. The small inset shows an electron transmission micrograph of the pore sculptured by a highly focused electron beam. Passage of individual species $k^+$ and $Cl^-$ through a synthetic nanopore [14], driven by a concentration gradient, is depicted in panel (b).

Nowadays, artificial nanopores (synthetic nanopores) are also available to characterize the ionic behaviors of molecules, like for example, DNA or RNA [15, 38, 44–49, 55] and also of ionic species like $k^+, Na^+$, and $Cl^-$ [13–15]. With recent technology, these synthetic nanopores can be made upon choice, allowing for effective control of the dimensions and the structure [14, 38, 44–46, 55]. In recent years, it has been of great interest to reveal the sequence and structural analysis of DNA and RNA molecules by passing them through the nanopores (voltage-driven translocation) [45–49, 53–55]. The translocation of structured polynucleotides through nanopores also allows one to determine their sequence and structure [53–55]. When a double stranded DNA molecule passes through the charged nanopore, each base pair exhibits its own distinct electronic signature because each DNA base is structurally and chemically different (see Fig. 1.4(a)) [4]. While present conventional methods to find out this sequence would take several months and are expensive, one can find the sequence of a human genome in a matter of hours at a potentially low cost using this new technology. A similar mechanism applies if a charged molecule or ion passes through a nanopore (see Fig. 1.4(b)) [5]. In this case different ionic species exhibit different ionic currents [13, 15].

[4] http://www.ks.uiuc.edu/Research/nanopore
[5] Z. Siwy *et al.,* Phys. Rev. Lett. **94**, 048102 (2005)

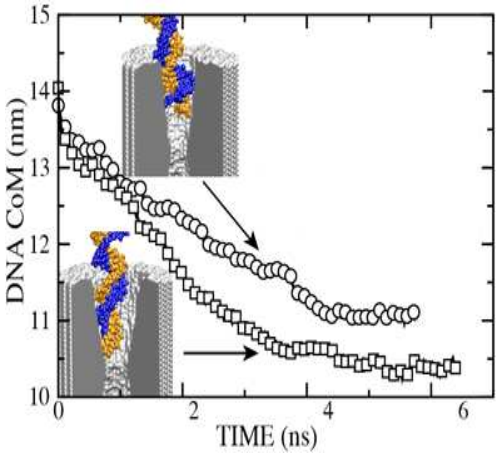


**Figure 1.5:** The position of the double stranded DNA center of mass relative to the tip of the nanopore against time [44] for two different bottleneck widths. It shows that apart from applied transmembrane bias the pore opening (bottleneck width) also plays a significant role in DNA translocation.

It has been found that the separation of DNA fragments in narrow channels [23–25, 38, 49] is largely influenced by their shape (see Fig. 1.5)[6]. The characteristic behavior of ionic currents of DNA molecules or individual species can effectively change if the pore opening (bottleneck) changes, see Fig. 1.5. In fact, if the pore opening is too small, then macro-molecules like DNA can jam in front of the bottleneck, for lack of space for the translocation. If the pore opening increases, then the translocation may be possible [48–52]. This feature is visible clearly in Fig. 1.5. Thus, there could be a threshold bottleneck width (pore opening) for a considered DNA molecule, but of course at a fixed low voltage bias across the translocation.

### Structural confinement

A common feature in the described systems (nanopores, zeolites, ion channels etc.) is the confinement arising from the presence of boundaries which very often exhibit an irregular geometry. Variations of the structural shape along the direction of propagation imply changes in the number of accessible states of the particles, see Fig. 1.6. Consequently, entropy is spatially varying, and the system evolves through entropic barriers which control transport, promoting or hampering the transfer of mass and energy to certain regions. Motion in the system can be induced by the presence of external driving forces supplying the particles with the energy necessary to proceed. The study of the kinetics of entropic transport, the properties of transport coefficients in far from equilibrium situations and the possibility for transport control mechanisms are objectives of major

[6] A. Aksimentiev *et al.* Biophys. J. **87**, 2086 (2004)

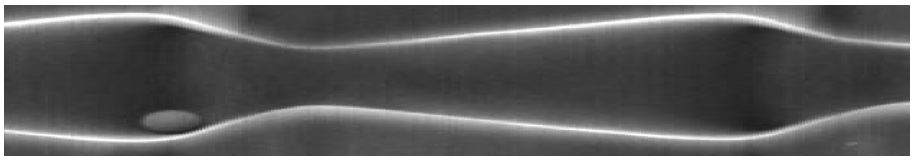

**Figure 1.6:** The situation of a Brownian particle which is confined within the two-dimensional channel [17, 18]. Entropic barriers arising due to variation in shape of the geometry along the propagation direction, and which may effectively control the transport characteristics of the system.

importance in the dynamical characterization of these systems.

Due to their enormous usage and various applicabilities of these systems, it is necessary to get a deeper understanding on their transport characteristics. Even though these materials have been studied widely, both experimentally [13, 14, 18, 19, 44, 45, 55, 56] and by numerical simulations [15, 58–63], there are unfortunately no analytical tools so far to calculate the transport characteristics of the underlying confined structures with complicated boundary conditions.

### Subject of this thesis

Within this work we provide an analytical tool, based on some approximations, to analyze transport characteristics in periodic confined structures. With the use of numerical simulations, we analyze the diffusion process in confined structures and, in fact, check the applicability and accuracy of the analytical predictions. Since entropy rule the diffusion process in confined structures, the transport characteristics may distinctly differ from that we usually observe in purely energetic systems. We identify the feature of universal scaling, a single parameter which can control the transport characteristics of a system which has entropic nature.

### Outline

The outline of this thesis is as follows: In chapter 2, as an overview, we discuss the free diffusion process, i.e., in the absence of any geometrical constraints, followed by the consideration of one-dimensional periodic potentials in the presence of an external bias.

In chapter 3, we set up the basic problem of the diffusion process in confined geometries and discuss the complications involved in calculating the transport characteristics in such systems. We introduce approximate methods, which allows for simplifying the complexity of the problem. We derive analytical expressions to calculate the transport characteristics for the defined problem. In chapter 4, we consider an arbitrary confined geometry, calculate its transport characteristics with the use of numerical simulations, analyze, and compare it with analytical predictions. Chapter 5 is devoted to the analysis of the diffusion process in geometric structures with different degrees of confinement,

including a detailed comparison between analytical predictions and numerical results.

Since we are considering approximate methods to analyze the diffusion process in confined geometries, we propose in chapter 6 the validity criteria for the applicability of the approximate methods by analyzing the characteristic times scales which are involved in the diffusion process of the Brownian particles inside the geometry. In chapter 7, we present our main conclusions together with an outlook.

# 2

# Energetic systems: Transport in 1D periodic potentials

In order to give a short outline, we discuss briefly the diffusion processes in the systems in the absence of geometrical constraints, and also discuss the known features of transport characteristics in purely energetic systems.

## Free diffusion

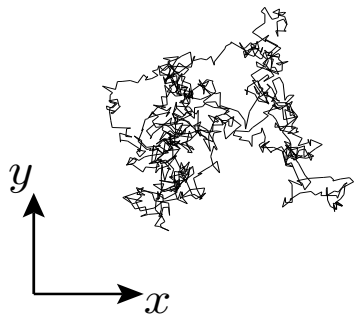


**Figure 2.1:** An exemplary trajectory of a Brownian particle in the absence of geometrical constraints/boundaries. The presence of thermal noise in the environment causes the zigzag motion.

In the absence of boundaries (see Fig. 2.1), i.e., for the free case, the Brownian particle obeys the fluctuation-dissipation theorem (Einstein relation) for asymptotically long times [1, 2]. The mean square displacement is proportional to time, and the diffusion constant reads

$$D_0 = \frac{k_\mathrm{B}T}{\eta}\,, \tag{2.1}$$

where $\eta$ is the friction coefficient, $k_\mathrm{B}$ the Boltzmann constant, and $T$ the temperature.

Here, the only particle property that enters the noise characteristics is the friction coefficient $\eta$. It is a remarkable feature that the diffusion in the present case does not depend on the mass of the Brownian particle [30]. Let's consider the case of an applied bias acting on the system, *only* along the $x-$ direction (see Fig. 2.1). Then, we can describe the system dynamics along the $x-$ direction with the Langevin equation, which in the over-damped limit [57] reads

$$\eta\,\dot{x}(t) = F + \sqrt{\eta\,k_{\mathrm{B}}\,T}\,\xi(t)\,, \tag{2.2}$$

where $\dot{x}(t)$ is the time derivative of the position coordinate of the particle at time $t$, and $F$ is a constant applied bias. The thermal fluctuations due to the coupling of the Brownian particle with the environment are modeled by the Gaussian white noise with zero mean

$$\langle \xi(t) \rangle = 0\,, \tag{2.3}$$

and the auto-correlation function

$$\langle \xi(t)\,\xi(t') \rangle = 2\,\delta(t-t')\,. \tag{2.4}$$

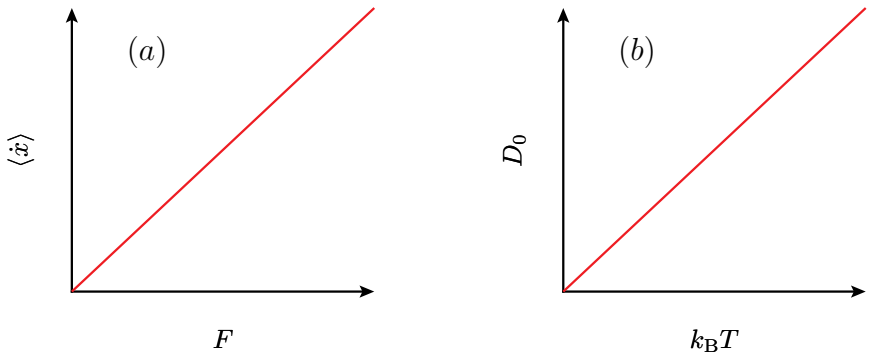


**Figure 2.2:** The behavior of transport coefficients in the free case. (a) The average particle current as a function of the applied bias and (b) the effective diffusion coefficient as a function of the thermal noise strength. Here, the average particle current is independent on thermal noise and the effective diffusion coefficient is invariant under the influence of an external bias.

From Eq. (2.2), and with the properties of Gaussian white noise (Eq. (2.3) and Eq. (2.4)), it is straightforward to conclude that in the steady-state the average particle current is proportional to the strength of the applied bias, see Fig. 2.2(a). For any

value of $k_{\mathrm{B}}T$, and for $\eta = 1$ it is equal to the value of the applied bias. The diffusion coefficient (Eq. (2.1)) does not change even if there is a constant external bias acting on the system, see Fig. 2.2(b). In the presence of a constant external bias, the transformation, $x(t) \to x(t) - Ft$ (for $\eta = 1$), leaves the diffusion coefficient invariant.

Note that, the very same diffusion process can be observed in the case of a flat channel where the Brownian particles do not experience any obstacles in the direction of propagation. In this case, channel walls (boundaries) along the transverse direction(s) do not show any impact on the transport properties along the channel direction because the motion in different directions is decoupled from each other. However, if we consider a long channel (2D or 3D) with irregular boundaries along the transverse direction(s) then the transport characteristics along the longitudinal direction can be strongly affected by the boundary conditions, and a decoupling is not possible.

In the following, we are considering the known and solvable case of motion of a Brownian particle in one-dimensional periodic potential.

## 1D periodic potentials

Thermal diffusion in tilted periodic potentials is of relevance in the context of Josephson junctions [64–66], rotating dipoles in external fields [67], diffusion of atoms and molecules on crystal surfaces [68], biophysical processes such as neural activity [69], and many other systems [30]. These, by nature, are purely energetic systems.

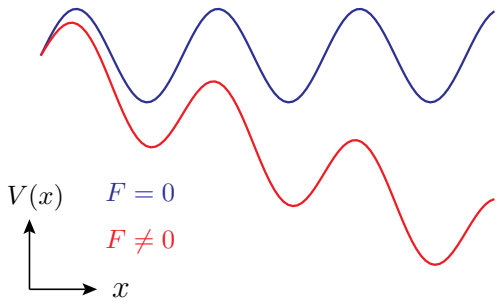


**Figure 2.3:** One-dimensional periodic potential $V(x) = U(x) - x\,F$ in the presence and in the absence of an applied bias.

The diffusion process in such systems has been studied widely from periodic systems to ratchet systems [70–78]. Analytical tools are available to calculate the relevant transport characteristics [70–73, 75–79]. The dynamics of the one-dimensional system with 1D periodic potential function considered here, can be described by the Langevin equation which in the over-damped limit [57] reads

$$\eta\,\dot{x}(t) = -V'(x) + \sqrt{\eta\,k_{\mathrm{B}}\,T}\,\xi(t)\,, \tag{2.5}$$

where $V(x) = U(x) - x\,F$ in the presence of an applied bias, $U(x) = U_0 \sin(2\pi x/L)$ is a periodic potential function with periodicity $L$, i.e., $U(x+L) = U(x)$, and $U_0$ determines the barrier height. A prime over the quantity refers to derivative with respect to spatial coordinate $x$.

The corresponding Fokker-Planck equation for the considered one-dimensional system reads [30, 75–77]

$$\frac{\partial P(x,t)}{\partial t} = D_0\,\frac{\partial}{\partial x}\left\{ e^{-\beta V(x)}\,\frac{\partial}{\partial x} e^{\beta V(x)} \right\} P(x,t)\,, \tag{2.6}$$

where $P(x,t)$ is the one-dimensional probability distribution and $\beta = 1/k_{\mathrm{B}}T$.

Fig. 2.3 is a sketch of an one-dimensional periodic potential in the presence and in the absence of an external bias $F$. For the considered potential, in the absence of external bias ($F = 0$), the potential function is spatially symmetric, and in the presence of the bias spatial symmetry breaks down.

### Transport characteristics

The transport characteristics, the average particle current and effective diffusion coefficient, for the considered one-dimensional periodic potential can be calculated by means of the Mean First Passage Time (MFPT) approach [72, 75–78], for which the analytical expressions are readily available [76, 77]. We discuss the MFPT approach later in detail in chapter 3.

The expression for the average particle current is given by [76, 77]

$$\langle \dot{x} \rangle = \frac{1 - e^{-\beta F L}}{\displaystyle\int_{x_0}^{x_0+L} \frac{\mathrm{d}x}{L}\, I_{\pm}(x)}\,, \tag{2.7}$$

and the effective diffusion coefficient reads [76, 77]

$$D_{\mathrm{eff}} = D_0\,\frac{\displaystyle\int_{x_0}^{x_0+L} \frac{\mathrm{d}x}{L}\, I_{\pm}(x)\, I_{+}(x)\, I_{-}(x)}{\left[\displaystyle\int_{x_0}^{x_0+L} \frac{\mathrm{d}x}{L}\, I_{\pm}(x)\right]^3}\,, \tag{2.8}$$

where the integral functions are given by

$$I_+(x) = \frac{1}{D_0}\, e^{\beta V(x)} \int_{x-L}^{x} \mathrm{d}y\, e^{-\beta V(y)} \tag{2.9}$$

and

$$I_-(x) = \frac{1}{D_0}\, e^{-\beta V(x)} \int_{x}^{x+L} \mathrm{d}y\, e^{\beta V(y)}\,. \tag{2.10}$$

The analytical expression for the average particle current equals the Stratonovich formula [70, 71].

### Dimensionless units

We can express the Langevin equation, Eq. (2.2), in a dimensionless form by scaling length with the periodicity $L$ and time by the characteristic time scale (as similar to we present in chapter 3, and see also Ref.[26, 28]). Thus, in the dimensionless form the Langevin equation reads

$$\dot{\tilde{x}}(\tilde{t}) = -\tilde{V}'(\tilde{x}) + \sqrt{\tilde{T}}\,\xi(\tilde{t})\,, \tag{2.11}$$

where

- $\tilde{x} = x/L$
- $\tilde{t} = t/\tau$
- $\tau = \eta\, L^2/k_\mathrm{B}\, T_\mathrm{R}$ with an arbitrary reference temperature $T_\mathrm{R}$
- $\tilde{T} = T/T_\mathrm{R}$ , which implies $\tilde{D_0} = D_0/(k_\mathrm{B}\, T_\mathrm{R}/\eta)$
- $\tilde{V}(\tilde{x}) = V(\tilde{x})/k_\mathrm{B}\, T_\mathrm{R} \; = (U_0\, \sin(2\pi\, \tilde{x}) - \tilde{x}\tilde{F})/k_\mathrm{B}\, T_\mathrm{R}$
- $\tilde{F} = F/F_\mathrm{R}$ with $F_\mathrm{R} = k_\mathrm{B}\, T_\mathrm{R}/L$
- $\tilde{U_0} = U_0/k_\mathrm{B}\, T_\mathrm{R}$

In the following, for convenience, we remove the tilde symbols on the coordinates. Note that, this dimensionless description is used only within this chapter.

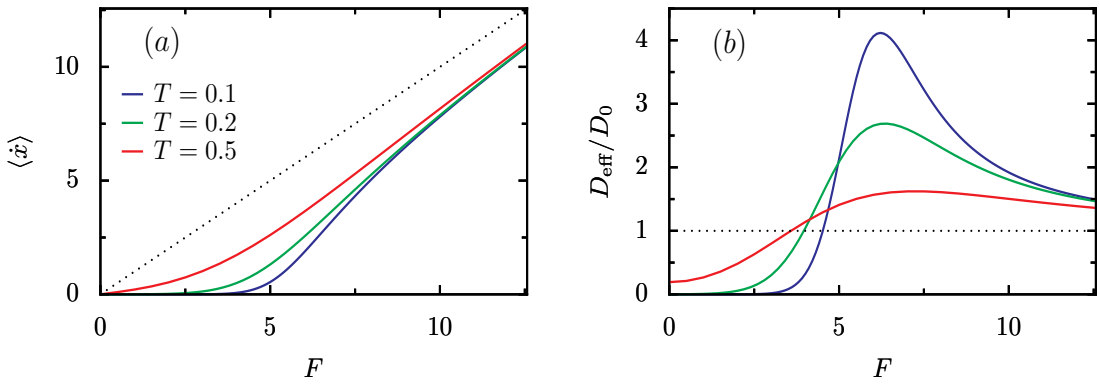


**Figure 2.4:** In dimensionless units, the behaviors of the scaled average particle current (a) and the ratio of scaled effective diffusion coefficient to the bulk diffusion coefficient (b), in a purely energetic system, as a function of the applied bias and at different noise strengths.

## 2.1 Diffusion process in energetic systems

The average particle current in the considered systems increases as the strength of the applied bias increases [79], see Fig. 2.4(a). For a very large applied bias, i.e., for a very large tilt, the average particle current tends to the value of applied bias described by the black dotted line in Fig. 2.4(a) for any thermal noise strength [79].

For the tilted energetic potentials, we can observe a *giant enhancement* in the effective diffusion near the threshold tilt [76–80]. The effective diffusion coefficient is greatly enhanced [76, 77, 79], see Fig. 2.4(b), and may exceed the bulk diffusion constant by many orders of magnitude. For the considered parameters the critical tilt $F_c$ is $2\pi$. Note that, near the critical tilt the effective diffusion is high for small thermal noise strengths and exhibits a resonance-like behavior [76, 77, 79, 81].

### 2.1.1 Kramers rate

The Kramers rate was first introduced for the so-called Kramers problem. The escape of a Brownian particle over a barrier in a cubic potential [82]. Principally, this may be extended to periodic systems [75].

For a potential $V(x)$ with a small static tilt and barrier height $\Delta V$ the escape rate of an over-damped Brownian particle from one well to the other in the presence of thermal noise is given by the Kramers rate [75, 82], in dimensionless units, for $\Delta V \gg T$,

$$r_{\mathrm{K}}(T) = \frac{\sqrt{V''(x_{\min})|V''(x_{\max})|}}{2\pi} \exp\left(-\Delta V/T\right) , \tag{2.12}$$

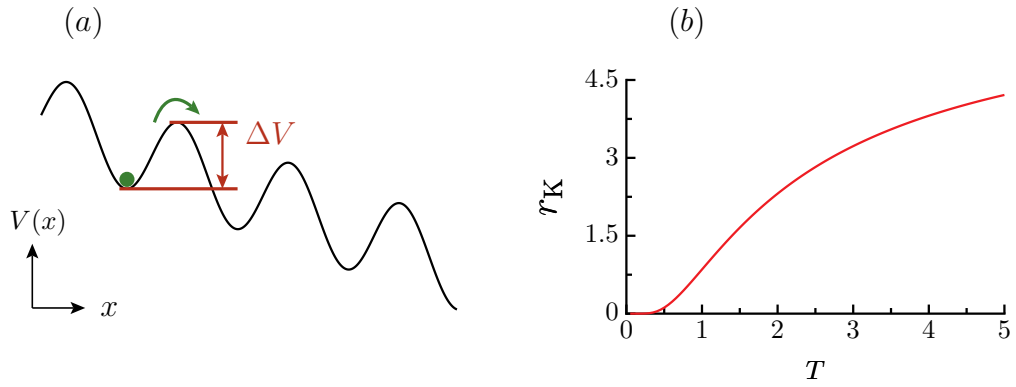


**Figure 2.5:** The sketch of an one-dimensional tilted periodic potential $V(x) = U(x) - x\,F$ with a barrier height $\Delta V$ is plotted in (a). In dimensionless units, the corresponding Kramers rate, Eq. (2.13), as a function of temperature is depicted in (b). Here, the value of $U_0$ is set to 1.

where $V''$ is second derivative of the effective potential function with respect to $x$, $x_{\max}$ and $x_{\min}$ indicate the positions of the maximum and minimum of the potential function, respectively. The barrier height $\Delta V$ denotes the activation energy necessary to proceed by one potential period [75, 82], see Fig. 2.5(a). With respect to the considered potential energy function $V(x) = U_0 \sin(2\pi\, x) - x\,F$, the corresponding Kramers rate for transitions from one cell to the next reads (for $F \ll 1$), in dimensionless units,

$$r_{\mathrm{K}}(T) = 2\pi\, U_0\, e^{-\,2U_0/T}\,. \tag{2.13}$$

The reaction rate increases monotonically with temperature, which implies that temperature facilitates the transition of Brownian particles from one potential minima to another by increasing the Arrhenius factor $\exp\left(-\Delta V/T\right)$ in Eq. (2.12), see Fig. 2.5(b).

### 2.1.2 Temperature dependence

Fig. 2.6 shows the behavior of transport characteristics as a function of thermal noise at different strengths of the applied bias. As we have observed from the reaction rate, temperature facilitates the activation to overcome the barrier, and the average particle current increases monotonically as temperature increases, see Fig. 2.6(a). For very high temperatures, the average particle current tends to reach the value of applied bias, illustrated by the dotted lines drawn at corresponding applied bias strengths in Fig. 2.6(a). If the strength of applied bias is lower than the critical tilt, the effective diffusion coefficient increases monotonically with thermal energy, starting from a value beneath the bulk diffusion constant [83]. Note that, for periodic potentials in the absence of applied

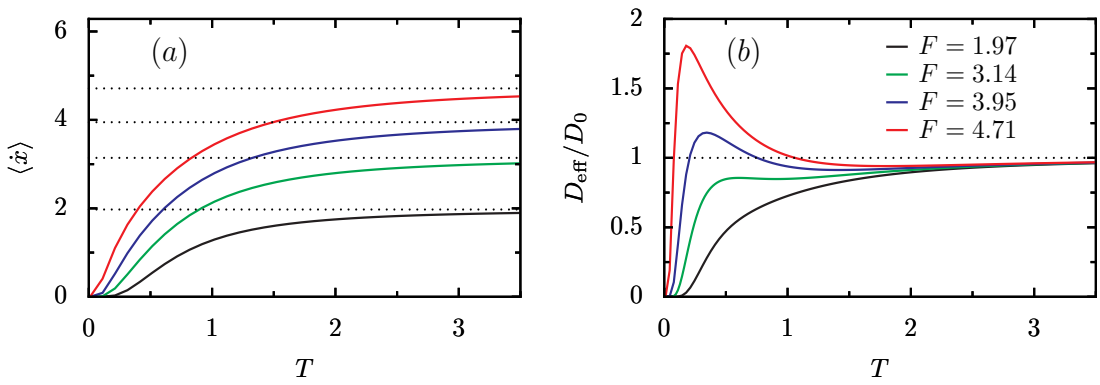


**Figure 2.6:** In dimensionless units, the behaviors of the scaled average particle current (a) and the ratio of scaled effective diffusion coefficient to the bulk diffusion coefficient (b) in a purely energetic system as a function of thermal noise and at different values of the applied bias. The dotted lines in graph (a) drawn at corresponding applied bias strengths. The dotted line in graph (b) is corresponding to $D_{\rm eff}/D_0 = 1$, which is reached in the limit $F \to \infty$.

bias the effective diffusion coefficient is lower than the bulk diffusion coefficient [83]. At very high temperatures, the effective diffusion coefficient tends to reach the bulk diffusion constant, see Fig. 2.6(b). Effective diffusion near and above the critical tilt is enhanced [76, 77, 79, 81], see Fig. 2.6(b), showing a resonance-like behavior.

## 2.2 Summary

In the absence of any boundaries, i.e., in the case of free diffusion, the mean square displacement of the Brownian particles proportional to thermal noise present in the system [1, 2]. If a Brownian particle is moving in a potential energy landscape diffusion process is subjected to change. In tilted one-dimensional periodic potentials, near the threshold tilt where deterministic running solutions set in, the diffusion is greatly enhanced [76, 77, 79] and exceeds the bulk diffusion constant. Below the threshold tilt, at lower and moderate thermal noise, the effective diffusion constant is lower than the bulk diffusion constant, and tends to reach the bulk diffusion constant in the strong noise limit.

In one-dimensional periodic potentials which are purely energetic systems, the reaction rate depends exponentially on temperature, i.e., temperature facilitates the activation process and helps the Brownian particles to overcome the potential energy barrier. Thus, the average particle current increases with the strength of thermal noise.

Now, an interesting question arises. If we consider a periodic system in higher dimensions where geometrical constraints may cause entropic barriers and control the transition rates between the potential minima, how is the diffusion process modified

then and how does the behavior of transport characteristics look like? in general, plenty of interesting questions arise concerning transport properties if the motion of Brownian particles is confined. In fact, this is the main motivation for the present work.

# 3

# Diffusion in confined structures

In typical transport processes through confined structures such as pores and channels or as a general example, the one depicted in Fig. 3.1 with an area of cross-section $\mathcal{A}(x)$, the transport of suspended Brownian particles is induced by the application of an external potential $V(\vec{r})$. In general, the dynamics of the Brownian particle inside the system is governed by the Langevin equation in the over-damped limit [57] with reflecting boundary conditions at the channel walls, reading

$$\eta\dot{\vec{r}}(\tilde{t}) = -\vec{\nabla}V(\vec{r}(\tilde{t})) + \sqrt{\eta\, k_{\mathrm{B}}\, T}\,\vec{\xi}(\tilde{t})\,, \tag{3.1}$$

where $\vec{r}$ is the position vector of a particle at time $\tilde{t}$. Thermal fluctuations due to the coupling of the Brownian particle to the environment are modeled by Gaussian white noise with zero mean, Eq. (2.3), and the auto-correlation function obeying Einstein's fluctuation-dissipation relation

$$\langle \xi(\tilde{t})\, \xi(\tilde{t}')\rangle = 2\,\delta_{ij}\,\delta(\tilde{t}-\tilde{t}') \;\text{ for } i,j = x,y,z\,. \tag{3.2}$$

Note that, Eq. (3.1) is not deduced from the previous chapter. The Langevin equation describing the dynamics of a Brownian particle within the channel, with an external force $\vec{F} = F\vec{e}_x$ acting along the direction of channel axis in the $x-$ direction, reads

$$\eta\,\dot{\vec{r}}(\tilde{t}) = \vec{F} + \sqrt{\eta\, k_{\mathrm{B}}\, T}\,\vec{\xi}(\tilde{t})\,, \tag{3.3}$$

with reflecting boundary conditions at the channels walls, confining the Brownian particles into the channel.

In order to further simplify the treatment of this model we introduce dimensionless variables, measuring all lengths in units of the period length $L$, i.e.,

$$\vec{r} = L\vec{x}\,, \tag{3.4}$$

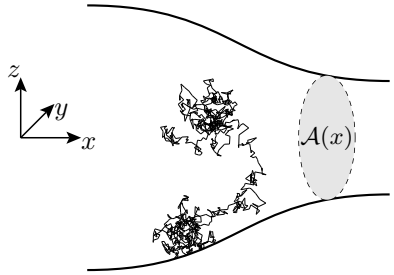


**Figure 3.1:** Confined structure with an area of cross section $\mathcal{A}(x)$. A Brownian particle explores the available space with in these boundaries, cf. trajectory.

where $\vec{x}$ denotes the dimensionless position of the particle. As unit of time $\tau$ we choose twice the time for the particle takes to diffusively overcome the distance $L$, which is given by $\tau = L^2\eta/(k_BT)$. Hence,

$$\tilde{t} = \tau t\,. \tag{3.5}$$

In these dimensionless variables the Langevin equation reads

$$\frac{\mathrm{d}\vec{x}}{\mathrm{d}t} = \vec{f} + \vec{\xi}(t)\,. \tag{3.6}$$

where $\langle \xi(t) \rangle = 0$, $\langle \xi_i(t)\, \xi_j(t') \rangle = 2\,\delta_{ij}\,\delta(t-t')$ for $i,j = x,y,z$, and the dimensionless force becomes

$$\vec{f} = f\vec{e}_x \quad \text{and } f = \frac{LF}{k_BT}\,. \tag{3.7}$$

The performed dimensionless scaling parameter $f$ characterizes the force as *the ratio of the work done on the particle along a distance of the period length $L$ and the thermal energy.* Note that, in the case of purely energetic systems, the driving force $F$ and the temperature $T$ are independent variables whereas in systems with entropic nature these two quantities can be coupled and tune the system's transport properties. In order to reach a certain value of $f$ one can modify either the bias strength or adjust the noise strength.

The corresponding Fokker-Plank equation that describes the time evolution of the probability distribution $P(\vec{x},t)$ takes the form [74, 84]:

$$\frac{\partial P(\vec{x},t)}{\partial t} = -\vec{\nabla}\cdot\vec{J}(\vec{x},t)\,, \tag{3.8a}$$

where $\vec{J}(\vec{x},t)$ is the probability current:

$$\vec{J}(\vec{x},t) = \left(\vec{f} - \vec{\nabla}\right) P(\vec{x},t)\,, \tag{3.8b}$$

Note that, for channels with similar geometry which are related by a scale transformation $\vec{r} \to \lambda\vec{r}$, $\lambda > 0$, the transport properties are determined by a single dimensionless parameter $f$ which subsumes the period lengths, the external forces and the temperature of the surrounding fluid.

The reflection of particles at the channel walls leads to a vanishing probability current at the boundaries. Due to the impenetrability of the channel walls, the normal component of the probability current $\vec{J}(\vec{x}, t)$ vanishes at the boundaries. Therefore, the boundary conditions at the channel walls are:

$$\vec{J}(\vec{x}, t) \cdot \vec{n} = 0 \quad \vec{x} \in \text{channel wall.} \tag{3.9}$$

where $\vec{n}$ denotes the normal vector at the channel walls.

The boundary of a 2D periodic channel which is mirror symmetric about the $x-$ axis is given by the periodic functions $y = \pm\omega(x)$, i.e., $\omega(x + 1) = \omega(x)$ for all $x$, where $x$ and $y$ are the cartesian components of $\vec{x}$. In this case, the boundary condition becomes

$$\frac{\mathrm{d}\omega(x)}{\mathrm{d}x}\left[fP(x, y, t) - \frac{\partial P(x, y, t)}{\partial x}\right] + \frac{\partial P(x, y, t)}{\partial y} = 0\,, \tag{3.10}$$

at $y = \pm\omega(x)$. Except for a straight channel with $\omega = const$, there are no periodic channel shapes for which an exact analytical solution of the Fokker-Planck equation (3.8, 3.8b) with boundary conditions (3.10) is known. Approximate solutions though can be obtained on the basis of a one-dimensional diffusion problem in an effective potential. Narrow channel openings, which act as geometric hindrances in the full model, show up as entropic barriers in this one-dimensional approximation [20–22, 26, 27, 85].

## 3.1 Equilibration assumption

Since the above mentioned system dynamics with special boundary conditions cannot be solved analytically one has to search for options in order to reduce the complexity of the situation by means of approximative methods. Let's assume that, *at any given time, the Brownian particles distribute uniformly along the transverse direction(s) of the confined structure*. Hence, by approximating *the concentration of Brownian particles along the transverse direction(s) as constant* (see Fig. 3.2) we can integrate out the transverse coordinate(s) between the lower and upper boundaries. This dramatically simplifies the complexity of the dynamics and leads to an entropic contribution (free energy term) to the reduced one-dimensional kinetic description, which can describe the full dynamics

of the system. This idea was originally proposed for systems in the absence of external bias, named the Fick-Jacobs equation [21]. Later on people made corrections to the equation [20, 22]. With this work we advance this approximation method by considering an additional external bias which is acting only along the length of the channel.

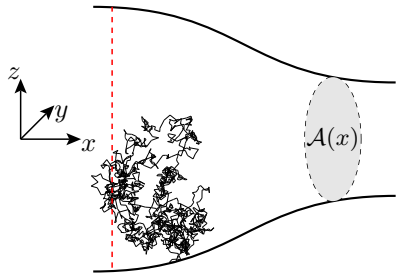


**Figure 3.2:** Equilibration along the transverse direction(s) in a confined structure with an area of cross section $\mathcal{A}(x)$.

The detailed mathematical description concerning the assumption of equilibration along the transverse direction(s), and the derivation of one-dimensional kinetic equation can be found in Appendix A.

After considering the equilibrium assumptions and integrating out the transverse coordinate(s), the final reduced one-dimensional kinetic equation with a free energy term that stems from the entropic contribution acquires the form [20, 22]

$$\frac{\partial P(x,t)}{\partial t} = \frac{\partial}{\partial x} D \left\{ \frac{\partial P(x,t)}{\partial x} + A'(x) P(x,t) \right\} , \tag{3.11}$$

where $P(x,t)$ is the reduced probability density. The dimensionless free energy $A(x)$ respectively reads, in the presence and in the absence of applied bias $f$,

$$A(x) = -\ln 2\Delta\omega(x) \qquad (f = 0) \tag{3.12a}$$

$$A(x) = -f\,x - \ln 2\Delta\omega(x) \qquad (f \neq 0)\,, \tag{3.12b}$$

where $2\Delta\omega(x)$ is the width of the channel in the two-dimensional (2D) system. The very same description holds for a three-dimensional (3D) system, except the width, $2\Delta\omega(x)$, of the channel should be replaced by the area of cross section $\pi\omega(x)^2$. For an illustration we have depicting the effective potential function $A(x)$, in Fig. 3.3 where we reduce the 2D system to an effective one-dimensional system.

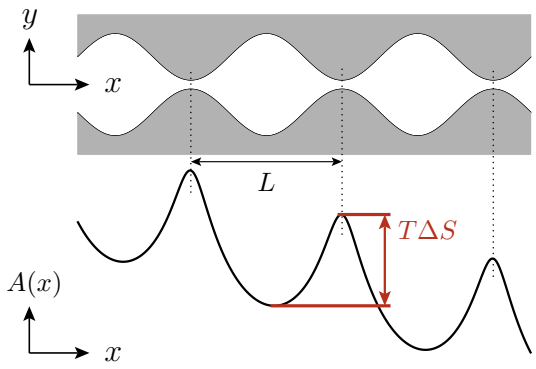


**Figure 3.3:** The free energy $A(x)$, Eq. (3.12), in the presence of applied bias as a function of the reaction coordinate $x$ if we reduce the 2D system, with the periodicity $L$, to an effective one-dimensional system with barrier height $T\,\Delta S(x)$.

Here, the temperature $T$ dictates the strength of the effective potential. An increase in temperature leads to an increase in barrier height while for purely energetic systems the barrier height is independent of the temperature [75].

## 3.2 Spatially dependent diffusion coefficient

After reducing the two-dimensional (or three-dimensional) kinetic equation to an one-dimensional one, one has to think about the influence of the boundary functions on the diffusion coefficient. Will there be the same constant diffusion everywhere inside the channel (or will there be changes) ?. Since the slope of the structure changes as the position along the $x-$ direction changes (see Fig. 3.1) the diffusion is possibly not constant everywhere inside the confined structure but could rather be a function of the position $x$. Taking these arguments into account, we can improve the accuracy of the reduced kinetic equation. In recent years there have been quite a few proposals in order to predict the form of a spatially dependent diffusion coefficient by considering the slope of the confined structure [20, 22, 85]. Here, we discuss the proposal of Zwanzig [20] predicted while making the corrections to the one-dimensional reduced kinetic equation as well as that of Reguera and Rubi [22] who proposed a scaling law for the diffusion coefficient by simple geometric arguments and finally that of Kalinay and Percus [85] who derived an expression by mapping procedures [86] while making the corrections to the Fick-Jacobs equation.

The spatially dependent diffusion coefficient suggested by Zwanzig results from a systematic expansion in terms of the gradient of the boundary function $\omega(x)$. In leading order, he obtained $D(x) = 1 - \alpha\omega'(x)^2 + \ldots$ where $\alpha = 1/3$ or $1/2$ in two or three dimen-

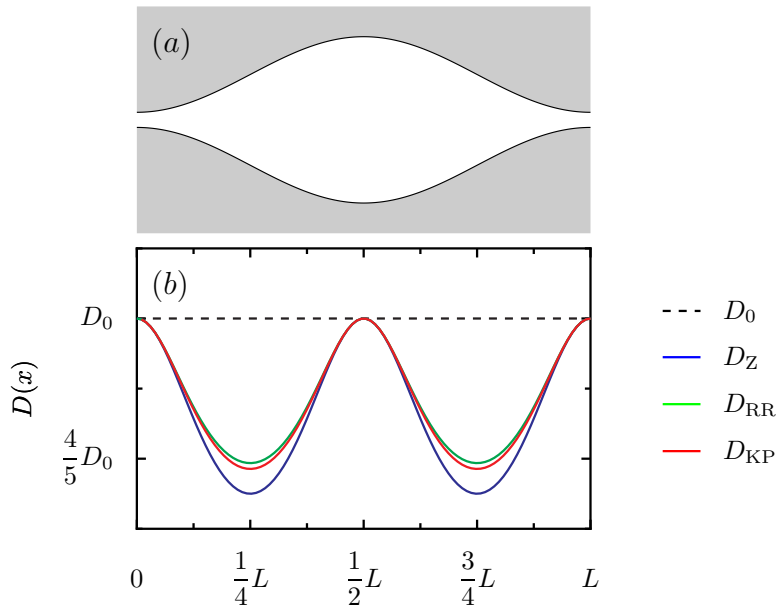


**Figure 3.4:** A single cell of the two-dimensional confined geometry with periodicity $L$ (a), and the behavior of $x-$ dependent diffusion coefficient (b). Blue line corresponds to Zwanzig's proposal, green line corresponds to Reguera-Rubi's proposal, red line corresponds to Kalinay-Percus's proposal, and black dashed line corresponds to the bare diffusion constant.

sions, respectively, and the prime denotes the derivative with respect to $x$. Interpreting this result as the first two terms of a geometric series, Zwanzig proposed his re-summed expression for the 1D diffusion coefficient [20] reading

$$D_{\mathrm{Z}}(x) = \frac{1}{[1 + \alpha\omega'(x)^2]}\,, \tag{3.13}$$

where $\alpha = 1/3, 1/2$ for two and three dimensions, respectively.

The expression given by Reguera and Rubi [22] in dimensionless units, is

$$D_{\mathrm{RR}}(x) = \frac{1}{[1 + \omega'(x)^2]^{\alpha}}\,. \tag{3.14}$$

This can simply be understood as follows: In the absence of applied bias the variance in the position of particles, due to thermal noise present in the environment, is proportional to time,

$$\Delta r^2 \sim t \tag{3.15a}$$

$$\Delta x^2 \left[1 + \left(\frac{\Delta y}{\Delta x}\right)^2\right] \sim t \tag{3.15b}$$

$$\frac{\Delta x^2}{t} \sim \left[1 + \left(\frac{\Delta y}{\Delta x}\right)^2\right]^{-1} , \tag{3.15c}$$

where $\Delta y/\Delta x = \omega'(x)$ gives the slope of the confined structure, and the spatially dependent diffusion coefficient along the $x-$ direction is $\Delta x^2/t$. This spatially dependent diffusion coefficient can also be considered as a re-summation of Zwanzig's perturbational result.

Kalinay and Percus proposed two different forms of spatially dependent diffusion coefficient for the 2D and 3D case [85]. In 2D case they obtained a geometric series,

$$D(x) \simeq 1 - \frac{\epsilon}{3}\omega'^2 + \frac{\epsilon^2}{5}\omega'^4 + ..... + \frac{(-\epsilon)^n}{2n+1}\omega'^{2n} \tag{3.16}$$

which results in

$$D_{\mathrm{KP}}(x) = \frac{\arctan\left[\sqrt{\epsilon}\omega'(x)\right]}{\sqrt{\epsilon}\omega'(x)} , \tag{3.17}$$

where $\epsilon = D_x/D_y$ is the ratio of the diffusion constants in the longitudinal and transverse directions, and $\omega(x)$ is the half-width of the channel.

In 3D they followed a similar analysis, and obtain a geometric series [85],

$$D(x) \simeq 1 - \frac{\epsilon}{2}\omega'^2 + \frac{3\epsilon^2}{8}\omega'^4 + ..... + \frac{(-\epsilon)^n(2n-1)!}{(2n)!}\omega'^{2n} \tag{3.18}$$

which results in

$$D_{\mathrm{KP}}(x) = \frac{1}{\sqrt{[1+\epsilon\,\omega'(x)^2]}} , \tag{3.19}$$

where $\omega(x)$ is radius of the channel.

Later on we are comparing these formulas with numerical results for an arbitrary confined structure and thus learn which one leads to better results.

The final form of the reduced one-dimensional kinetic equation in the presence of entropic barriers with spatially dependent diffusion coefficient reads

$$\frac{\partial P(x,t)}{\partial t} = \frac{\partial}{\partial x} D(x) \left\{\frac{\partial P(x,t)}{\partial x} + A'(x)P(x,t)\right\} \tag{3.20}$$

## 3.3 Mean First Passage Time (MFPT) approach

The transport characteristics, the average particle current and effective diffusion coefficient, of Brownian particles within a periodic channel can be calculated in terms of the moments of the first passage time by a well-known analytical method, namely the Mean First Passage Time (MFPT) approach [75–78]. In order to calculate the moments of the first passage time *we consider an arbitrary but fixed point ($x_0 = 0$), and we denote $t(x_0 \to x_0 + 1)$ the time until the fixed point $x_0 + 1$ is reached for the first time.* Then, the $n$th moment of the first passage time is given by the ensemble average of $t^n$, i.e

$$T_n(x_0 \to x_0 + 1) := \langle t^n(x_0 \to x_0 + 1)\rangle. \tag{3.21}$$

for $n \in \mathbb{Z}$ and with $T_0(a \to b) = 1$. The mathematical details of calculating these moments can be found in Appendix B.

For any non-negative bias the average particle current in periodic structures can be obtained from [76, 77]

$$\langle \dot{x}\rangle = \frac{1}{T_1(x_0 \to x_0 + 1)}\,, \tag{3.22}$$

where $T_1$ is the first moment of the first passage time (Eq. (B.15)). Note that, the averages in Eq. (3.21) may diverge for zero bias. A positive bias prevents the particle from traveling too far to the left, and hence leads to a finite mean first passage time as well as to a finite current.

The effective diffusion coefficient reads [76, 77]:

$$D_{\text{eff}} = \frac{\Delta T_2(x_0 \to x_0 + 1)}{2\,[T_1(x_0 \to x_0 + 1)]^3}\,, \tag{3.23}$$

where $\Delta T_2$ is the dispersion of the second moment of the first passage time (Eq. (B.43)). The final expression for the average particle current which is similar to the Stratonovich formula [70] with a free energy term reads

$$\langle \dot{x}\rangle = \frac{1 - e^{-f}}{\displaystyle\int_{x_0}^{x_0+1} \mathrm{d}x\, I(x)}\,, \tag{3.24}$$

and the effective diffusion coefficient becomes

$$D_{\text{eff}} = \frac{\displaystyle\int_{x_0}^{x_0+1} \mathrm{d}x \int_{x-1}^{x} \frac{D(z)}{D(x)}\, e^{[A(x)-A(z)]}\, \mathrm{d}z\ [I(z)]^2}{\left[\displaystyle\int_{x_0}^{x_0+1} \mathrm{d}x\, I(x)\right]^3}\,, \tag{3.25}$$

where the integral function $I(x)$ acquires the form

$$I(x) = \frac{e^{A(x)}}{D(x)} \int_{x-1}^{x} \mathrm{d}y\, e^{-A(y)}\,. \tag{3.26}$$

Now, the analytical expressions are available for the constructed effective one-dimensional kinetic description.

## 3.4 Summary

In this chapter we have discussed the complications involved in calculating the transport characteristics of a higher dimensional system (2D or 3D) with impenetrable boundaries. Here, the boundary functions complicate the problem which hence cannot be solved with the available analytical tools. Therefore, we have constructed an approximation method, assuming an equilibrium distribution along the transverse directions. It leads to a reduction of dimensionality, and we finally end up at an effective one-dimensional kinetic description with an entropic contribution to the energy profile. In this connection, the complexity of the problem is reduced allowing for an analytical solution concerning the transport properties. The reduction of dimensionality impacts the diffusion coefficient by modifying it from a constant to a position dependent one. Finally, the reduced effective one-dimensional kinetic equation in the presence of entropic barriers and with a spatially dependent diffusion coefficient reads

$$\frac{\partial P(x,t)}{\partial t} = \frac{\partial}{\partial x}\, D(x) \left\{ \frac{\partial P(x,t)}{\partial x} + A'(x) P(x,t) \right\}.$$

Concerning the reduced one-dimensional kinetic description, the analytical expressions for the transport characteristics, the average particle current and effective diffusion coefficient are derived with the use of the Mean First Passage Time (MFPT) approach. We found a scaling parameter $f = FL/k_{\text{B}}T$, i.e., the ratio of the work done to the particle and the available thermal energy, which is a genuine property of entropic systems and can be used to tune the system's transport characteristics.

# 4

# Entropic transport

In the previous chapter, we have constructed an approximative mechanism to calculate the transport characteristics for a given confined structure. We have obtained analytical expressions for the average particle current and the effective diffusion coefficient for the one-dimensional kinetic description. Now we shall check it's applicability, the consistency, and the accuracy. We are considering a higher dimensional system (2D or 3D) and calculate the transport characteristics by using numerical simulations we are then comparing these results with those obtained from the one-dimensional kinetic description.

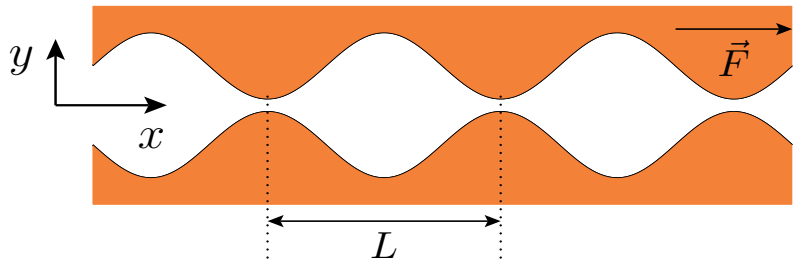


**Figure 4.1:** Schematic diagram of a two-dimensional channel confining the motion of biased Brownian particles. The half-width $\omega(x) = a\sin(2\pi x) + b$ is a periodic function of $x$ with periodicity $L$. Here, the constant applied bias $F$ acts only along the channel direction, and the thermal bath the particles are coupled to is modelled by Gaussian white noise with zero mean.

In doing so, we consider as a model system a two-dimensional symmetric channel confining the Brownian particles, with periodicity $L$ and a constant bias $F$ acting along the channel length. The shape of the structure is defined by the function [1] Here, $a$ is the parameter that controls the slope of the channel wall, the width of the channel is $2\,\omega(x)$, the width at the bottleneck is $2\,(b-a)$ and the full width of the channel is $2\,(b+a)$. In principle, we can consider the similar structure in 3D also but due to constraints in computational time we have restricted ourselves to the two-dimensional case. In the

[1] Note: In dimensionless units, the half-width $\omega(x)$ is scaled with the periodicity $L$.

following, the term *cell* is used to define the part of the structure reading from one bottleneck to the other.

## 4.1 Numerical simulations

As described above, we have considered a two-dimensional system for the numerical simulations, see Fig. 4.1. The transport characteristics as predicted in the previous chapter have been corroborated by Brownian dynamic simulations performed within the stochastic Euler-algorithm by integration of the dimensionless Langevin equation in the over-damped limit [57] reading

$$\frac{\mathrm{d}\vec{x}}{\mathrm{d}t} = \vec{f} + \vec{\xi}(t) \tag{4.1}$$

with reflecting boundary conditions at the channel walls confining the Brownian particles inside the channel. Here, the scaled bias $f$ acts only along the length of the channel. For the numerical simulations the single integration steps read :

- modification of the $x-$ coordinate

$$x_{\mathrm{new}} = x_{\mathrm{old}} + f\Delta t + \sqrt{\Delta t}\,\zeta_1 \tag{4.2}$$

- modification of the $y-$ coordinate

$$y_{\mathrm{new}} = y_{\mathrm{old}} + \sqrt{\Delta t}\,\zeta_2\,, \tag{4.3}$$

where $\zeta_1$ and $\zeta_2$ are two Gaussian distributed random numbers. If the new desired position is not allowed in the sense that it is lying outside the channel then the boundary conditions have to be considered, i.e the simulation step is discarded. For the numerical simulations, we have considered more than $3 \cdot 10^4$ realizations to improve accuracy and minimize statistical errors. An initial distribution at time $t = 0$ starts in the middle of a cell. The new positions for each realization, Eq. (4.2) and Eq. (4.3), along the $x-$ and $y-$ directions depend on strength of the scaling parameter $f$. In order to provide the requested accuracy of the system dynamics time step was chosen to be smaller than $10^{-4}$.

For an illustration, Fig. 4.2 shows numerically evaluated density snap-shots of the Brownian particles at different times $t$ in a symmetric two-dimensional channel with a shape defined by the half width $\omega(x) = (1/2\pi)\sin(2\pi x) + (1.02/2\pi)$, mapped into a single

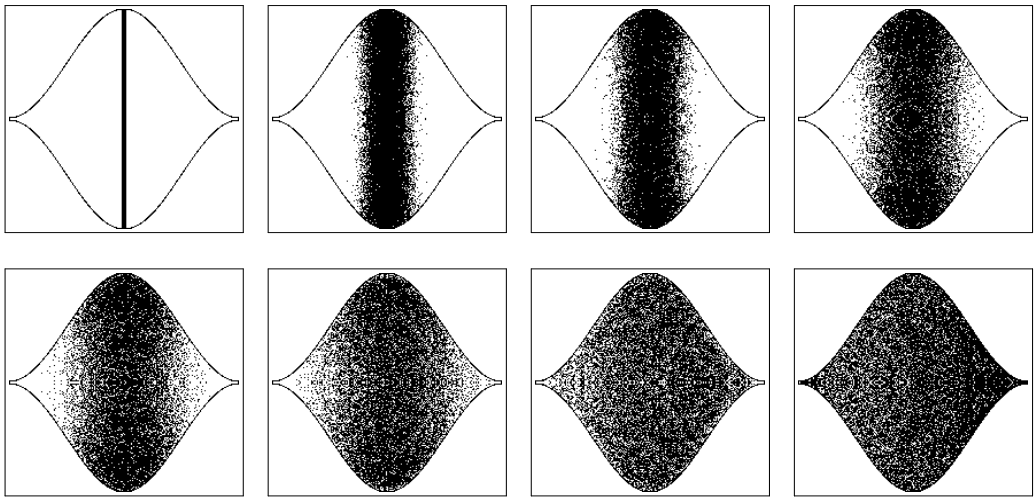

**Figure 4.2:** Numerically obtained, density snap-shots of the Brownian particles at different values of time $t$ in a symmetric two-dimensional channel with the shape defined by the half width $\omega(x) = (1/2\pi)\sin(2\pi x) + (1.02/2\pi)$ mapped into a single cell at the scaling parameter value $f = 1.0$ . Upper row correspond to $t = 0, 6, 13$, and 25 (left to right). Bottom row correspond to $t = 38, 50, 126$, and 5000 (left to right). The initial distribution of the Brownian particles start at the middle of a cell, at time $t = 0$ (top left panel), diffuse within the channel geometry and in the long time limit the distribution reaches a steady-state (bottom-right panel), i.e., the initial conditions have completely died out.

cell. The scaling parameter value is chosen as $f = 1.0$. Brownian particles which initially start at time $t = 0$ in the middle of a single cell will distribute over the available space within the channel geometry. Thermal noise that is present in the system enables the particles to roam around and the applied bias acting along the length of the channel drags the particle in the same direction. Finally, after a very long time the Brownian particles will reach a steady-state, i.e., after the initial conditions have been died out. During this process the Brownian particles may cross a high number of cells, but for convenience, in Fig. 4.2, we have mapped all Brownian particles into one single cell as the channel is periodic with a periodicity $L$. Fig. 4.3 shows the corresponding normalized probability distribution of the Brownian particles along the $x-$ direction (channel direction) during the time evolution. The initial delta-distribution at time $t = 0$ will broader as time increases. In the long time limit the distribution reaches a steady-state.

Since our main motive is to compare the transport characteristics obtained from the reduced one-dimensional kinetic equation with the results obtained from numerical simulations, we will calculate the transport coefficients only along the $x-$ direction. The expressions for the transport characteristics, the mean particle velocity and effective diffusion coefficient which we used for the numerical simulations are given by [26, 27]

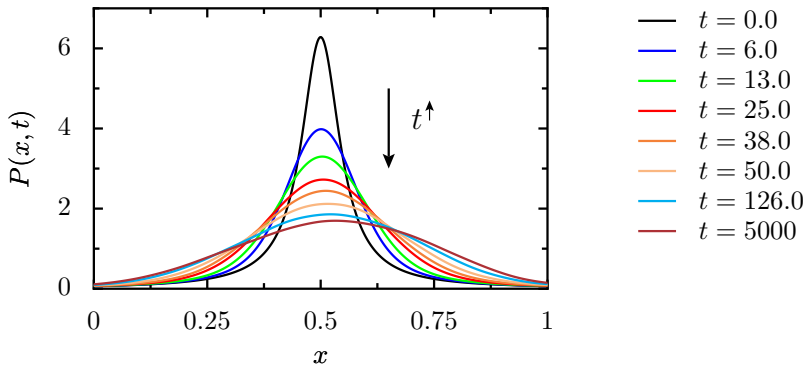


**Figure 4.3:** Normalized probability distribution of the Brownian particles along the $x-$ direction $P(x,t)$, with in a single cell, as the evolution time increases (extracted from Fig. 4.2)

The average particle current in the $x$- direction,

$$\langle \dot{x} \rangle = \lim_{t \to \infty} \frac{\langle x(t) \rangle}{t} \tag{4.4}$$

and the effective diffusion coefficient

$$D_{\text{eff}} = \lim_{t \to \infty} \frac{\langle x^2(t) \rangle - \langle x(t) \rangle^2}{2\,t}\,. \tag{4.5}$$

Both the average particle current and the effective diffusion coefficient along the transverse direction ($y$) are zero since there is no force acting along that direction.

Fig. 4.4 shows the behavior of the key quantities of interest, i.e., the average particle current and the effective diffusion coefficient, as functions of time. Depending on the system's initial preparation, both the average particle current and the effective diffusion coefficient start at an arbitrary value. During the time evolution process the values may change, fluctuate, and finally reach a steady-state in the long time limit, i.e., after the initial conditions have been completely died out. Even then one could observe unavoidable small fluctuations which lead to some statistical error. In order to minimize it one has to consider a large number of realizations. In our simulations, the relative error in calculating the transport coefficients, the average particle current and effective diffusion coefficient is less than 0.01.

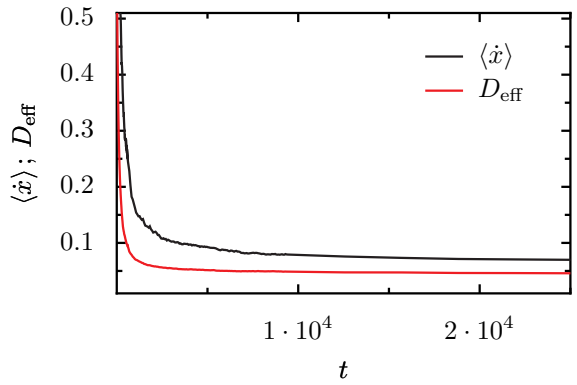


**Figure 4.4:** The behavior of the key quantities of interest, the average particle current and the effective diffusion coefficient, as the time changes in a symmetric two-dimensional channel with the shape defined by the half width $\omega(x) = (1/2\pi)\sin(2\pi x) + (1.02/2\pi)$ at the scaling parameter value $f = 1.0$. At very long time, both the quantities reach the steady-state.

## 4.2 Transport characteristics

In this section we present the transport characteristics, the average particle current and effective diffusion coefficient of a two-dimensional system obtained from the numerical simulations. In the present entropic system the transport quantities may be expressed in terms of a single scaling parameter $f := FL/k_{\text{B}}T$. But in this section, we analyze the influence of applied bias $F$ and temperature $T$, that is on the transport characteristics in order to observe the system behavior and for better comparison with the situation in purely energetic system, i.e., in the absence of entropic barriers.

Therefore, like in chapter 2 we adopt an arbitrary reference temperature $T_{\text{R}}$, as well as the corresponding characteristic diffusion time at this temperature,

$$\tau_{\text{R}} = \frac{\eta L^2}{k_{\text{B}} T_{\text{R}}}\,, \tag{4.6a}$$

and the reference force,

$$F_{\text{R}} = \frac{k_{\text{B}} T_{\text{R}}}{L}\,. \tag{4.6b}$$

### 4.2.1 Biased transport

The results for the average particle current and effective diffusion coefficient obtained from numerical simulations as functions of applied bias $F/F_{\text{R}}$ for a symmetric two-dimensional channel with a shape defined by the half-width $\omega(x) = (1/2\pi)\sin(2\pi x) + (1.02/2\pi)$ has been presented in Fig. 4.5 for different values of temperature $T/T_{\text{R}}$.

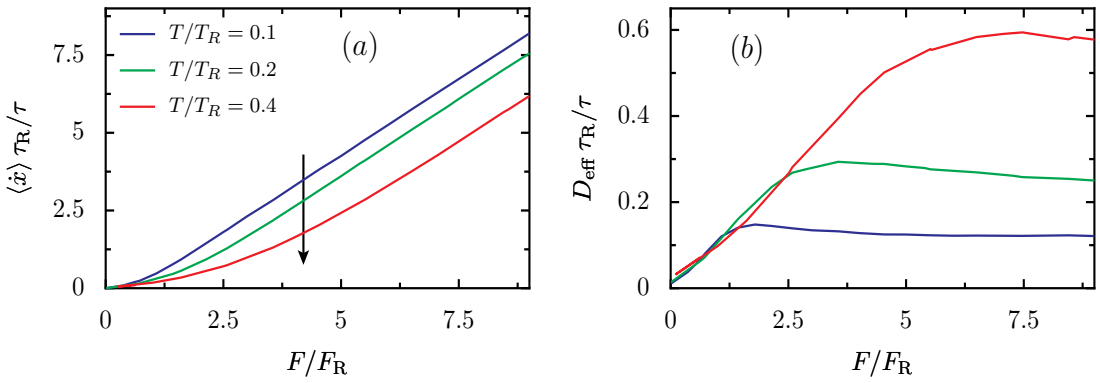


**Figure 4.5:** Numerically determined force dependence of the average particle current (a), and the effective diffusion coefficient (b), for a symmetric two-dimensional channel with the shape defined by the half width $\omega(x) = (1/2\pi)\sin(2\pi x) + (1.02/2\pi)$.

The average particle current increases monotonically as the strength of the applied bias increases (see Fig. 4.5(a)). The effective diffusion coefficient exhibits a non-monotonic behavior including the appearance of a peak, see Fig. 4.5(b). It's value is higher than in the case of bulk diffusion, and the peak position shifts to higher values of applied bias $F/F_{\rm R}$ as the strength of the thermal noise increases. The common feature of increasing average particle current with applied bias can also be observed even in the case of a purely energetic system, i.e., in the absence of entropic barriers [75]. But, the interesting feature we can observe in Fig. 4.5(a) is that upon increasing the strength of thermal noise $k_{\rm B}T$ the average particle current decreases at a constant value of applied bias $F/F_{\rm R}$. This makes an *inverse temperature dependence* which is not obvious in purely energetic systems where increasing temperature leads to an increase in the particle current. This interesting feature of noise-controlled transport solely arises from the entropic nature of the system. We will discuss this feature in more detail in the following section.

### 4.2.2 Anomalous temperature dependence

Fig. 4.6 shows the temperature dependence of the average particle current and the effective diffusion coefficients as functions of thermal noise strength $k_{\rm B}T$ at a constant applied bias $F/F_{\rm R}$ and for a symmetric two-dimensional channel with a shape defined by the half-width $\omega(x) = (1.0/2\pi)\sin(2\pi x) + (1.0/2\pi)$.

In the case of a purely energetic system, an increasing temperature leads to an increase in the average particle current (see Fig. 2.6(a)). But from Fig. 4.6(a) we observe that the average particle current decreases upon increasing thermal noise strength which is an opposite effect that we usually encounter in purely energetic system.

In the purely energetic case, increasing temperature increases the transition rates from

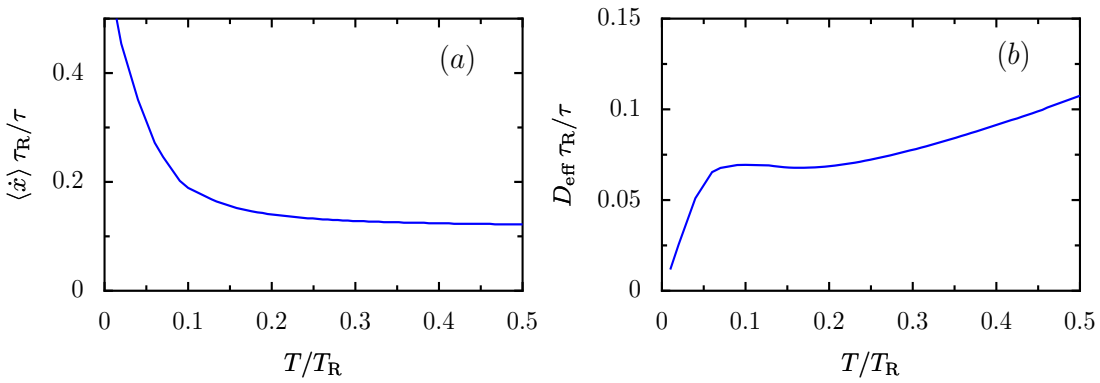


**Figure 4.6:** Numerically determined temperature dependence of the average particle current (a), and the effective diffusion coefficient (b), for a symmetric two-dimensional channel with the shape defined by the half width $\omega(x) = (1.0/2\pi)\sin(2\pi x) + (1.0/2\pi)$, at the force value $F/F_R = 0.628$.

one period to the next (see Fig. 2.5) [75]. This means that temperature facilitates the activation by overcoming the potential barrier thus an increase in temperature leads to an increase in the average particle current. For a one-dimensional periodic system with an entropic potential, temperature dictates the strength of the potential function (Eq. (3.12)) and an increase in temperature leads to an increase in the barrier height (see Fig. 3.3) and results in a decrease of the average particle current.

The effective diffusion coefficient exhibits a peak over a wide range of temperatures. This behavior we can observe even in the case of purely energetic system. In purely energetic systems the reaction rate depends exponentially on temperature, while this is not the case for entropic systems. Hence, due to this exponential dependence one would expect a *giant enhancement* in the effective diffusion coefficient [76, 77] in purely energetic systems, while for purely entropic systems this is not the case. An important feature that we can extract from Fig. 4.6(b) is that over a range of temperatures the effective diffusion coefficient increases upon decreasing the temperature, which only is a consequence of the entropic nature of the system. We are discussing this feature in more detail in the following.

### Effective diffusion coefficient in energetic and entropic systems

Fig. 4.7 shows the behavior of effective diffusion coefficient, in the presence and in the absence of applied bias, as a function of the thermal noise strength $k_B T$ in a flat channel geometry and in a two-dimensional system. For a flat channel, i.e., in the absence of geometrical constraints along the propagation direction of the Brownian particles, the effective diffusion coefficient equals the bare diffusion constant. In a confined system (2D or 3D), and in the absence of applied bias ($f = 0$), the effective diffusion coefficient

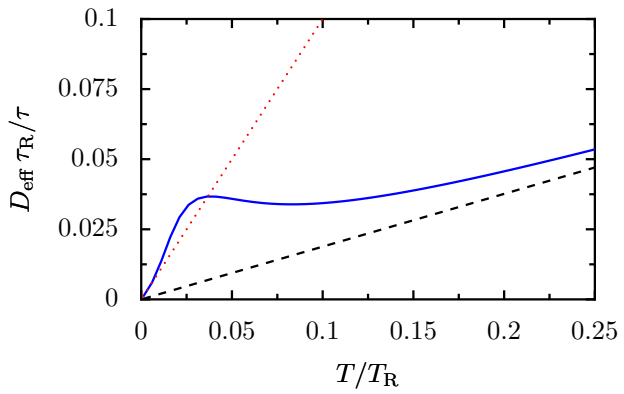


**Figure 4.7:** Numerically determined temperature dependence of the effective diffusion coefficient for a flat channel geometry corresponds to dotted red line, and for the periodic potential $\omega(x) = (1/2\pi)\sin(2\pi x) + (1.02/2\pi)$ corresponds to dashed black line (for $F/F_{\mathrm{R}} = 0$) and solid blue line (for $F/F_{\mathrm{R}} = 0.05$).

is still proportional to time (linear behavior, normal diffusion) but the slope of the line is less than that for the flat channel which is due to entropic effects arising from the confinement of the geometrical structure.

In the confined system in the presence of applied bias the value of the effective diffusion coefficient initially follows the red line which is corresponding to the flat channel case, see Fig. 4.7(a). At this stage applied bias $F/F_{\mathrm{R}}$ rules the dynamics rather than thermal noise strength $k_{\mathrm{B}}T$, and the entropic contribution to the free energy is negligible ($A(x) \approx -f\,x$). At very high values of thermal noise strength the effective diffusion curve follows the dashed black line which corresponds to the purely entropic case ($F/F_{\mathrm{R}} = 0$). At this stage the entropic contribution to the free energy is very high ($A(x) \approx -\ln 2\Delta\,\omega(x)$), and the entropic nature of the system rules the transport characteristics.

Over a wide range of temperatures, i.e., making a cross-over region from a purely energetic to a purely entropic nature, the effective diffusion coefficient exhibits a striking peak where it even exceeds the bare diffusion constant. The stationary distribution acquires a finite width in the transversal direction with a "crowded" region in front of the narrowest region of the channel [27]. Transport becomes more noisy and, consequently, the effective diffusion exceeds the bare diffusion constant. From these arguments we can conclude that noise strength plays an important role in entropic systems and dictates the transport characteristics.

So far, we have analyzed the peculiar behaviors of the transport characteristics, the average particle current and the effective diffusion coefficient, obtained from the numerical simulations for an arbitrary 2D periodic geometry. Now, let us compare these results with the analytical predictions derived in the previous chapter.

## 4.3 Analytics versus Numerics

Within our numerical simulations we have examined the transport characteristics of a given confined system. Now we are comparing these results with the analytical ones obtained from the Mean First Passage Time (MFPT) approach, see appendix B. Before doing that, for the analytical expressions we choose the *best* spatially dependent diffusion coefficient out of the available forms which we have discussed in the previous chapter 3.

### Spatially dependent diffusion coefficient

In order to check the consistency of the various spatially dependent diffusion coefficients available, we have considered the two-dimensional confined structure depicted in Fig. 4.1 with a constant applied bias acting along its length and calculated the first moment, the average particle current as a function of applied bias by using our reduced 1D kinetic equation. The analytical expression for the average particle velocity is given by Eq. (3.24).

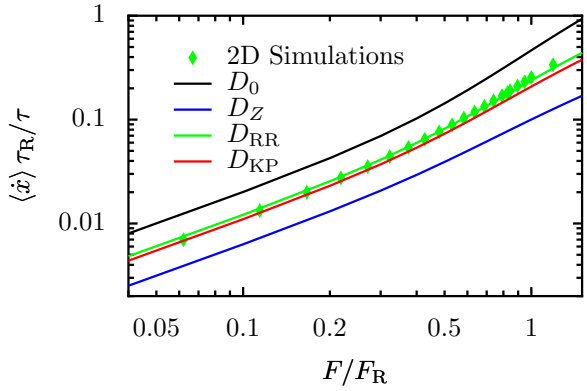


**Figure 4.8:** Numerically simulated (symbols) and analytically calculated (lines) force dependence of the average particle current is depicted with different diffusion coefficients for a symmetric two-dimensional channel.

From Fig. 4.8 we can clearly see that, if we are dealing with a confined structure we have to consider the spatially dependent diffusion coefficient $D(x)$, which will account for the impacts of geometrical constraints on the transport properties, rather than a constant diffusion coefficient $D_0$, which is independent of the geometrical shape of the structure.

The second message from Fig. 4.8 is that the position dependent diffusion constant proposed by Reguera and Rubí [22] is in good agreement with our 2D simulation results and improves the quality of our kinetic equation compared to other expressions proposed by Zwanzig [20] or Kalinay and Percus [85]. In the present situation of biased diffusion in

confined structures, the spatially dependent diffusion coefficient proposed by Kalinay and Percus doesn't provide a higher accuracy as the use of $D_{\mathrm{RR}}(x)$, proposed by Reguera and Rubi. Therefore, we are considering the later proposal of a spatially dependent diffusion coefficient [22] for our analytical expression for the transport characteristics.

### Comparison

For a fixed confined periodic system the analytical expressions for the transport characteristics, the nonlinear mobility and effective diffusion coefficient with a spatially dependent diffusion coefficient in terms of the scaling parameter $f$ are given by Eq. (4.7) and Eq. (4.8).
The expression for the nonlinear mobility $\mu(f)$ is

$$\mu(f) = \frac{\langle \dot{x} \rangle}{f} = \frac{1}{f} \frac{1 - e^{-f}}{\int_0^1 \mathrm{d}x\, I(x)}\,, \tag{4.7a}$$

with the integral function $I(x)$

$$I(x) = \frac{e^{A(x)}}{D(x)} \int_{x-1}^{x} \mathrm{d}y\, e^{-A(y)}\,. \tag{4.7b}$$

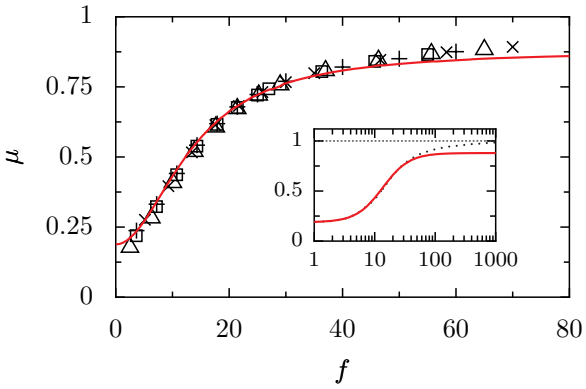


**Figure 4.9:** Graph for the nonlinear mobility for the periodic potential $\omega(x) = (1/2\pi)\sin(2\pi x) + (1.02/2\pi)$. In the Langevin simulation the different symbols correspond to different values of $T/T_R$: 0.01 (crosses), 0.1 (pluses), 0.2 (squares), 0.4 (triangles). The relative error of the simulation results is 0.01. The analytical results, Eq. (4.7), correspond to the solid lines. The inset depicts the long range behavior (the dotted line depicts the numerical results). The numerical values for the nonlinear mobility approach, in the limit $f \to \infty$, the value 1 (dashed horizontal line).

Fig. 4.9 shows the nonlinear mobility as a function of the scaling parameter. By defining this universal scaling parameter all the curves in Fig. 4.5(a) collapse into one

single one. The nonlinear mobility increases monotonically with the scaling parameter $f := FL/k_{\mathrm{B}}T$. Since, by definition, a decrease of $f$ means an increase of $k_{\mathrm{B}}T$, the nonlinear mobility decreases. The same behavior we have observed in the average particle current as a function of thermal noise, see Fig. 4.5. For very large values of the scaling parameter $f$ the nonlinear mobility approaches to the value 1, i.e., the deterministic limit.

The corresponding effective diffusion coefficient,

$$D_{\mathrm{eff}} = \frac{\displaystyle\int_0^1 \mathrm{d}x \int_{x-1}^{x} \mathrm{d}z\, \mathcal{N}(x,z,f)}{\left[\displaystyle\int_0^1 \mathrm{d}x\, I(x)\right]^3}\,, \tag{4.8a}$$

where the function $\mathcal{N}(x,z,f)$ is

$$\mathcal{N}(x,z,f) = \frac{D(z)}{D(x)}\, e^{[A(x)-A(z)]}\, [I(z)]^2\,. \tag{4.8b}$$

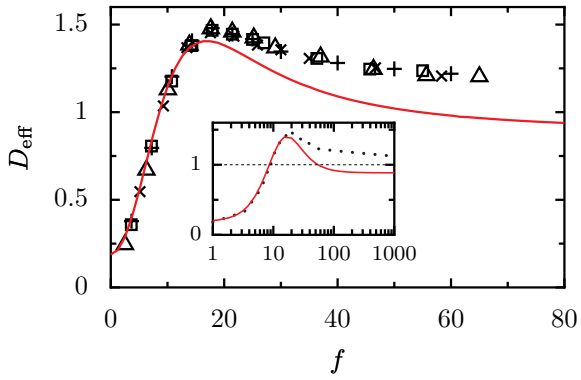


**Figure 4.10:** Same as in Fig. 4.9, but for the effective diffusion coefficient. The relative error of the simulation results is 0.1. The analytical results, Eq. (4.8), correspond to the solid lines. The inset depicts the long range behavior (the dotted line depicts the numerical results). In the limit $f \to \infty$, the numerical values for the scaled effective diffusion coefficient approach to the value 1 (dashed horizontal line).

Another interesting effect can be observed for the effective diffusion if considered as a function of the force $f$, see Fig. 4.10. Similar to that of non-linear mobility, all the curves in Fig. 4.5(b) collapse into one single one obeying the scaling behavior. Already the expression for the effective diffusion, Eq. (4.8), which follows rigorously from the one-dimensional kinetic equation displays a maximum as a function of $f$ which may even

exceed the bare diffusion, see Fig. 4.10. For $f \to \infty$ the effective diffusion coefficient approaches to the value 1. This behavior was already discussed in the previous section Fig. 4.7.

We can see from the figures (Fig. 4.9 and Fig. 4.10) that, the equilibrium assumption holds perfectly in confined structures where the entropic nature is more dominant. Transport characteristics can be tuned by a single scaling parameter $f$. The approximation method holds nicely up to a large value of this scaling parameter and it starts to fail as $f$ increases. For $f \to \infty$ the scaled nonlinear mobility and effective diffusion coefficient values different from the unity. The accuracy of the one-dimensional kinetic description worsens at large $f$ because the assumption of equilibration in the transverse direction, which supports the elimination of the transverse coordinate(s), fails if applied bias becomes too strong. The accuracy can substantially improve when the shape of the channel does not change too fast, i.e., when $|\omega'(x)|$ is smaller (smooth channels). We focus on this aspect in the following chapter.

## 4.4 Applications

An example in which the entropic nature of the transport becomes more evident is the case of micro and nanoporous materials such as zeolites. These materials exhibit a regular structure with channels of different width and well-defined geometry. This peculiar structure confers them an outstanding ability to act as molecular sieves that is currently exploited in chemically clean separation of mixtures, ion exchange and petrochemical cracking. Driven by their economic and scientific importance, these materials have been studied extensively experimentally and, more recently, by computer simulations. For instance, the diffusion has been found to decrease with temperature in some range of temperatures [58]; and the existence of an optimal value of the diffusion as a function of the temperature has also been observed [59]. In fact, the dependence of the effective diffusion coefficient on temperature reported in Ref. [59] behaves just as the one predicted here with Fig. 4.6. Finally, values of diffusion coefficients higher than the bulk, consistent with the phenomenon of diffusion enhancement predicted by our model have also been reported [60]. Our model thus accounts for all these behaviors and shows that they are not specific for a particular zeolites structure but rather arise from the entropic nature of the transport.

## 4.5 Summary

In this chapter, we have examined the one-dimensional kinetic description in the presence of an applied bias with an arbitrary 2D channel. First, we analyzed the diffusion process in the considered geometry by means of accurate numerical simulations and identified different transport behaviors. If the entropic nature is more dominant, we observe a

different temperature dependence which is quite unusual compared to a purely energetic system. The average particle current decreases upon increasing thermal noise strength $k_{\mathrm{B}}T$ which is in contrast to that we observe in purely energetic systems [75]. We observed an enhancement in the effective diffusion coefficient, similarly to the case of purely energetic systems, and notice that the maximum effective diffusion coefficient always exceeds the bulk diffusion constant.

We have compared these analytical predictions with numerical simulations for the transport coefficients, the non-linear mobility and effective diffusion coefficient, in terms of the proposed scaling parameter $f := FL/k_{\mathrm{B}}T$, noticing an excellent agreement up to a very large scaling parameter. We found out that tuning the scaling parameter $f$, we can effectively control the transport properties by modifying either the strength of the applied bias $F/F_{\mathrm{R}}$ or the thermal noise strength $k_{\mathrm{B}}T$, which is a genuine property of entropic systems. In the case of a purely energetic system, these quantities $F/F_{\mathrm{R}}$ and $k_{\mathrm{B}}T$ enter as independent parameters.

However, for a large scaling parameter $f$, the one-dimensional kinetic description starts to fail. This can be improved for instance, if the roughness of the channel is not very extreme, i.e for rather smooth channels the one-dimensional kinetic description provides a very good approximation to the transport for values of the external work of some tens of $k_{\mathrm{B}}\,T$'s. In fact, this is the range of energies relevant to most transport processes in biological systems [44, 49, 50, 56].

# 5

# Role of geometrical confinement

The applicability of the one-dimensional kinetic description for a fixed geometry with an arbitrary smoothness has been discussed in the previous chapter. The diffusion process in a given confined structure can be calculated accurately with the use of the one-dimensional kinetic equation for small scaling parameters $f$. In the range of moderate values of $f$ the one-dimensional kinetic description still leads to reasonable results but the relative error is slightly higher. On further increase in $f$ the one-dimensional kinetic description starts to fail, and in the regime of very large $f$ ($f \to \infty$) it cannot capture the adequate values for the non-linear mobility and effective diffusion coefficient.

The one-dimensional kinetic description has been constructed based on the equilibrium assumption along the transverse direction(s), which in principle holds for smooth channels, i.e., if the shape of the geometry does not change too fast. However, the use of a spatially dependent diffusion coefficient may extend the applicability of the one-dimensional kinetic description to moderately rough channels.

In the modified Fick-Jacobs description for the derivation of an effective one-dimensional kinetic equation, given by Zwanzig [20], the slope of the channel wall is the only parameter which can control applicability of the one-dimensional description. However, the bottleneck width at the channel opening also plays an important role. As we have discussed in chap 1 (Fig. 1.5) the electrical signature of the macromolecules or individual species may be widely effected by the width of the bottleneck opening of the nanopore [14, 15, 48, 49]. In fact, for narrow openings the macromolecule could jam *in front* of the bottleneck and may not pass through the pore [48, 49]. This implies that the geometric structure and degree of confinement play an important role in the accuracy and applicability of the one-dimensional kinetic description. Therefore, we discuss the impact of the slope of the geometry and the bottleneck width on the transport characteristics in more detail in the following.

## 5.1 Geometric scaling of the structure

The shape of the geometry under consideration, is given by the function

$$\omega(x) = a\sin(2\pi x) + b\,, \tag{5.1}$$

The parameters $a$ and $b$ decide the maximal width $2w_{\max}$ and minimal bottleneck width $2w_{\min}$ of the channel. In addition, $a$ controls the slope of the geometry since it enters in the first derivative of $\omega(x)$.

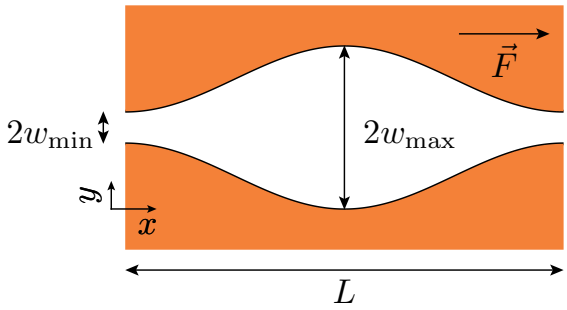


**Figure 5.1:** Geometry of a single channel with the periodicity $L$, where the shape of the structure is defined by Eq. (5.1). In the geometry, $w_{\max}$ defines the maximal half-width and $w_{\min}$ defines the minimal bottleneck half-width. The constant applied bias $F$ acts along the length of the channel.

- minimal bottleneck half-width : $w_{\min} = b - a\,, \quad b > a$
- maximal half-width : $w_{\max} = b + a$

which implies

$$a = \frac{w_{\max} - w_{\min}}{2} \quad \text{and} \quad b = \frac{w_{\max} + w_{\min}}{2}\,.$$

Note that, these widths are scaled with the period length $L$. We can rewrite the expression, Eq. (5.1), in terms of $w_{\max}$ and $w_{\min}$ reading

$$\omega(x) = \frac{w_{\max} - w_{\min}}{2}\sin(2\pi x) + \frac{w_{\max} + w_{\min}}{2}\,. \tag{5.2}$$

The width ratio [1], being a dimensionless constant, is defined as the ratio of minimal bottleneck half width to the maximal half-width, and reads

$$\epsilon = \frac{w_{\min}}{w_{\max}}\,, \qquad 0 < \epsilon \leq 1\,. \tag{5.3}$$

[1]Note: Here, the symbol $\epsilon$ has nothing to do with the geometric series in Eq. (3.16) and Eq. (3.18)

The case $w_{\min} = 0$, which implies $\epsilon = 0$, refers to a closed single cell, and $w_{\min} = w_{\max}$, implying $\epsilon = 1$, refers to a flat channel. The general form of the geometric function in terms of the maximal half-width $w_{\max}$ and the width ratio $\epsilon$ reads

$$\omega(x) = \frac{w_{\max}}{2}(1-\epsilon)\left\{\sin(2\pi x) + \frac{1+\epsilon}{1-\epsilon}\right\}. \tag{5.4}$$

Thus, by altering $w_{\max}$ and $\epsilon$ in the above expression for the geometric function, the confinement of the geometry can be varied. Therefore, we modify $w_{\max}$ and $\epsilon$, systematically, by considering two cases: Geometric scaling I and Geometric scaling II. In the former case, we modify the maximal half-width $w_{\max}$ by keeping the width ratio $\epsilon$ as constant, i.e., since $\epsilon = w_{\min}/w_{\max}$ we modify the minimal bottleneck half-width $w_{\min}$ as well in order to maintain $\epsilon$ value constant. In the later case, we change the width ratio $\epsilon$ by keeping the maximal half-width $w_{\max}$ constant.

### 5.1.1 Geometric scaling I

In Geometric scaling I, lowering $w_{\max}$ makes the geometry smooth and the applicability of the one-dimensional description may improve.

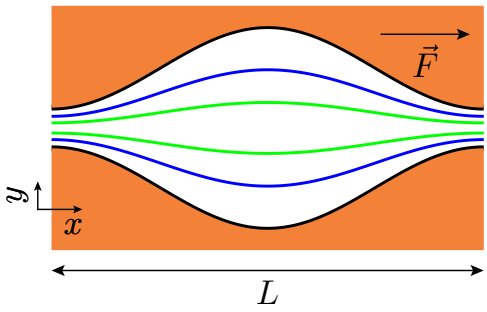


**Figure 5.2:** Geometry of a single channel with the periodicity $L$, and for different maximal half-widths $w_{\max}$ and for a constant width ratio $\epsilon$ (Eq. (5.3)). The shape of the structure is defined by Eq. (5.4). The constant applied bias $F$ acts along the length of the channel.

Fig. 5.2 illustrates the considered geometric structure with different maximal half-widths $w_{\max}$, where the width ratio $\epsilon$ remaining constant. Note that, a smaller $w_{\max}$ corresponds to smoother channel (less confined geometry) and larger $w_{\max}$ corresponds to rough channel (more confined geometry).

### Transport characteristics

Transport characteristics for Geometric scaling I with different smoothness are analyzed in the following.

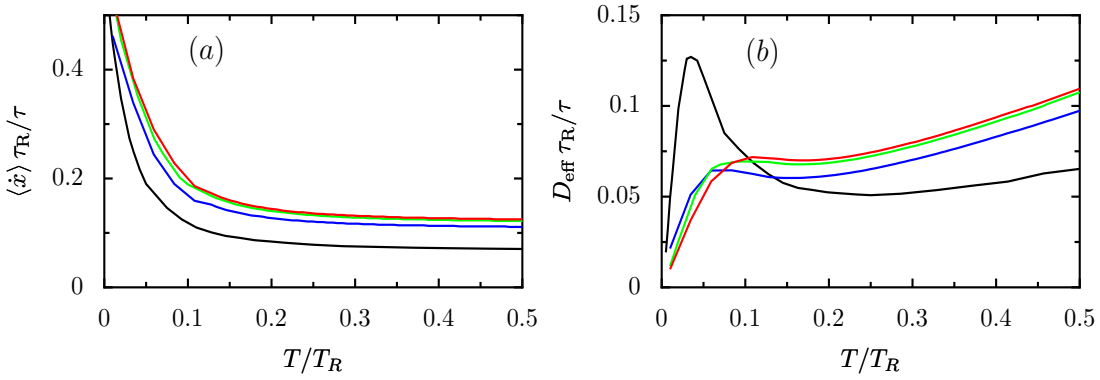


**Figure 5.3:** Numerically determined temperature dependence of the average particle current (a) and the effective diffusion coefficient (b) for the two-dimensional channel with the shape defined by Eq. (5.4), at the force value: $F/F_{\rm R} = 0.628$ and for different smoothness of the channel, i.e., for different values of the maximal half-width $w_{\rm max}$. Black line: $w_{\rm max} = 2.02$; blue line: $w_{\rm max} = 2.02/\pi$; green line: $w_{\rm max} = 2.02/2\pi$; red line: $w_{\rm max} = 2.02/3\pi$.

From Fig. 5.3 we can extract the influence of geometrical smoothness and also the impact of the system's entropic nature on transport characteristics. Since temperature controls the strength of entropic potential, the average particle current decreases upon increasing temperature, Fig. 5.3(a). The effective diffusion coefficient exhibits a striking peak over a range of temperatures, Fig. 5.3(b). As the geometry smoothness increases, i.e., lowering $w_{\rm max}$, the strength of entropic potential reduces. The influence of geometrical roughness on transport characteristics becomes more visible when the behavior of the effective diffusion coefficient as a function of thermal noise is considered. In rough structures, referring to large values of maximal half-width $w_{\rm max}$, the effective diffusion coefficient is greatly enhanced. Another important feature we can extract from Fig. 5.3(b) is that over a range of temperatures the effective diffusion coefficient increases upon decreasing temperature, and this feature is more visible in rough structures.

Fig. 5.4 depicts the comparison between results obtained from the numerical simulations and analytical predictions for the non-linear mobility and effective diffusion coefficient, as a function of the scaling parameter $f$, for different smoothness of the channel. The qualitative behavior of non-linear mobility, Fig. 5.4(a), is same for any value of maximal half-width $w_{\rm max}$. But the range of validity, in terms of the scaling parameter $f$, in which the numerical results and the analytical predictions agree, varies by changing $w_{\rm max}$. For $w_{\rm max} = 2.02$ the range of validity is up to the scaling parameter value of $\sim 10$ and for $w_{\rm max} = 2.02/2\pi$ it is $\sim 50$. The value increases further more by

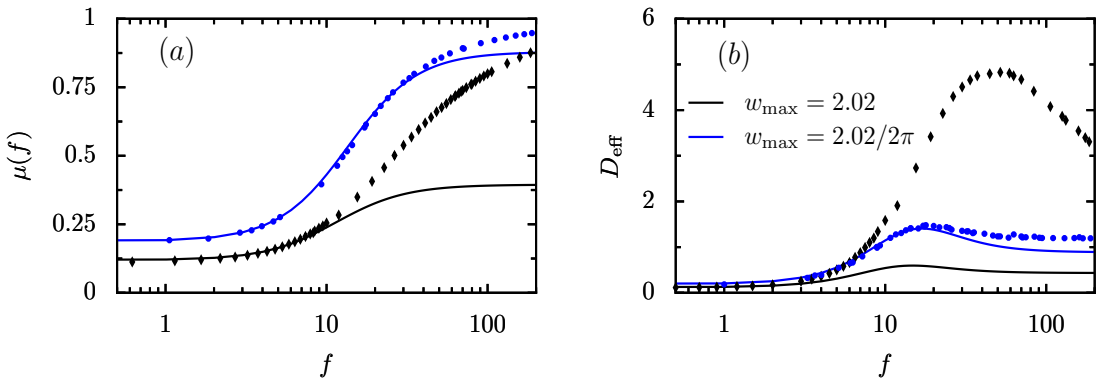


**Figure 5.4:** Numerically simulated (symbols) and analytically calculated (lines) dependence of the nonlinear mobility $\mu(f)$ *vs.* the scaling parameter $f$ is depicted in (a) for the two-dimensional channel with the shape defined by Eq. (5.4), with different maximal half-widths $w_{\max}$. The corresponding scaled effective diffusion coefficient as a function of the scaling parameter $f$ for the same values of $w_{\max}$ is depicted in (b).

decreasing $w_{\max}$ value.

The effective diffusion coefficient, Fig. 5.4(b), exhibits a striking peak over a range of scaling parameter values. This characteristic feature has been encountered before in chapter 4 (see Fig. 4.7 and Fig. 4.10). The main observation from Fig. 5.4(b) is that for large values of maximal half-width $w_{\max}$ the effective diffusion is enhanced, and exceeds the bulk diffusion constant. This phenomena can be observed also in the case of purely energetic systems [76, 77, 79, 81]. In Fig. 5.4(b) the maximum of effective diffusion reduces upon increasing the smoothness of the geometry.

From Fig. 5.4 we can conclude that the one-dimensional description holds nicely for rather smooth channels, and the validity range depends on the quantity we consider. It is due to the fact that the non-linear mobility corresponds to the first moment in $x$ and effective diffusion coefficient corresponds to the second moment in $x$.

### Péclet number and $Q$ factor

In order to obtain more information of entropic nature of the geometry on transport characteristics we consider a quantity called Péclet number $P_e$ [87–89] expressed in terms of the scaling parameter $f = FL/k_{\mathrm{B}}T$. Originally, the Péclet number was used in the context of heat transfer in fluids, and defined as the ratio of heat transfer in horizontal direction of the fluid surface to the diffusion [87–89]. Large Péclet numbers correspond to ordered and directed motion whereas small Péclet numbers correspond to irregular motion. For the considered system the Péclet number in terms of scaling parameter $f$ reads:

$$P_e = \frac{\langle \dot{x} \rangle}{D_{eff}} = \frac{\mu}{D_{eff}} f \,. \tag{5.5}$$

The inverse of Péclet number is called $Q-$ factor (in the context of chromatography, it's called retention parameter) and is defined as

$$Q = \frac{2}{P_e} \,. \tag{5.6}$$

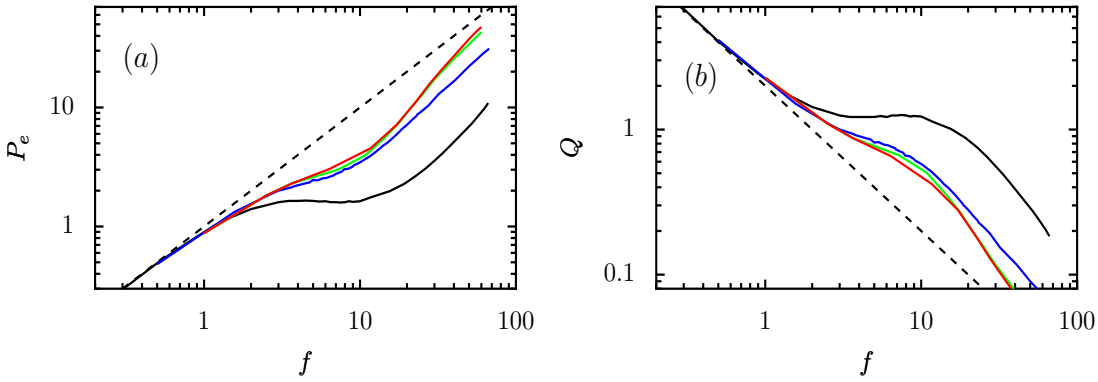


**Figure 5.5:** Numerically determined the Péclet number $P_e$, panel (a), and $Q-$factor, panel (b), as a function of the scaling parameter $f$ for the two-dimensional channel with the shape defined by Eq. (5.4), with different maximal half-widths $w_{\max}$. Black line: $w_{\max} = 2.02$; blue line: $w_{\max} = 2.02/\pi$; green line: $w_{\max} = 2.02/2\pi$; red line: $w_{\max} = 2.02/3\pi$. The behaviors of the Péclet number and $Q-$factor are shown in (a) and (b), respectively, in dashed black line for the flat channel geometry.

Fig. 5.5 depicts the influence of confinement of the geometry when compared to a flat channel. As one could expect, in the case of a more confined geometry, i.e., large values of $w_{\max}$, the non-linear mobility $\mu$ is less, which leads to an increase of $Q$. For smooth channels, corresponding to small values of maximal half-width $w_{\max}$, system exhibits better transport close to the free case, correspond to the dynamics in a flat geometry. In this case the irregular nature of the Brownian particles is less leads to small diffusion. An interesting feature we can observe from the behavior of these quantities is that, over a wide range of scaling parameters $f = FL/k_{\mathrm{B}}T$ there is a decrease in $Q$ (and an increase in $P_e$) upon increasing noise strength $k_{\mathrm{B}}T$. This corresponds to a decrease in the effective diffusion coefficient upon increasing temperature (this we can see clearly in Fig. 5.3(b)), a feature which is rather obvious in more confined structures.

### 5.1.2 Geometric scaling II

In the analysis for a given geometric structure the ratio of the maximal width to the minimal bottleneck width has been maintained as a constant so far whereas in the following, this ratio is subject to alternation, i.e., we fix the maximal width of the geometry to the value 2.02 and vary the minimal bottleneck width as shown in Fig. 5.6.

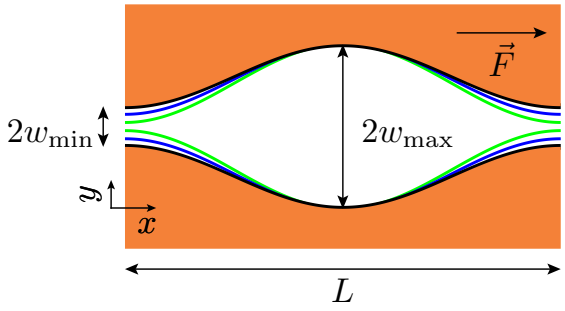


**Figure 5.6:** Geometry of a single channel with the periodicity $L$, for different minimal bottleneck half-widths $w_{\min}$ and at a constant maximal half-width $w_{\max}$. The shape of the structure is defined by Eq. (5.4). The constant applied bias $F$ acts along the length of the channel.

Fig. 5.6 illustrates the geometric structure with different values for the width ratio $\epsilon$ and a constant maximal width $2\,w_{\max}$. Small $\epsilon$ correspond to a narrow bottleneck width of the channel opening, and vice versa. $\epsilon = 1.0$ corresponds to the flat channel geometry.

#### Transport characteristics

An increase in the width of the bottleneck of the geometry, while the maximal width of the channel kept constant, reduces the strength of the entropic nature of the system.

Fig. 5.7 shows how the influence of entropic barriers reduce systematically as we increase the bottleneck width of the geometry. The influence of entropic nature of the system is high for small values of the width ratio $\epsilon$ leading to a decrease in the average particle current, and the effective diffusion coefficient exhibits a peculiar behavior. A similar behavior has been encountered also in Geometric scaling I (Fig. 5.3). The strength of entropic nature of the system starts to decrease upon increasing the value of the width ratio $\epsilon$. At moderate values of $\epsilon$ we can still observe a decrease in the average particle current but the peculiarity in the diffusional behavior, i.e., increase in the effective diffusion coefficient upon decreasing the thermal noise, starts to vanish. On further increase in the width ratio $\epsilon$, i.e., moving to a flat channel geometry, the influence of entropic barriers is almost negligible. The average particle current tends to reach the value of applied bias ($\langle \dot{x} \rangle \to F$) for any value of noise strength, see the black dotted

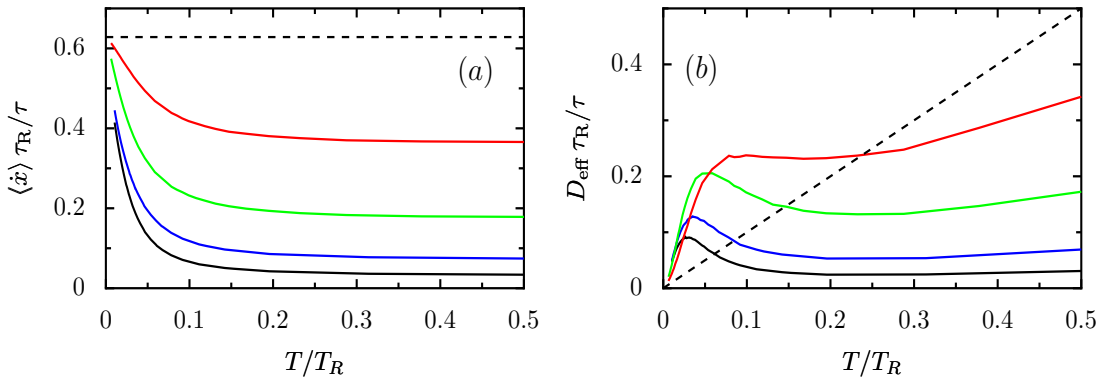


**Figure 5.7:** Numerically determined temperature dependence of the average particle current (a) and effective diffusion coefficient (b) for a symmetric two-dimensional channel with the shape defined by Eq. (5.4) at the force value $F/F_{\rm R} = 0.628$, and for various values of the width ratio $\epsilon$. Red line : $\epsilon = 0.3$ ; green line : $\epsilon = 0.074$ ; blue line : $\epsilon = 0.01$ ; black line : $\epsilon = 0.0025$. The behaviors of the average particle current and effective diffusion coefficient are shown in (a) and (b), respectively, in dashed black line for the flat channel geometry (i.e., for the width ratio $\epsilon = 1$).

line in Fig. 5.7(a). The effective diffusion coefficient tends to reach the bare diffusion constant.

Fig. 5.8 shows the behavior of the scaled nonlinear mobility and the effective diffusion coefficient as a function of the scaling parameter $f$ for various values of the width ratio $\epsilon$. For a very small value of $\epsilon$, a less number of Brownian particles diffuse to the neighboring cells, which results in reduced mobility and also less effective diffusion. The non-linear mobility increases with the width ratio $\epsilon$ (see Fig. 5.8(a)). The effective diffusion coefficient also increases due to hindering of particles in every cell which leads to a border distribution in the steady-state probability density. System approaches the flat channel geometry when the value of $\epsilon$ is increases further. In that case, the value of the non linear mobility tends to reach one, and the effective diffusion would reach the bare diffusion constant, for any value of the scaling parameter $f$.

### Péclet number and $Q$ factor

Fig. 5.9 shows the behavior's of the Péclet number and the $Q$ factor for the considered geometry with different bottleneck widths, as a function of scaling parameter $f$. The peak value in $Q$ factor (correspondingly, the optimal value in Péclet number) varies as the value of the width ratio $\epsilon$ increases, see Fig. 5.9. We didn't encounter this feature in the previous case of Geometric scaling I, but we are going to discuss it in more detail in the following section, comparing the behavior of the effective diffusion coefficient in both scenarios Geometric scaling I and Geometric scaling II.

Interestingly, in Geometric scaling II, very small bottleneck openings lead to less

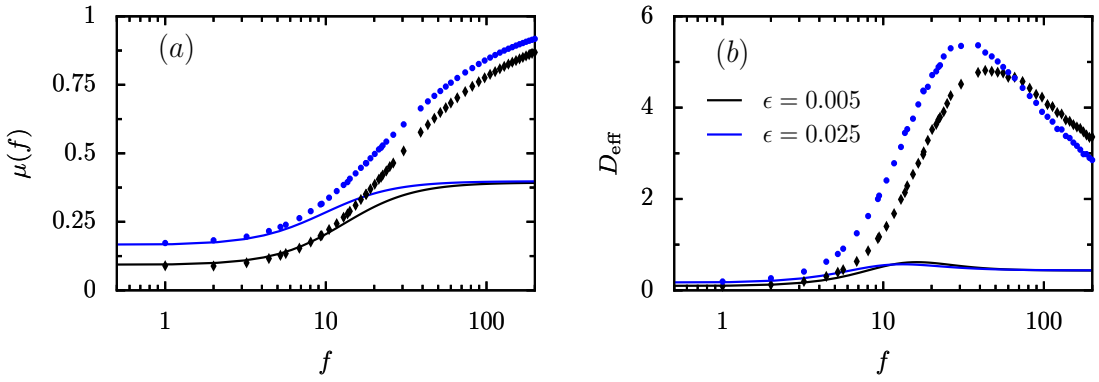


**Figure 5.8:** Numerically simulated (symbols) and analytically calculated (lines) dependence of the nonlinear mobility $\mu(f)$ as a function of the scaling parameter $f$ is depicted in (a) for the two-dimensional channel with the shape defined by Eq. (5.4), and for various values of the width ratio $\epsilon$. The corresponding scaled effective diffusion coefficient as a function of the scaling parameter $f$ for the same $\epsilon$ values is depicted in (b).

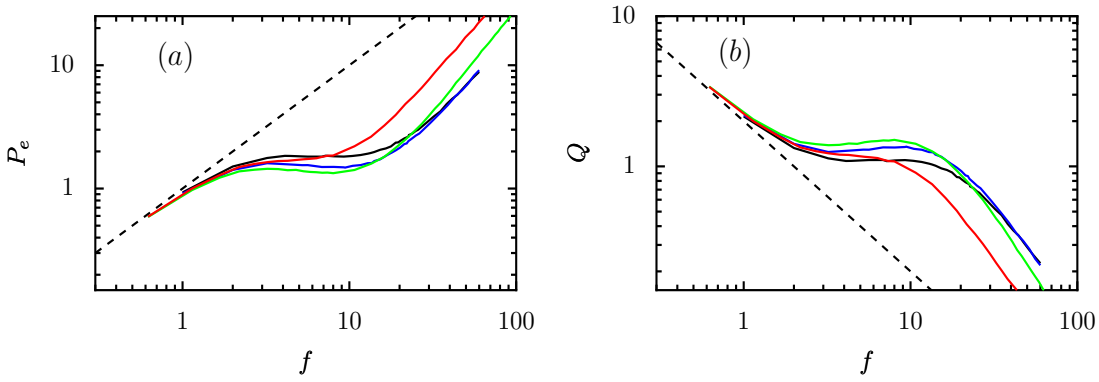


**Figure 5.9:** Numerically determined the Péclet number as a function of the scaling parameter $f$ for different values of the width ratio $\epsilon$ is depicted in (a) for the two-dimensional channel with the shape defined by Eq. (5.4), and for various values of the width ratio $\epsilon$. Solid black line : $\epsilon = 0.0025$; solid blue line : $\epsilon = 0.01$; solid green line : $\epsilon = 0.074$; solid red line : $\epsilon = 0.3$. The corresponding $Q$ factor as a function of scaling parameter $f$ for the same values $\epsilon$ depicted in (b). The behaviors of the Péclet number and $Q-$factor are shown in (a) and (b), respectively, in dashed black line for the flat channel geometry. (i.e., for the width ratio $\epsilon = 1$).

diffusion, lower values of $Q$ and higher Péclet numbers. This suggests that system may exhibit a better transport. An increase of the width ratio $\epsilon$ spoils the quality of transport by increasing $Q$ and decreasing Péclet number. On further increase of the width ratio $\epsilon$ the quality of transport is improved again, see Fig. 5.9. Thus, by varying the width ratio $\epsilon$ one can encounter different transport regimes, i.e., at a particular scaling parameter $f$, by changing $\epsilon$ one can tune the quality of transport, see Fig. 5.9. However, in practice, it is the other way around: The optimal transport regime is reached via controlling $f$ while $\epsilon$ is given for a specific system. This feature is slightly visible in Fig. 5.9 and it is even more pronounced in very rough geometries, see Fig. 5.5.

## 5.2 Enhancement of the effective diffusion in confined geometries

The diffusion process in Geometric scaling II is quite different from that in Geometric scaling I. In order to gain a deeper understanding, we are analyzing the diffusion behaviors in both scenarios in the following.

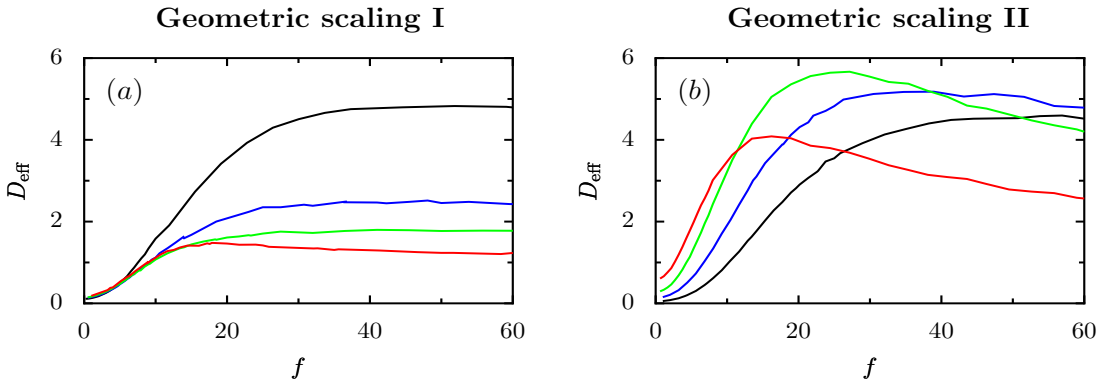


**Figure 5.10:** Numerically determined the behavior of the effective diffusion coefficient in Geometric scaling I (a) and in Geometric scaling II (b) as a function of the scaling parameter $f$. Panel (a) corresponds to Geometric scaling I with different maximal half-widths. Black line: $w_{\max} = 2.02$; Blue line: $w_{\max} = 2.02/2.0$; Green line: $w_{\max} = 2.02/3.0$; Red line: $w_{\max} = 2.02/2\pi$. Panel (b) corresponds to Geometric scaling II for different values of the width ratio $\epsilon$. Black line: $\epsilon = 0.025$; Blue line: $\epsilon = 0.01$; Green line: $\epsilon = 0.075$; Red line: $\epsilon = 0.3$.

From Fig. 5.10 we can observe that the diffusion behavior is quite different in each geometrical structure. It may depend on many factors such as the slope of the structure, the width of the channel opening, the strength of the applied bias, and thermal noise present in the system. The maximum effective diffusion a geometry could exhibit depends on both the maximal half-width and the bottleneck opening whereas the maximum can appear at different scaling parameter values. In Geometric scaling I, the

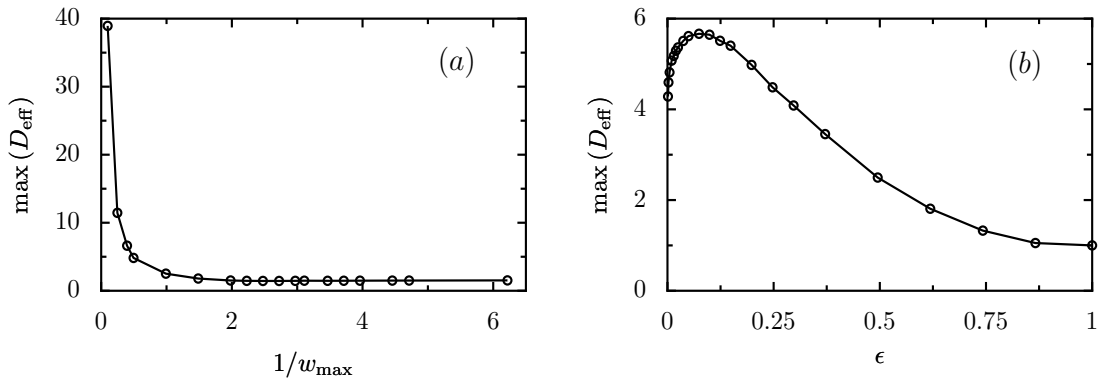


**Figure 5.11:** Numerically determined the behavior of the maximum effective diffusion coefficient as a function of the maximal half-width in Geometric scaling I (a), and in Geometric scaling II (b) for different values of the width ratio $\epsilon$.

maximum effective diffusion coefficient (the peak value in Fig. 5.10(a)) decreases as the maximal half-width decreasing. In Geometric scaling II, the maximum effective diffusion coefficient (the peak value in Fig. 5.10(b)) exhibits a peculiar behavior. Initially, it increases by increasing the width ratio $\epsilon$, but then it starts to decrease upon further increase of $\epsilon$. There is an optimal value where the system exhibits an higher effective diffusion coefficient. We can extract this maximum value (e.g. from Fig. 5.10), for both Geometric scaling I and Geometric scaling II.

Fig. 5.11(a) shows the maximum effective diffusion coefficient as a function of the maximal half-width in Geometric scaling I. The maximum value of the effective diffusion coefficient (peak value) decreases monotonically as the maximal half-width of the geometry decreases, i.e., by increasing the smoothness of the geometry, (see Fig. 5.11(a)). This is due to the decreasing influence of entropic barriers upon an increase of geometry smoothness. Thus, the hindrance of particles in every cell during the propagation decreases leading a decrease in the effective diffusion coefficient.

Fig. 5.11(b) shows the maximum effective diffusion exhibited in Geometric scaling II for different values of the width ratio $\epsilon$. In the range of $\epsilon = [0, 1]$, the maximum effective diffusion coefficient initially increases, reaches the maximum, then starts to decrease and tends to approach unity which corresponds to the bare diffusion constant. The effective diffusion peak is found at the width ratio $\epsilon \sim 0.075$ (see Fig. 5.11). In order to understand this nature we should keep in mind that we are moving from a closed system, to a confined system and finally reaching a flat channel geometry. The described above can then be understood as follows: For a closed system with zero bottleneck widths, particles are confined within a single cell irrespectively of the strength of the applied bias. In the steady-state limit both the average particle current and the effective diffusion coefficient vanish. Increasing the bottleneck width allows movement of particles from one cell to

an other which leads to an increase in the average particle current (correspondingly the non-linear mobility) and also the effective diffusion. This increase in the effective diffusion, due to the fact that some portion of particles get stuck at the bottlenecks and lag behind those are rapidly moved to the other cells, results in a broad distribution over many number of cells with a large half-width. On further increase in the bottleneck width of the geometry which means that we move towards a flat channel geometry, the influence of entropic barriers vanishes. The maximum effective diffusion coefficient starts to decrease, tending to approach the value of the bare diffusion constant, and the non-linear mobility increases, tending to unity.

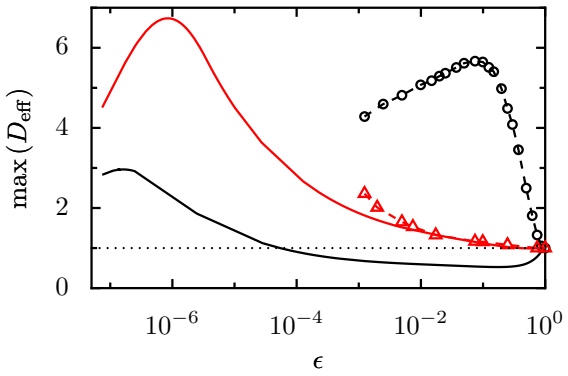


**Figure 5.12:** The behavior of the maximum effective diffusion coefficient as a function of the width ratio $\epsilon$ at two different values of the maximal half-width $w_{\max}$. The solid black line corresponds to analytical prediction for $w_{\max} = 2.02$, the solid red line corresponds to analytical prediction for $w_{\max} = 2.02/2\pi$.

The qualitative feature of raising and falling down of the maximum effective diffusion can be captured analytically. Fig. 5.12 shows the maximum effective diffusion coefficient for different values of the width ratio $\epsilon$ with different maximal half-widths of the geometry (see figure caption). The applicability of the one-dimensional kinetic description to very rough structures is limited, but the qualitative behavior of the maximum effective diffusion, raising and falling down, can be observed in any constrained channel, irrespectively of the smoothness.

Capturing the peak of maximum effective diffusion is not accessible, numerically, for our choice of $w_{\max} = 2.02/2\pi$. The lowest accessible value of the width ratio $\epsilon$ is 0.001, which means the bottleneck width is 1000 times smaller than the maximal width of the channel, and any value beyond it is quite hard to reach. The numerical value of the position of the maximum effective diffusion peak (for $w_{\max} = 2.02$) is found at a different value of the width ratio $\epsilon$ and is different from the analytical prediction. This is of course due to the failure of the one-dimensional kinetic description for very rough channels. For rather smooth channels, the agreement between the analytics and the numerics is better, see Fig. 5.12.

## 5.3 Summary

In this chapter, the geometric structure of a confined system has been modified in two different ways in order to vary the degree of confinement, named Geometric scaling I and Geometric scaling II. The transport characteristics have been analyzed in both cases, and the applicability of the one-dimensional kinetic description has been observed. In Geometric scaling I, as the channel maximal half-width decreases, the range of the applicability of our one-dimensional kinetic description increases. In Geometric scaling II, for a fixed maximal half-width of the geometry, the range of applicability is just moderate for small values of the width ratio $\epsilon$ corresponding to small bottleneck widths, and the validity range decreases upon increasing the width ratio $\epsilon$ value.

We have encountered that the diffusion process is different in Geometric scaling I and Geometric scaling II. In Geometric scaling I, as the maximal half-width of the geometry decreases the particle diffusion decreases. In Geometric scaling II, as we move from a very confined geometry to a flat channel geometry the diffusion process exhibits a peculiar behavior.

In both geometric scalings, during the crossover region from a purely energetic regime to entropy dominated regime, optimal transport could be observed, suggesting that by increasing $k_{\mathrm{B}}T$ the system may exhibit better transport, i.e., larger Péclet number or smaller $Q-$ factor. Tuning the parameters $\epsilon$, $k_{\mathrm{B}}T$ and the maximal half-width $w_{\max}$, one can effectively regulate the transport characteristics in these confined geometries. However, in general, controlling the width ratio $\epsilon$ and the maximal half-width $w_{\max}$ of the geometry may not be feasible, but, tuning the scaling parameter $f$ one can arrive at an optimal transport regime.

# 6

# The hypothesis of equilibration and validity conditions

Diffusion processes in confined structures in the range of small applied bias can be calculated accurately with the use of the one-dimensional kinetic equation. The applicability of the one-dimensional kinetic equation increases as the smoothness of the geometry increases and it is more accurate in geometries with small bottleneck openings. The one-dimensional kinetic description fails at very high values of the scaling parameter $f$. On the other hand, it doesn't make any sense to apply the approximative method which is based on an assumption that demands an uniform distribution of the particles along the transverse direction(s) of the geometric structure at large $f$ values. In this regime the impact of the geometrical constraints is almost negligible. Therefore, if we can construct a tailored criteria (in other words the limits of applicability) for the one-dimensional kinetic description, in terms of the applied bias, smoothness and the bottleneck width of the channel then, we can apply it more safely to calculate the transport characteristics in confined systems.

Since, the applicability and accuracy of the one-dimensional kinetic description depends on the smoothness and the bottleneck width of the channel, in the following we are examining more deeply the diffusion processes in both Geometric scaling I and Geometric scaling II.

## 6.1 Equilibrium conditions in Geometric scaling I

Here, we consider a two-dimensional periodic structure with different maximal half-widths ($w_{\max}$) and a constant width ratio $\epsilon$, i.e., Geometric scaling I (Fig. 5.2). First, we take a rather rough structure, and analyze the steady-state distribution of the particles inside the cell at different values of the scaling parameter $f$. Later, we fix the scaling parameter $f$ to a moderate value, and vary the maximal half-width $w_{\max}$ of the geometry to analyze the steady-state distributions.

### 6.1.1 Fixed channel geometry

In this section, we examine the diffusion process in a geometry with a fixed maximal half-width $w_{\max}$ and a fixed width ratio $\epsilon$. Shape of the geometrical structure is defined by the function

$$\omega(x) = \frac{w_{\max}}{2}\,(1-\epsilon)\,\left\{\sin(2\pi x) + \frac{1+\epsilon}{1-\epsilon}\right\}\,.$$

#### Steady-state particle distribution

Here, we check the steady-state distribution of the particles at different scaling parameter values. During the evolution process, at a given circumstance, each particle may cross many number of cells, to reach the steady-state. Since, the channel is periodic, for the convenience, we map the positions of all the particles into a single cell.

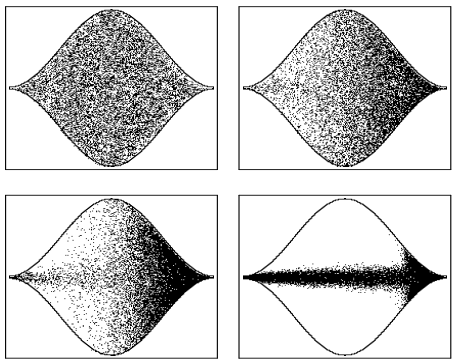

**Figure 6.1:** Steady-state particle distribution mapped into a single cell of a 2D channel with the maximal half-width $w_{\max} = 2.02$, for the width ratio $\epsilon = 101$ and for different values of the scaling parameter $f$. Upper left panel: $f = 0.2$; upper right panel: $f = 3.0$; lower left panel: $f = 7.0$; lower right panel: $f = 50$.

Fig. 6.1 shows the steady-state distribution of the Brownian particles mapped into a single cell, in a rough channel ($w_{\max} = 2.02$) at different values of the scaling parameter $f$. At small scaling parameter values, particles distribute uniformly along the transverse direction at every position of $x$ along the channel satisfying the equilibrium assumption (see upper left panel in Fig. 6.1). Therefore, for this parameter range, the one-dimensional description is expected to hold nicely. With increasing the scaling parameter $f$, there is still a large number of particles which could exhibit almost an uniform

distribution in the transverse direction to satisfy the equilibrium assumption but may be with some small error (see upper right panel in Fig. 6.1).

On further increase of the scaling parameter $f$ the Brownian particles tend to focus at the middle of the channel because the work done on the particles is greater than the thermal noise present in the system, which leads a spread out in the longitudinal direction (see lower left panel in Fig. 6.1). For very high values of the scaling parameter $f$, the Brownian particles are almost focused at the middle of the channel and obtaining an uniform distribution along the transverse direction is then not possible. At this stage, the equilibrium assumption completely fails (see lower right panel in Fig. 6.1).

We can observe another feature from Fig. 6.1, namely, the accumulation of the Brownian particles at the exit of the cell. This feature can be observed for moderate to large scaling parameter values. This accumulation is due to, if a Brownian particle enters a cell through the bottleneck, the applied bias tries to drag the particle in it's direction (a straight line motion) and at the same time the thermal noise tries to deviate the straight line motion by giving freedom to the Brownian particle. Therefore, as a result the Brownian particle stick to the channel wall at the exit of the cell, and it takes some time to move to the next cell. This behavior play an important role in the diffusion process and results in enhancement of the effective diffusion coefficient. Practically, this feature is more pronounced in rough channels due to high confinement.

For scaling parameters $f \to \infty$, the Brownian particles would not feel any boundaries. It is then a direct transport and the accumulation at the exit of the channel practically disappears. The later is true in any kind of channel whether it is rough or smooth. A more detailed analysis on distribution of the Brownian particles could be provided by checking the normalized steady-state probability distributions in the transverse and in the channel directions.

#### Probability distribution along the transverse direction

In this section we analyze the normalized steady-state probability distribution in the transverse direction at a given $x-$ position. The expression is given by

$$P_x^{\mathrm{st}}(y) := \frac{P^{\mathrm{st}}(x,y)}{\displaystyle\int_{-\omega(x)}^{\omega(x)} \mathrm{d}y\, P^{\mathrm{st}}(x,y)}\,, \tag{6.1}$$

where $P^{\mathrm{st}}(x,y)$ is the 2D steady-state probability distribution and $P_x^{\mathrm{st}}(y)$ is the local distribution of the Brownian particles, at a given $x$, between the lower $(-\omega(x))$ and upper boundary $(\omega(x))$.

Fig. 6.2 depicts the steady-state probability distribution of the Brownian particles at three different locations along the channel, i.e., at $x = 0.2$, $x = 0.5$ and $x = 0.8$, for

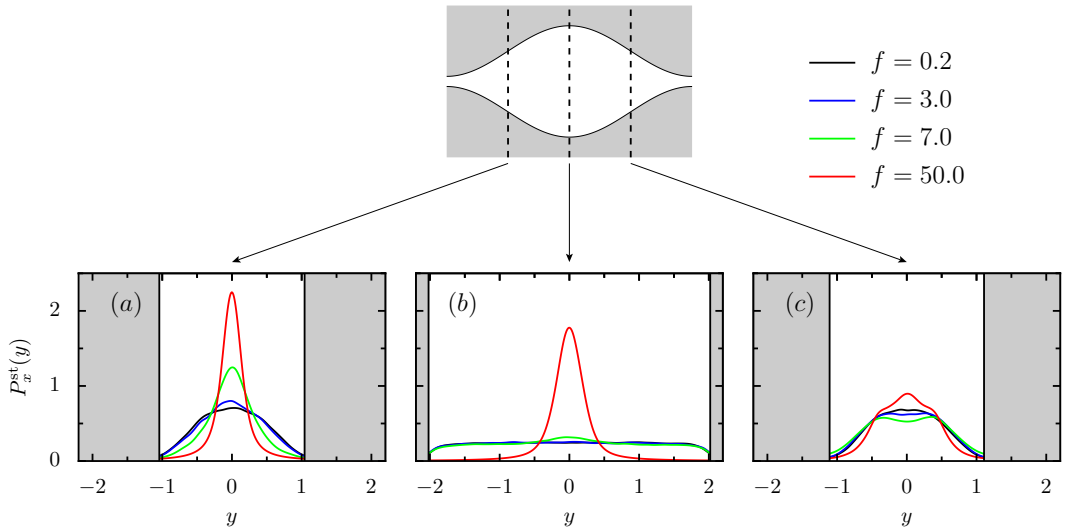


**Figure 6.2:** Normalized steady-state probability distribution of the particles in the $y-$ direction (see Eq. (6.1)) for different values of the scaling parameter $f$, at different positions along the length of a 2D channel with the maximal half-width $w_{\max} = 2.02$ and the width ratio $\epsilon = 101$. $x = 0.2$ (panel (a)), $x = 0.5$ (panel (b)) and $x = 0.8$ (panel (c)). The grey regions indicate the outside of the channel.

different values of the scaling parameter $f$. At $x = 0.5$ where $\omega'(x) = 0$ (at the middle of the channel) the $P_x^{\mathrm{st}}(y)$ is flat, for small values of $f$, indicating a perfect uniform distribution (box distribution) in the transverse direction. However, at $x = 0.2$ and $x = 0.8$, the system is not completely equilibrated and $P_x^{\mathrm{st}}(y)$ is bell shaped. Notice that, for $x = 0.2$ and $x = 0.8$, the distributions are very much similar for small values of $f$, but as $f$ value increases the distributions are different, corroborating that the equilibration depends on $\omega'(x)^2$, and not just on $\omega'(x)$.

For moderate values of the scaling parameter $f$, as we observed in Fig. 6.1, a perfect uniform distribution along the transverse direction is quite hard and the particles tend to gather at the middle of the channel resulting in a bell shape distribution. At very large force strengths, particles concentrate along the axis of the channel. In this situation, the assumption of equilibration along the transverse direction fails completely. The Brownian particles would only feel the presence of the boundaries when they are close to the bottlenecks. Hence, in the limit of very large force values, the influence of the entropic barriers practically disappears. In this limit, the correction in the diffusion coefficient leading to a spatial dependency, i.e., $D(x)$, overestimates the influence of the entropic barriers.

### Probability distribution along the channel direction

In this section we analyze the normalized steady-state probability distribution of the particles in the channel direction. The expression is given by

$$P^{\mathrm{st}}(x) := \frac{\int_{-\omega(x)}^{\omega(x)} \mathrm{d}y P^{\mathrm{st}}(x,y)}{\int_0^L \mathrm{d}x \int_{-\omega(x)}^{\omega(x)} \mathrm{d}y\, P^{\mathrm{st}}(x,y)}, \tag{6.2}$$

where $P^{\mathrm{st}}(x,y)$ is the 2D steady-state probability distribution and $P^{\mathrm{st}}(x)$ is the normalized marginal steady-state distribution over a period length.

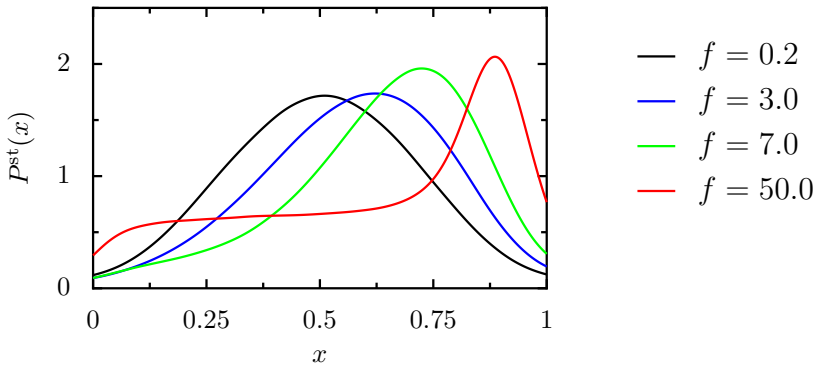


**Figure 6.3:** Normalized steady-state probability distribution of the particles along the length of the channel $P^{\mathrm{st}}(x)$ for different values of the scaling parameter $f$. Here, the channel maximal half-width $w_{\max} = 2.02$ and the width ratio $\epsilon = 101$.

Fig. 6.3 depicts the normalized steady-state probability distribution of the Brownian particles in the $x$-direction at various scaling parameter values. At very low values of the scaling parameter $f$, particles are uniformly distributed over the period length and the normalized probability distribution $P^{\mathrm{st}}(x)$ scales with the cross-section of the channel. On increasing the scaling parameter $f$, the distribution $P^{\mathrm{st}}(x)$ exhibits an uneven shape and the mean position of $P^{\mathrm{st}}(x)$ starts to shift towards the exit of the cell. For large values of the scaling parameter $f$, particles accumulate *in front* of the bottleneck. A similar behavior we have encountered in Fig. 6.1. On further increase in $f$, $P^{\mathrm{st}}(x)$ is almost constant over a wide range of $x-$ values, indicating a minor influence of the shape of the structure on the dynamics of the particles. For $f \to \infty$ the plateau extends and covers the whole period. In this situation, a deterministic treatment of the 2D problem leads to adequate results.

### 6.1.2 Influence of the channel smoothness

In the previous section, we analyzed the distribution of the Brownian particles inside a cell in a rough channel, and in the following, we do the same but changing the maximal half-width $w_{\max}$ of the channel by keeping both the width ratio $\epsilon$ and the scaling parameter $f$ constant.

#### Steady-state particle distribution

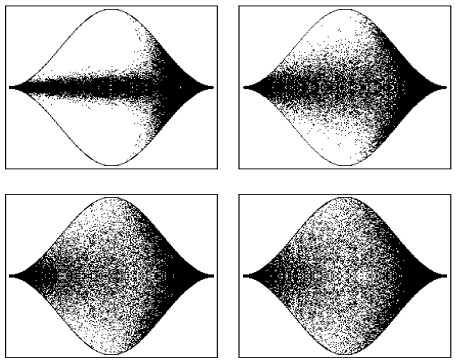

**Figure 6.4:** Steady-state distribution of the particles mapped into a single period of a 2D channel with the width ratio $\epsilon = 101$, at the scaling parameter value $f = 24.0$ and for different values the maximal half-widths. Upper left panel: $w_{\max} = 2.02$; upper right panel: $w_{\max} = 2.02/\pi$; lower left panel: $w_{\max} = 2.02/2\pi$; lower right panel: $w_{\max} = 2.02/3\pi$. Note that, even though each panel is corresponds to different maximal half-widths of the channel, for better visual perceptibility the mapped single cells are presented in the same scale.

Fig. 6.4 shows the steady-state probability distribution of the Brownian particles, inside a single cell, for the channel geometries with different smoothness. In the present case the scaling parameter $f$ is fixed to a moderate value ($f = 24.0$). Upper left panel in Fig. 6.4 corresponds to the distribution of the particles in a rough channel ($w_{\max} = 2.02$) and as we have observed previously, particles would not exhibit an uniform distribution along the transverse direction. At this stage particles exhibit a more direct transport, but still one could observe an accumulation at the exit of the cell because $f$ is not extremely high.

The situation improves slowly as the maximal half-width of the channel decreases. In Fig. 6.4, moving from upper left panel to bottom right panel in $Z$ like motion, particles tend to distribute uniformly along the transverse direction. In the bottom left panel of Fig. 6.4, corresponding to the maximal width $w_{\max} = 2.02/3\pi$, particles exhibit an uniform distribution along the transverse direction, and the equilibrium assumption can satisfy. At this stage the one-dimensional kinetic description leads to better results, may

be with a very small relative error. The situation may improve drastically by further increasing the smoothness of the channel.

From Fig. 6.4 we see clearly, that as the maximal half-width of the channel decreases the applicability of the one-dimensional kinetic description increases. Similar to the situation that we encountered in the previous section, the distribution of the Brownian particles is not the same at every $x-$ position along the channel direction in any geometric structure. For further details on the distribution of the Brownian particles along the transverse direction and along the length of the channel, we analyze the situation in more detail as like in the previous section.

### Probability distribution along the transverse direction

Here, we analyze the probability distribution of the Brownian particles along the transverse direction of the cell for different maximal half-widths of the channel. The mathematical expression is given by Eq. (6.1).

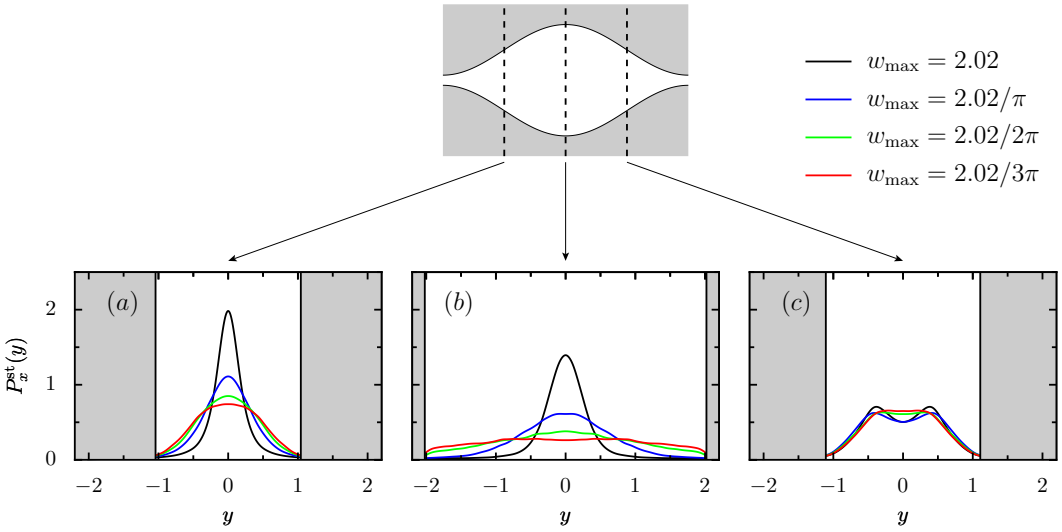


**Figure 6.5:** Normalized steady-state probability distribution of particles in the $y-$ direction (see Eq. (6.1)) for different values of the maximal half-widths $w_{\max}$, at different positions along the length of a 2D channel with the width ratio $\epsilon = 101$ and the scaling parameter $f = 24.0$. $x = 0.2$ (panel (a)), $x = 0.5$ (panel (b)), and $x = 0.8$ (panel (c)). The grey regions indicate the outside of the channel. Note that, each line in the graph corresponds to different maximal half-widths of the channel, but for better visual perceptibility the widths (correspondingly the probability distributions) are maintained at same scale.

Fig. 6.5 depicts the normalized steady-state probability distribution of the particles at three different locations along the channel, i.e., at $x = 0.2$, $x = 0.5$ and $x = 0.8$, with different maximal half-widths, and at the scaling parameter $f = 24.0$. For the

maximal half-width $w_{\max} = 2.02$, corresponding to a rough channel geometry, particles do not exhibit an uniform distribution along the transverse direction at the middle of the channel, i.e., at $x = 0.5$ ($\omega'(x) = 0$). But as the smoothness of the channel increases, i.e., decreasing $w_{\max}$, particles begin to exhibit an uniform distribution (box like distribution) along the transverse direction. For $w_{\max} = 2.02/3\pi$, corresponding to a smooth channel geometry, we can observe a perfect uniform distribution in $P_x^{\rm st}(y)$, see panel (b) in Fig. 6.5. At $x = 0.2$ and $x = 0.8$, the system is not equilibrated enough for rough channels, i.e., for high values of $w_{\max}$. Particles are mostly concentrated in the middle of the cell (see panel (a) in Fig. 6.5). By decreasing $w_{\max}$, the distribution becomes broader. At $x = 0.8$, particles almost exhibit an uniform distribution along the transverse direction for moderate smoothness of the channel (see panel (c) in Fig. 6.5). At this position, accumulation feature at the exit of the cell starts to disappear as the smoothness of the channel increasing (see panel (c) in Fig. 6.5).

### Probability distribution along the channel direction

Here, we analyze the probability distribution of the Brownian particles along the channel direction for different maximal half-widths of the channel. The mathematical expression is given by Eq. (6.2).

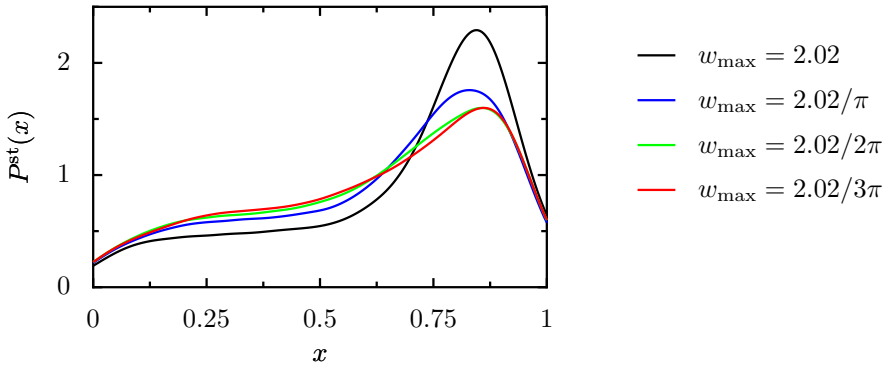


**Figure 6.6:** Normalized steady-state probability distribution of the particles along channel direction $P^{\rm st}(x)$, at the scaling parameter $f = 24.0$ and for different values the maximal half-widths. Here the width ratio $\epsilon = 101$. Note that, each line in the graph corresponds to different maximal half-widths of the channel, but for better visual perceptibility the widths (correspondingly the probability distributions) are maintained at the same scale.

Fig. 6.6 shows the normalized steady-state distribution of the Brownian particles in the $x-$ direction with different maximal widths, and at the scaling parameter value of 24.0. In rough channels, i.e., for high values of $w_{\max}$, the distribution of the particles along the channel direction is almost constant up to a moderate value of $x$, indicating a minor influence of the shape of the structure on the dynamics of the particles. In

this case, the particles do not explore the available space inside the cell, and do not exhibit an uniform distribution along the transverse direction. It results, a failure of the one-dimensional kinetic description. But the situation improves upon decreasing the maximal half-width of the channel. For $w_{\max} = 2.02/3\pi$ particles tries to distribute uniformly along the transverse direction, and not just accumulating at one position (see Fig. 6.6). This situation improves even further by increasing the smoothness of the channel. Thus, for rather smooth channels the one-dimensional description is expected to provide accurate results.

## 6.2 Equilibrium conditions in Geometric scaling II

In this section, we consider geometry with a constant maximal half-width ($w_{\max}$) and for different values of the width ratio $\epsilon$, i.e., Geometric scaling II (Fig. 5.6). The expression is given by

$$\omega(x) = \frac{w_{\max}}{2}(1-\epsilon)\left\{\sin(2\pi x) + \frac{1+\epsilon}{1-\epsilon}\right\},$$

here the value of the maximal half-width is set to 2.02 (gives a rough geometry), and for the analysis the value of scaling parameter $f$ is 5.0. Like before, we analyze the steady-state distributions of the particles in the channel geometry with different width ratios.

### Steady-state particle distribution

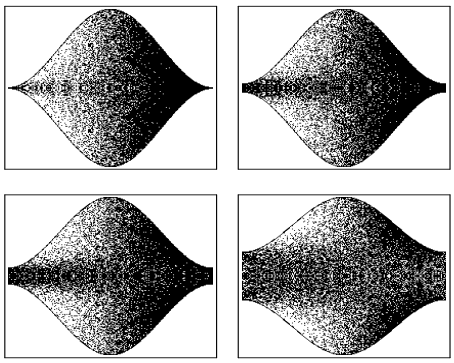

**Figure 6.7:** Steady-state particle distribution mapped into a single cell of a 2D channel with maximal half-width $w_{\max} = 2.02$, for the scaling parameter value $f = 5.0$ and for different values of the width ratio $\epsilon$. Upper left panel: $\epsilon = 0.005$; upper right panel: $\epsilon = 0.01$; lower left panel: $\epsilon = 0.05$; lower right panel: $\epsilon = 0.1$.

Fig. 6.7 shows the steady-state distribution of the Brownian particles mapped into a single cell of a 2D channel with different values of the width ratio $\epsilon$. For a very small value of the width ratio $\epsilon$, i.e., for very small bottleneck width, surprisingly, there are enough number of particles which could exhibit an uniform distribution along the transverse direction. But most of the particles gather at the exit of the cell. By increasing the width ratio $\epsilon$, i.e., increasing the bottleneck opening, particles follow more directed transport which means, less number of particles occupy the extreme regions in the $y-$ direction, and most of the particles gather at the middle of the cell (see Fig. 6.7 bottom panels). System exhibits an uniform distribution along the transverse direction up to $\epsilon \sim 0.05$ (see Fig. 6.7 top panels and bottom left panel), and on further increase in $\epsilon$ spoils the uniform distribution. For narrow openings, more number of particles reflect at the channel walls close to the bottleneck. These particles resides a longer time inside a cell and therefore have more time to explore diffusively the full region along the transverse directions. Therefore, in Geometric scaling II, the one-dimensional description holds for very small values of the width ratio $\epsilon$ and starts to fail as the $\epsilon$ value increases.

### Probability distribution along the transverse direction

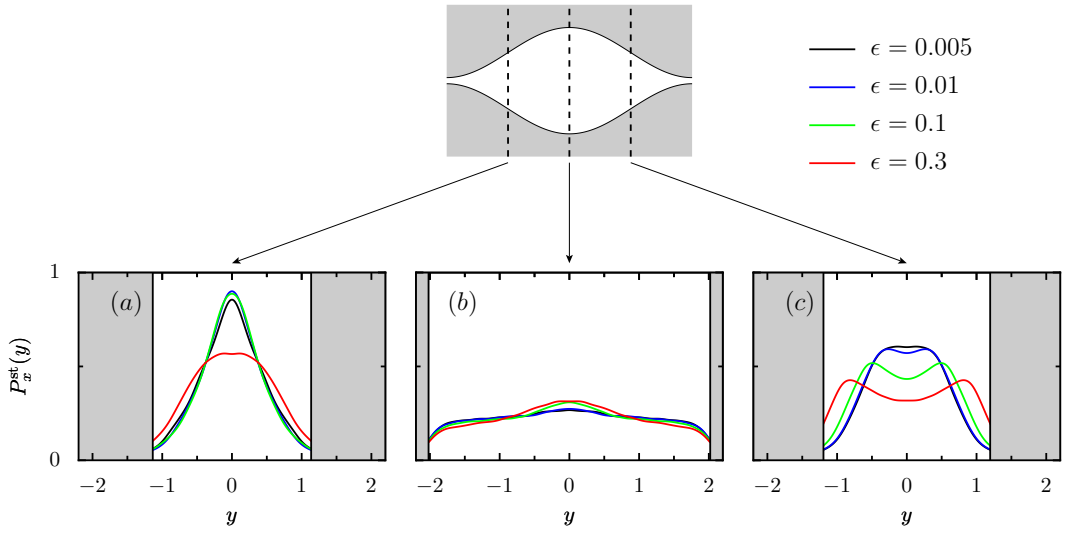


**Figure 6.8:** Normalized steady-state probability distribution of the particles in the $y$-direction $P_x^{\rm st}(y)$ (see Eq. (6.1)) for different values of the width ratio $\epsilon$, at different positions along the length of a 2D channel with the maximal half-width $w_{\rm max} = 2.02$ and the scaling parameter $f = 5.0$. $x = 0.2$ (panel (a)), $x = 0.5$ (panel (b)) and $x = 0.8$ (panel (c)). The grey regions indicate the outside of the channel.

For very small values of the width ratio $\epsilon$, corresponding to small bottleneck openings, the Brownian particles exhibit a perfect uniform distribution along the transverse

direction at the middle of the cell (see panel (b) in Fig. 6.8). As we have observed in Fig. 6.7, for increasing $\epsilon$ more number of particles gather at the center line of the cell axis exhibiting a bump like feature (see panel (b) in Fig. 6.8). This feature is more pronounced as the width ratio $\epsilon$ increases. Like in Geometric scaling I, the distribution of the particles is position dependent (see panel (a) and (c) in Fig. 6.8). At the beginning of the cell particles exhibit a Gaussian like distribution for small values of the width ratio $\epsilon$, and as the value increases the distribution becomes flat.

In situation where the geometries with large width ratio, if the Brownian particles enter a cell, from a neighboring one, particles are less deviated and exhibit a more directed transport. But the behavior of the steady-state distribution, before the exit of the cell, is quite different (see panel (c) in Fig. 6.8). For very small values of the width ratio $\epsilon$, system exhibits an uniform distribution and as $\epsilon$ value increases uniform distribution breaks down. For rather high values of the width ratio $\epsilon$ the Brownian particles exhibit a two-peak behavior in the distribution along the transverse direction which is due to, at these moderate values of $\epsilon$, particles get stuck at the channel walls at the exit of the cell. Notice that, for $\epsilon = 1.0$ (flat geometry) the system shows a perfect uniform distribution along the transverse direction at any $x-$ position along the cell.

### Probability distribution along the channel direction

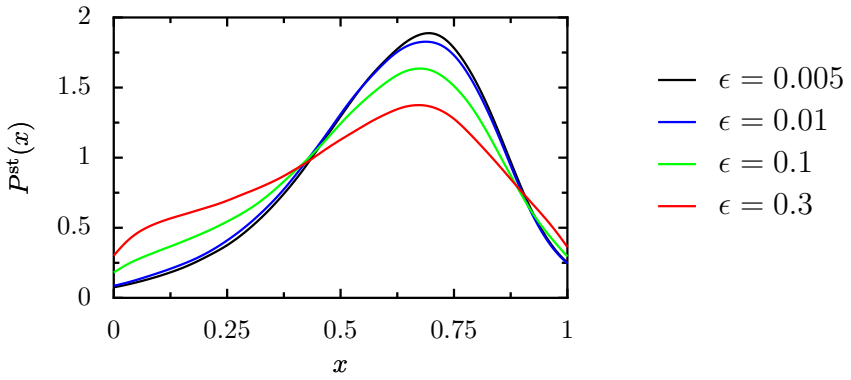


**Figure 6.9:** Normalized steady-state probability distribution of the particles along the channel direction $P^{\rm st}(x)$ for different values of the width ratio $\epsilon$, and at the scaling parameter $f = 5.0$. Here, the maximal half-width $w_{\rm max}$ of the 2D channel is 2.02.

Fig. 6.9 shows the steady-state distribution of the Brownian particles along the channel direction for different values of the width ratio $\epsilon$. For small values of $\epsilon$ and at lower value of the scaling parameter $f$, the system exhibits an uniform distribution of the particles along the transverse direction. But, some portion of the particles gather at exit of the cell (see Fig. 6.9). Increasing the value of the width ratio $\epsilon$, particles tend to occupy the

full region along the channel direction, instead of accumulating at one position. At this stage particles obey more directed transport. At the moderate values of the width ratio $\epsilon$, by looking at Fig. 6.9, one can assume that system may exhibit an uniform distribution in both transverse and channel direction, but it is not true. At this stage, particles not completely occupy the extreme regions in transverse direction since, particles obey more directed transport (see Fig. 6.7 lower panels). For very high values of the width ratio $\epsilon$, we can observe a flat distribution along the channel direction. A similar distribution we can observe along the transverse direction as well.

We have analyzed the diffusion process in both Geometric scaling I and Geometric scaling II so far, and we can draw some conclusions from the above observations. (i) The distribution of the Brownian particles inside a cell is not the same at every position of $x$ along the channel direction, for any geometry irrespective of the Geometric scaling. (ii) The failure of the one-dimensional description at large values of the scaling parameter $f$ in both Geometric scaling I and Geometric scaling II. (iii) An increase of validity regime for the one-dimensional description as the maximal half-width of the channel decreases in Geometric scaling I. (iv) Upon decreasing the bottleneck width, the applicability of the one-dimensional description increase in Geometric scaling II. By taking into account of these arguments we can construct the validity criteria for the one-dimensional kinetic description, in terms of the maximal half-width $w_{\max}$, the with ratio $\epsilon$, and the scaling parameter $f$ by analyzing the characteristic time scales which characterize the diffusion process in these confined systems.

## 6.3 Validity of the equilibrium assumption

The reduction of dimensionality done in the formulation of the one-dimensional kinetic equation relies on the assumption of equilibration in the transverse direction. An estimate of the conditions under which equilibration occurs can be made by analyzing the different time scales involved in the problem. For the sake of simplicity, let us focus on the situation of a 2D channel, although the same discussion can readily be extended to 3D. One can formulate two different sets of criteria determining first, whether the one-dimensional kinetic equation describes the relaxation towards the stationary state, say in presence of periodic boundary conditions, or second, whether the stationary state, but not necessarily the relaxation towards this state, can be described by the one-dimensional kinetic equation.

Although we here are mainly interested in the second criterion which is sufficient to guarantee the validity of the transport properties predicted by the one-dimensional kinetic equation, we shortly formulate a stronger criterion which must be satisfied if the one-dimensional kinetic equation is employed to determine the relaxation towards equilibrium. Then, of course, the time scale of equilibration in transversal direction must be short compared to the relevant time scales in longitudinal direction [27].

### 6.3.1 Characteristic timescales

When the diffusion process takes place inside the system, there are different kinds of characteristic time scales which should be considered. The characteristic time scales, for a Brownian particle to diffuse inside the system depend on the space available, thermal noise present in the system, and also depend on the external conditions like whether there is any bias acting on the system or not. By keeping all these in mind, one can identify three different characteristic time scales.

- The time scale $\tau_{\mathrm{T}}$ can be estimated as the time it takes for the Brownian particle to diffusively cover the transversal distance of the channel, and which depends on the position $x$. It is given by

$$\tau_{\mathrm{T}} = \frac{\omega(x)^2}{2}. \tag{6.3}$$

  As we have observed in Fig. 6.1 and Fig. 6.4 the distribution of the Brownian particles is not the same at every position of $x$ along the channel direction. If the position $x$ changes, the width of the cell changes, i.e., $\omega(x)$, and in turn $\tau_{\mathrm{T}}$ changes.

- One time scale characterizing the longitudinal motion is the diffusion time $\tau_{\mathrm{d}L}$ over the length of a period, which reads in dimensionless variables

$$\tau_{\mathrm{d}L} = \frac{1}{2}\,. \tag{6.4}$$

- In the presence of an applied bias, the time $\tau_{\mathrm{f}L}$ it takes to drag a particle over a period length is given by

$$\tau_{\mathrm{f}L} = \frac{1}{f}\,, \tag{6.5}$$

With these characteristic times scales we can construct a validity criteria for the one-dimensional kinetic description for both Geometric scaling I and Geometric scaling II.

In the absence of bias, $f = 0$, a perfect uniform distribution of the Brownian particles along the transverse direction(s), the basic assumption, could be observed only when the diffusion time for the Brownian particles to reach the channel walls (cover the full width of the channel) is less than the diffusion time for the Brownian particles to travel the distance of one period, i.e., $\tau_{\mathrm{T}}/\tau_{\mathrm{d}L} \ll 1$. It can be achieved in rather smooth channels.

In the presence of an applied bias, acting along the length of the channel direction, a necessary condition that the one-dimensional kinetic description reliably describes transient processes can be formulated when $\tau_{\mathrm{T}}/\tau_{\mathrm{f}L} \ll 1$. Thus, a more general criteria for the equilibrium condition reads

$$\omega(x)^2 \ll \min(1/2, 1/f)\,. \tag{6.6}$$

As already mentioned in the presence of periodic boundary conditions in the longitudinal direction, the particle distribution described by the Fokker-Planck equation Eq. (3.8) approaches a stationary distribution. Even in the case if the first criterion Eq. (6.6) is violated, the stationary solution of the one-dimensional kinetic equation Eq. (3.20) may still yield the correct marginal probability density, provided transversal cuts of the two-dimensional stationary probability density are practically constant. Such a uniform distribution in transversal direction strictly holds in the absence of externally imposed concentration differences if the force $f$ vanishes or if the channel is straight. For channels with varying width the narrow positions confine the positions of particles. From there they are dragged by the force and at the same time they perform a diffusive motion until the channel narrows again. The required uniform distribution in the transversal direction can only be achieved if the diffusional motion is fast enough in comparison to the deterministic drift under the influence of $f$. In other words, the diffusional spreading within the time the force drags the particle from the narrowest to the widest place in the channel must be at least of the order of the widest channel width. This leads to the second, criterion

$$\omega(x)^2 \leq \frac{2}{f} \quad \Leftrightarrow \quad f \leq \frac{2}{\omega(x)^2}\,. \tag{6.7}$$

Eq. (6.7) provides a quite stringent criterion that indicates when the one-dimensional kinetic description is expected to be valid. Note also that, this is a local criterion. There will be regions associated with drastic changes in the shape of the channel where equilibration in the transverse direction is not feasible, whereas in other regions it is fulfilled. The distribution of the Brownian particles along the transverse direction is not the same at every position of $x$ along the channel direction, see Fig. 6.1 and Fig. 6.4. Therefore, it is then more convenient to work with a global criterion of validity rather than with a local one. One way of getting that global condition is by averaging the local criterion over the period of the channel, i.e., taking the average width along the transverse direction over the channel period length, Eq. (6.7) results in

$$f \leq \frac{2}{\langle \omega(x)^2 \rangle}\,, \tag{6.8}$$

where the average is defined as

$$\langle \omega(x)^2 \rangle = \int_0^1 \omega(x)^2 \mathrm{d}x\,. \tag{6.9}$$

For the geometric function

$$\omega(x) = \frac{w_{\max}}{2}(1-\epsilon)\left\{\sin(2\pi x) + \frac{1+\epsilon}{1-\epsilon}\right\}, \tag{6.10}$$

the average value reads

$$\langle \omega(x)^2 \rangle = \frac{w_{\max}^2 (3\epsilon^2 + 2\epsilon + 3)}{8}. \tag{6.11}$$

Substituting the above equation in Eq. (6.8), the final global criterion reads

$$f \leq \frac{16}{w_{\max}^2 (3\epsilon^2 + 2\epsilon + 3)}. \tag{6.12}$$

Eq. (6.12) provides an estimate of the minimum forcing above which the one-dimensional kinetic description is expected to fail in providing an accurate description of the transport properties in the long time limit. The quantitative value of the critical force depends on the level of the prescribed accuracy. The criterion demonstrates how the validity of the equilibrium approximation depends on the relevant parameters of the problem. In the following, we analyze the validity criterions for both Geometric scaling I and Geometric scaling II.

### 6.3.2 Validity criterion for Geometric scaling I

Eq. (6.12) indicates that the critical scaling parameter $f_c$ scales asymptotically as $1/w_{\max}^2$, for a fixed width ratio $\epsilon$, i.e.,

$$f_c \propto \frac{1}{w_{\max}^2}. \tag{6.13}$$

In order to verify the criterion we have proposed, we extract the critical scaling parameter values by comparing the analytical results with the numerical results, for the non-linear mobility, up to which the agreement is perfect within some relative error. For an illustration see Fig. 6.10. Here, one can also consider the effective diffusion, the second moment in $x$. For $w_{\max} = 2.02/2\pi$, the agreement between the analytics and numerical simulations is up to the scaling parameter value of $\sim 40$, and for $w_{\max} = 2.02$ it's up to 10. Thus, as the maximal half-width decreases the critical scaling parameter value increases. Similarly, we can extract the critical scaling parameter values for different maximal half-widths of the channel geometry.

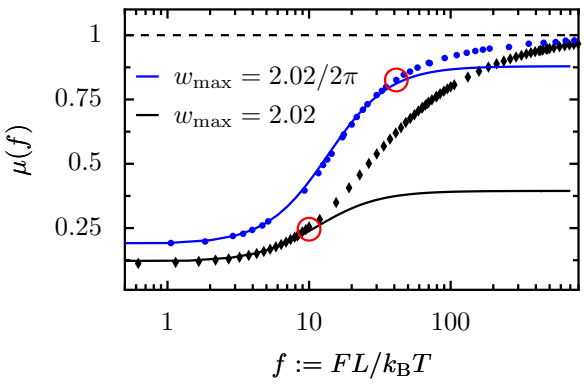


**Figure 6.10:** The critical scaling parameter values $f_c$ for different maximal half-widths $w_{\max}$ of the channel (Geometric scaling I) by comparing the numerical simulations results with the analytically predicted behaviors within a small relative error. Decreasing $w_{\max}$ leads to an increase in the critical scaling parameter value.

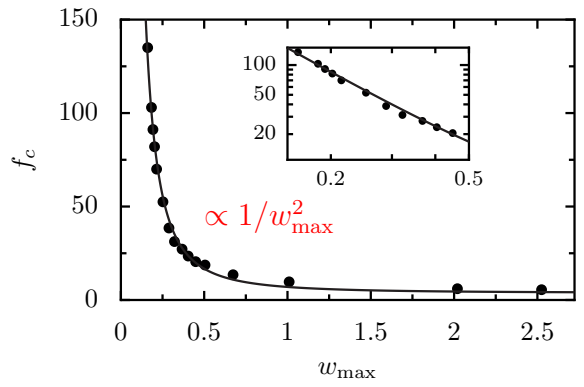


**Figure 6.11:** The dependence of the critical value of the scaling parameter $f_c$ on the maximal half-width of the channel (Geometric scaling I) is depicted. For $f < f_c$ the relative error of the one-dimensional kinetic description is less than 1%. The solid line is a $1/w_{\max}^2$ -fit of the critical scaling parameter values obtained by comparison of the approximative analytic and the exact numerical results, see Fig. 6.10. The inset depicts the behavior of $f_c$ as a function of $w_{\max}$ in a log plot.

Fig. 6.11 shows the value of the critical scaling parameter, with a tolerance of 1%, as a function of the maximal half-width. Each point in the graph corresponding to the critical scaling parameter value for a particular smoothness of the geometry. The critical value of the scaling parameter depends *inverse quadratically* on the smoothness, as predicted by Eq. (6.12). For rough channels, i.e., for large values of $w_{\max}$, the range of validity of the one-dimensional description is small and it increases upon decreasing the value of $w_{\max}$.

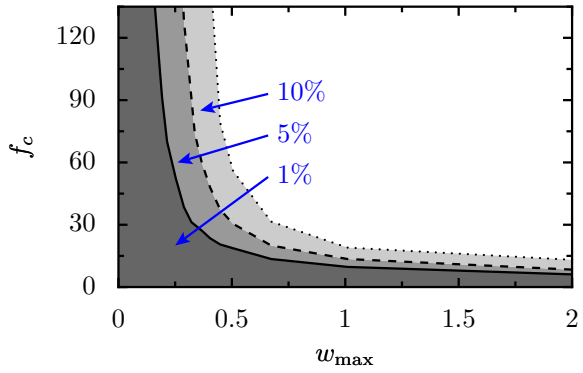


**Figure 6.12:** The *validity diagram* of the one-dimensional description for biased diffusion is obtained upon a comparison between the precise numerics with the approximative analytic solution (see Eq. (4.7)) for Geometric scaling I. The dependence of the critical value of the scaling parameter on the maximal half-width $w_{\max}$ is depicted for three different relative errors; 1%: solid line, 5%: dashed line and 10%: dotted line. Below these limiting lines the analytic treatment agrees within the corresponding prescribed relative error.

In Fig. 6.12 we illustrate, for the considered two-dimensional channel, the regions where the one-dimensional kinetic description is accurate when compared with the simulations. We depict the dependence on the maximal half-width ($w_{\max}$) of the critical scaling parameter, obtained by comparing numerical results with the analytic solution for the non-linear mobility, for different required relative errors. The qualitative behavior of $f_c$ as a function of $w_{\max}$ is same for small relative error, but only the quantitative behavior changes. This diagram shows the regions in parameter space in terms of $f$ and $w_{\max}$ for which an accurate solution is provided. Thus, it is possible to provide an accurate result by using the analytic solution over a wide range of the scaled parameter $f$ and the maximal half-width $w_{\max}$.

### 6.3.3 Validity criterion for Geometric scaling II

We have observed in the previous chapter that the applicability of the one-dimensional kinetic description is very little for the rough channels. The validity criterion for Geometric scaling II, for a fixed maximal half-width $w_{\max}$, reads,

$$f_c \propto \frac{1}{g(\epsilon)}\,, \tag{6.14}$$

where $g(\epsilon)$ is a quadratic function of $\epsilon$.

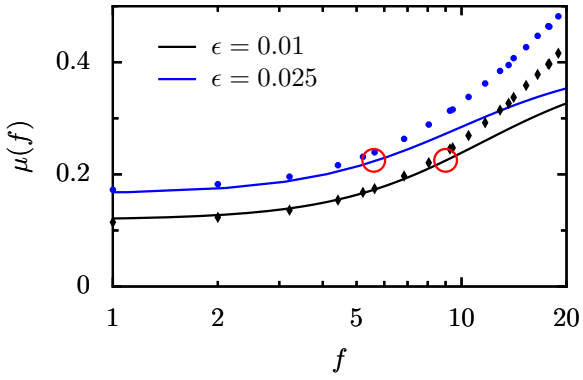


**Figure 6.13:** The critical scaling parameter values $f_c$ for different width ratios $\epsilon$ of the channel (Geometric scaling II) by comparing the numerical simulations results with the analytically predicted behaviors within a small relative error.

In order to verify the criterion we have proposed for Geometric scaling II, we extract the critical scaling parameter values by comparing the analytical results with the numerical results, for the non-linear mobility, up to which the agreement to perfect within some relative error, for an illustration see Fig. 6.13. For $\epsilon = 0.01$, the agreement between the analytics and numerical simulations is up to the scaling parameter value of $\sim 9$, and for $\epsilon = 0.025$ it's up to 6. Here, we can see that as the width ratio $\epsilon$ value increases the critical scaling parameter value decreases. Thus, we can extract the critical scaling parameter values for different value of the width ratio $\epsilon$.

Fig. 6.14 shows the value of the critical scaling parameter, with a tolerance of 1%, as a function of the width ratio $\epsilon$. Each point in the graph corresponding to the critical scaling parameter value for a particular value of $\epsilon$. The critical value of the scaling parameter depends as an *inverse quadratic function* of the width ratio $\epsilon$, as predicted in the Eq. (6.14). For small values of the width ratio $\epsilon$, i.e., for small bottleneck openings, the range of validity of the one-dimensional description is high, and it decreases upon increasing the value of $\epsilon$. Notice that, as the width ratio $\epsilon \to 0$, $f_c$ tends to reach a constant value. If we imagine a closed system, an isolated single cell with some degree of smoothness, for small values of scaling parameter $f$, the Brownian particles occupy the full region along the transverse direction and system exhibits a perfect uniform distribution, and the one-dimensional description holds nicely. This validity regime continue up to some critical value of the scaling parameter $f_c$, and then it may start

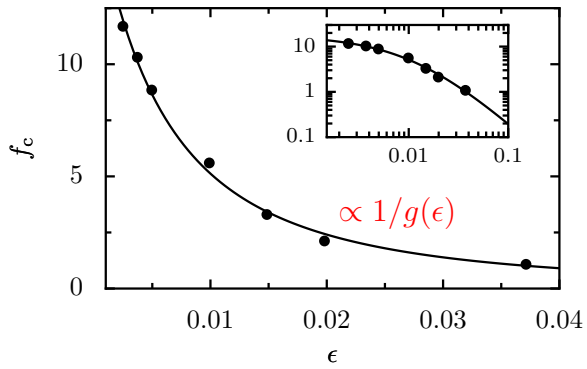


**Figure 6.14:** The dependence of the critical value of the scaling parameter $f_c$ on the width ratio $\epsilon$ for Geometric scaling II. For $f < f_c$ the relative error of the one-dimensional kinetic description is less than 1%. The solid line is $g(\epsilon)$ -fit of the critical values obtained by comparison of the approximative analytic and the exact numerical results, see Fig. 6.13. Thereby $g(\epsilon)$ is a quadratic function in $\epsilon$.

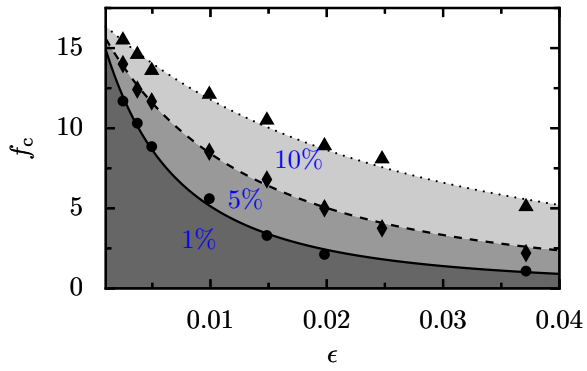


**Figure 6.15:** The *validity diagram* of the one-dimensional description for biased diffusion is obtained upon a comparison between the precise numerics with the approximative analytic solution (see Eq. (4.7)) for Geometric scaling II. The dependence of the critical value of the scaling parameter on the width ratio $\epsilon$ is depicted for three different relative errors; 1%: solid line, 5%: dashed line and 10%: dotted line. Below these limiting lines the analytic treatment agrees within the corresponding prescribed relative error.

to fail. This critical value depends on the maximal half-width of the channel. In the present case we are considering $w_{\max} = 2.02$, and the limiting value for $f_c$ is $\approx 10.5$. On further increase in $w_{\max}$ this constant value may increase.

Fig. 6.15 shows, the dependence of the maximal critical scaling parameter on the width ratio $\epsilon$, obtained by comparing numerical results with the analytic solution for the non-linear mobility, for different required relative errors. The qualitative behavior of $f_c$ as a function of the width ratio $\epsilon$ is same for small relative error, but only the quantitative behavior changes. This diagram shows the regions in parameter space in terms of $f$ and $\epsilon$ for which an accurate solution is provided. Thus, it is possible to provide an accurate result by using the analytic solution over a wide range of the scaled parameter $f$ and the width ratio $\epsilon$.

## 6.4 Summary

In this chapter we have investigated the validity conditions under which the one-dimensional kinetic description provides an accurate description of the biased diffusion of the Brownian particles in both Geometric scaling I and Geometric scaling II. We have investigated, numerically, the conditions for a fast equilibration in the transverse direction which is vital for the accurateness of the one-dimensional kinetic description. The presented results evidence the usefulness of the one-dimensional description with a spatially dependent diffusion coefficient up to a moderate value of the scaling parameter. We have established the validity criteria, formulated in terms of the sinuosity of the channel $\omega(x)$, as done in the unbiased case [20–22, 85], and on the scaling parameter that causes forced diffusion. This scaling parameter compares the work done on a particle travelling a channel period with the available thermal energy. Interestingly, the critical value of this scaling parameter up to which the one-dimensional kinetic equation holds for an arbitrary channel geometry, with an arbitrary maximal half-width and the ratio of bottleneck width to the full width, reads

$$f \leq \frac{16}{w_{\max}^2 \left(3\epsilon^2 + 2\epsilon + 3\right)} .$$

This dependence follows from the analysis of the different time scales that rule the biased, diffusive dynamics. We have analyzed this validity criteria, separately for Geometric scaling I and Geometric scaling II. For Geometric scaling I, for a constant width ratio $\epsilon$, the critical value of the scaling parameter up to which the one-dimensional kinetic equation holds depends *inverse quadratically* on the maximal half-with $w_{\max}$. For Geometric scaling II, with a constant maximal half-width, the critical scaling parameter is an *inverse quadratic function* of the width ratio $\epsilon$.

# 7

# Conclusions and Outlook

With this work we have analyzed the transport characteristics in geometrically confined systems where entropic barriers play an important role. Practically, solving the full problem for arbitrary boundary functions is quite difficult, and so far there have been no corresponding analytical tools. Therefore, we have developed an approximative method based on the equlibriation assumption in order to reduce the complexity of the problem. This essentially leads to an effective one-dimensional kinetic description within a free energy landscape where the entropic contribution arises coming from the geometric confinement. Reducing a higher dimensional system (3D or 2D) to an effective one-dimensional one, the geometrical confinement modifies the diffusion process in the system, implying a spatially dependent diffusion coefficient. The reduced one-dimensional kinetic description can be improved by including the spatially dependent diffusion coefficient.

We have shown that transport phenomena in confined systems in the presence of entropic barriers exhibit some features which are radically different from those we observe in purely energetic systems [75–77, 79]. The effect of confinement can be recast in terms of an entropic potential, and the dynamics of the system can be accurately described by means of the one-dimensional kinetic equation. If the entropic nature is more dominant, we observe a different temperature dependence [26–28] which is not present in purely energetic systems. The average particle current decreases upon increasing the strength of thermal noise [26], contrary to the behavior that usually found in purely energetic systems.

Similar to purely energetic systems, we observed an enhancement in the effective diffusion coefficient whose maximum always exceeds the bulk diffusion constant [26–28, 60, 91–95]. In tilted energetic potentials, near the critical tilt (or critical bias), there is an enhancement in the effective diffusion coefficient, whereas below this critical tilt the effective diffusion is lower than the bulk diffusion constant [83]. Values of diffusion coefficient in excess of the bulk being consistent with the phenomenon of diffusion enhancement predicted by our model have been reported in Ref.[60] by means of molecular dynamic studies of $n-$ pentane and isopentane in one-dimensional channels of $AIP0_4$-5, as well as in Ref.[91–95]. Related to our observation that the effective diffusion coeffi-

cient decreases with temperature in certain temperature ranges, a similar effect has been reported concerning the self-diffusion of ethane molecules in Linde type A zeolites [58]. Furthermore, the existence of an optimal value of the diffusion as a function of temperature has been watched [59] by molecular dynamics simulations on the self-diffusion of ethane, methane and propane molecules in LTA and LTL type zeolites.

Our model thus describes all above mentioned phenomena and shows that they are not specific for a particular zeolite structure but rather arise from the entropic nature of transport. The particle current and the effective diffusion coefficient are controlled by a single parameter $f := FL/k_{\mathrm{B}}T$ that measures the ratio of external work applied to the particle and thermal energy, which is one of the major result of this work. In purely energetic systems, applied bias $F$ and temperature $T$ are independent parameters and cannot be coupled in this fashion.

The applicability of the equilibrium assumption depends on the degree of confinement of the geometric structure. If the roughness of the channel is not extremely distinct, i.e., rather smooth, the one-dimensional kinetic description provides a very good approximation to the transport for values of the external work of some tens of $k_{\mathrm{B}}\,T$'s. In fact, which is the range of energy relevant to most transport processes in biological systems [44, 49, 50, 56]. The diffusion process varies upon changing the bottleneck opening of the confined geometry. One could observe a similar effect in the case of DNA translocation through solid nanopore [44, 49, 56]. There is a critical bottleneck opening related to a maximum effective diffusion coefficient. This feature is more visible in highly confined geometries. Brownian particles, at moderate values of scaling parameter, get stuck at the exit of the channel before they can transfer to the neighbored one, a similar feature can also be observed in translocation of DNA molecules or individual species through nanopores, where the former molecules sojourn in front of the bottleneck openings [44, 49, 56].

Since we are using an approximative method to analyze the transport characteristics of the system, we also need to discuss it's limitations. We have established general criteria for the applicability of the one-dimensional kinetic description by analyzing the characteristic time scales [27, 28] that rule the dynamics in terms of the sinuosity of the channel, and the scaling parameter $f$ that causes the forced diffusion [27, 28]. Recently, there have been some new proposals emerging [96–98] to explain the transport characteristics in periodic confined systems in the presence of an applied bias with the use of the Macro-transport theory [92, 99].

Our one-dimensional kinetic description can be applied in a wide variety of situations, such as biological transport through ion channels and membrane or synthetic pores, or the portage in molecular sieves, where entropic effects play a very important role. The scaling in $f$ thus opens up the possibility of tuning and controlling the efficiency of transport in confined systems by a proper combination of temperature and applied bias. In situations where temperature can only be varied in a very limited range, like in biological systems, the existence of scaling implies that the same regime of transport

may be accomplished by the variation of an external force.

Incidentally, our one-dimensional kinetic description for calculating the transport characteristics in periodic symmetric and asymmetric channels (ratchet systems) has already been applied in several investigations [15, 61, 100–107]. In particular, our kinetic description could be applied to the translocation of ionic species through nanopores [15]. Moreover, applying our kinetic description in asymmetric channels and replacing the constant applied bias with a fluctuating one or an additional noise source to the system, one can observe a finite current [62, 105–107]. In these systems, the adaptability of the one-dimensional kinetic description can vary upon the direction of the external bias [108].

After having gained all this knowledge by analyzing the diffusion process in confined systems, it would be interesting in addition to this to observe all the characteristic features which are known in purely energetic systems in entropically dominant situations. In particular, the influence of entropic barriers on resonance property calls for further investigation.

# A

# Reduction of dimensionality

We present in this appendix some mathematical details of the equilibrium assumption along the transverse direction(s) of a confined structure, as it's shown in Fig.A.1. This allows to reduce the complexity of the dynamics and leads to an effective one-dimensional kinetic equation which describes the dynamics of the full system [20, 22, 26].

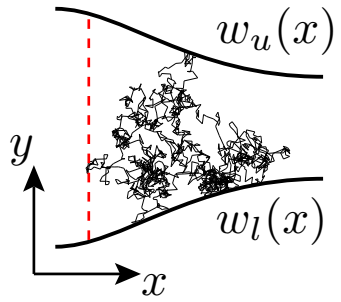


**Figure A.1:** A two-dimensional geometry which is confined between the lower boundary $w_l(x)$ and upper boundary $w_u(x)$. The Brownian particles explore the available space within these boundaries. An assumption of uniform distribution of the Brownian particles along the transverse direction(s), leads to a reduction of dimensionality, results in obtaining an effective one-dimensional kinetic equation with an entropic contribution which is arising from the boundary functions.

As we have described in Fig. A.1, the marginal probability distribution of the Brownian particles at a position $x$, at a given time $t$, along the length of the geometry is nothing but the integration of the total probability density along the transverse direction(s) at that position of $x$. The expression reads

$$P(x,t) = \int P(x,y,z,t)\,\mathrm{d}y\,\mathrm{d}z\,. \tag{A.1}$$

Now, consider the Smoluchowski equation in the absence of an applied bias, i.e. $F = 0$, which is

$$\frac{\partial}{\partial t}P(\vec{x},t) = \pounds\, P(\vec{x},t)\,, \tag{A.2}$$

where $P(\vec{x},t)$ is probability distribution of the Brownian particles. The operator $\pounds$ has the form

$$\pounds = \vec{\nabla}\, D\, e^{-U(\vec{x})}\, \vec{\nabla}\, e^{U(\vec{x})}\,, \tag{A.3}$$

where $D$ is diffusion coefficient and $U(\vec{x})$ is dimensionless potential function (scaled with $k_{\mathrm{B}}T$).

By using Eq. (A.1), Eq. (A.2) can be written as

$$\frac{\partial}{\partial t}P(x,t) = \int \pounds\, P(x,y,z,t)\,\mathrm{d}y\,\mathrm{d}z\,. \tag{A.4}$$

Define $A(x)$, a thermodynamic potential, which takes care of the boundary conditions by confining the particles with in the geometric structure, neglecting the irrelevant constants it reads

$$e^{-A(x)} = \int e^{-U(x,y,z)}\,\mathrm{d}y\,\mathrm{d}z\,. \tag{A.5}$$

Under the equilibrium conditions along the transverse direction(s), i.e. the probability distribution of the Brownian particles along the transverse direction(s) can be written as the Boltzamnnn distribution, we can define a conditional local distribution, at a given $x$, which will have the form [20]

$$\rho(y,z;x) = e^{-U(x,y,z)}\, e^{A(x)} \tag{A.6}$$

where $\rho(y,z;x)$ is normalized. The total probability distribution $P(x,y,z,t)$ can be expressed in terms of the conditional probability $\rho(y,z;x)$, which reads [20]

$$P(x,y,z,t) \cong P(x,t)\,\rho(y,z;x)\,. \tag{A.7}$$

This is our main assumption of equlibriation along the transverse direction(s). After using the above assumptions, Eq. (A.4) modifies into [20, 22, 26]

$$\frac{\partial}{\partial t}P(x,t) = \frac{\partial}{\partial x}\, D\, e^{-A(x)} \frac{\partial}{\partial x} e^{A(x)} P(x,t)\,, \tag{A.8}$$

gives the approximative reduced one-dimensional (1D) kinetic equation with a free energy term $A(x)$ containing an entropic contribution coming from the boundary functions. A more general form of the free energy function reads

$$A(x) = -\ln h(x)\,, \tag{A.9}$$

where $h(x) = \pi\omega(x)^2$, the cross sectional area of the geometry, when we reduce a 3D system to 1D, and $h(x) = 2\Delta\omega(x)$, the width of the geometry, from a 2D system to 1D.

# B

# Mean First Passage Time approach

We present in this appendix the details about the moments of the first passage time to calculate the transport quantities, the average particle current and the effective diffusion coefficient.

We start with the reduced one-dimensional kinetic equation, Eq. (3.20)

$$\frac{\partial P(x,t)}{\partial t} = \pounds\, P(x,t)\,, \tag{B.1}$$

where $\pounds$ is the Fokker-Plank operator will have the form

$$\pounds = \frac{\partial}{\partial x}\left\{ D(x)\, e^{-A(x)}\, \frac{\partial}{\partial x}\, e^{A(x)} \right\}. \tag{B.2}$$

The corresponding backward Smoluchowski operator has the form

$$\pounds^{+} = e^{A(x)}\, \frac{\partial}{\partial x}\left\{ D(x)\, e^{-A(x)}\, \frac{\partial}{\partial x} \right\} \tag{B.3}$$

Then, for our reduced one-dimensional description, the moments of the first passage time, for a particle starting out at an arbitrary position $x_a$ and reaching at an arbitrary position $x_b$, expressed in a closed analytical recursion (Ref.[75] and further references there in)

$$\pounds^{+} T_n = -n T_{n-1}\,, \tag{B.4}$$

where $T_n$ with $n = 1, 2, 3, ...,\ n \in \mathbb{Z}$, are the moments of the first passage time with $T_0 = 1$.

Now, we calculate the first moment of the first passage times $\pounds^{+} T_1 = -1$, i.e. for $n = 1$,

$$e^{A(x)}\, \frac{\partial}{\partial x}\left\{ D(x)\, e^{-A(x)}\, \frac{\partial}{\partial x} \right\} T_1 = -1 \tag{B.5}$$

$$\frac{\partial}{\partial x}\left\{D(x)\,e^{-A(x)}\,\frac{\partial}{\partial x}\right\}T_1 = -e^{-A(x)}\,. \tag{B.6}$$

Integrating on both sides we get

$$D(x)\,e^{-A(x)}\,\frac{\partial}{\partial x}T_1 = -\int_c^x e^{-A(z)}\mathrm{d}z + K_1\,, \tag{B.7}$$

where $c$ is an arbitrary point with in the domain, and $K_1$ is a constant. Now, we have to determine the constant $K_1$ by imposition absorbing boundary conditions, i.e ${T_1}'(x \to -\infty) \to 0$

$$K_1 = \int_c^{-\infty} e^{-A(z)}\mathrm{d}z \tag{B.8}$$

substituting back in Eq. (B.7) we get

$$\frac{\partial}{\partial x}T_1 = \frac{e^{A(x)}}{D(x)}\left\{-\int_c^x e^{-A(z)}\mathrm{d}z + \int_c^{-\infty} e^{-A(z)}\mathrm{d}z\right\} \tag{B.9}$$

summing up the integrals leads to

$$\frac{\partial}{\partial x}T_1 = -\frac{e^{A(x)}}{D(x)}\int_{-\infty}^x e^{-A(z)}\mathrm{d}z\,. \tag{B.10}$$

Now, again integrating on both side to calculate $T_1$ we get

$$T_1 = -\int_c^x \frac{e^{A(y)}}{D(y)}\mathrm{d}y\int_{-\infty}^y e^{-A(z)}\mathrm{d}z + K_2\,, \tag{B.11}$$

where $K_2$ is constant. Again, we impose boundary conditions to calculate the constant $K_2$. Since $T_1(x+1) = 0$

$$-\int_c^{x+1} \frac{e^{A(y)}}{D(y)}\mathrm{d}y\int_{-\infty}^y e^{-A(z)}\mathrm{d}z + K_2 = 0 \tag{B.12}$$

which gives

$$K_2 = \int_c^{x+1} \frac{e^{A(y)}}{D(y)}\mathrm{d}y\int_{-\infty}^y e^{-A(z)}\mathrm{d}z\,, \tag{B.13}$$

by substituting $K_2$ back into the Eq. (B.11) and summing the integrals we get

$$T_1(x \to x+1) = \int_x^{x+1} \frac{e^{A(y)}}{D(y)} \mathrm{d}y \int_{-\infty}^{y} e^{-A(z)} \mathrm{d}z \tag{B.14}$$

The final equation for the first moment of the first passage time, from a fixed point $x_0$ to $x_0 + 1$, reads

$$T_1(x_0 \to x_0+1) = \int_{x_0}^{x_0+1} \frac{e^{A(x)}}{D(x)} \mathrm{d}x \int_{-\infty}^{x} e^{-A(y)} \mathrm{d}y \,. \tag{B.15}$$

For simplification we define

$$T_1(x_0 \to x_0+1) = \int_{x_0}^{x_0+1} \tilde{I}(x)\, \mathrm{d}x \,, \tag{B.16}$$

where the quantity

$$\tilde{I}(x) := \frac{e^{A(x)}}{D(x)} \int_{-\infty}^{x} e^{-A(y)}\, \mathrm{d}y \,. \tag{B.17}$$

Notice that, since $A(x)$ and $D(x)$ are periodic functions, i.e. $A(x+1) = A(x) + f$ and $D(x+1) = D(x)$, $\tilde{I}(x+1) = \tilde{I}(x)$. Then, the average particle current is given by the ratio of distance, in the present case the distance is the period length which is equal to 1, and mean time the particle needs to overcome the distance

$$\langle \dot{x} \rangle = \frac{1}{T_1(x_0 \to x_0+1)} \,. \tag{B.18}$$

Now, we calculate the effective diffusion coefficient which is defined as

$$D_{\text{eff}} = \frac{\Delta T_2(x_0 \to x_0+1)}{2\, [T_1(x_0 \to x_0+1)]^3} \,. \tag{B.19}$$

In order to calculate the effective diffusion coefficient we need to know dispersion $\Delta T_2$ of the second moment of the first passage time, $T_2$. Therefore we consider the recursion relation, Eq. (B.4), and the explicit form is given by [75–77]

$$T_n(x_0 \to x_0+1) = n \int_{x_0}^{x_0+1} \frac{e^{A(x)}}{D(x)}\,\mathrm{d}x \int_{-\infty}^{x} e^{-A(y)}\,\mathrm{d}y \cdot T_{n-1}(y \to x_0+1)\,. \tag{B.20}$$

The second moment of the first passage time, i.e. for $n = 2$, reads

$$T_2(x_0 \to x_0+1) = 2 \int_{x_0}^{x_0+1} \frac{e^{A(x)}}{D(x)}\,\mathrm{d}x \int_{-\infty}^{x} e^{-A(y)}\,\mathrm{d}y \cdot T_1(y \to x_0+1) \tag{B.21}$$

$$= 2 \int_{x_0}^{x_0+1} \frac{e^{A(x)}}{D(x)}\,\mathrm{d}x \int_{-\infty}^{x} e^{-A(y)}\,\mathrm{d}y \int_{y}^{x_0+1} \tilde{I}(z)\,\mathrm{d}z\,, \tag{B.22}$$

where in the last step we inserted the expression for $T_1$. Rewrite the above equation by splitting the intervals, we get

$$T_2(x_0 \to x_0+1) = 2 \int_{x_0}^{x_0+1} \frac{e^{A(x)}}{D(x)}\,\mathrm{d}x \int_{-\infty}^{x} e^{-A(y)}\,\mathrm{d}y \times \left( \int_{y}^{x} \tilde{I}(z)\,\mathrm{d}z + \int_{x}^{x_0+1} \tilde{I}(z)\,\mathrm{d}z \right) \tag{B.23}$$

$$T_2(x_0 \to x_0+1) = 2 \int_{x_0}^{x_0+1} \frac{e^{A(x)}}{D(x)}\,\mathrm{d}x \int_{-\infty}^{x} e^{-A(y)}\,\mathrm{d}y \int_{y}^{x} \tilde{I}(z)\,\mathrm{d}z + R_e\,, \tag{B.24}$$

where the residue $R_e$ reads

$$R_e = 2 \int_{x_0}^{x_0+1} \frac{e^{A(x)}}{D(x)}\,\mathrm{d}x \int_{-\infty}^{x} e^{-A(y)}\,\mathrm{d}y \int_{x}^{x_0+1} \tilde{I}(z)\,\mathrm{d}z \tag{B.25}$$

$$= 2 \int_{x_0}^{x_0+1} \mathrm{d}x\, \tilde{I}(x) \int_{x}^{x_0+1} \mathrm{d}z\, \tilde{I}(z) \tag{B.26}$$

$$= 2\,[T_1(x_0 \to x_0+1)]^2 - 2 \int_{x_0}^{x_0+1} \tilde{I}(x)\,\mathrm{d}x \int_{x_0}^{x} \mathrm{d}z\, \tilde{I}(z)\,. \tag{B.27}$$

Switch the integrals in the second part of the above equation, we get

$$R_e := 2\,[T_1(x_0 \to 1)]^2 - 2 \int_{x_0}^{x_0+1} \tilde{I}(z)\mathrm{d}z \int_{z}^{x_0+1} \tilde{I}(x)\,\mathrm{d}x \tag{B.28}$$

$$:= 2\,[T_1(x_0 \to 1)]^2 - R_e \tag{B.29}$$

$$:= [T_1(x_0 \to 1)]^2\,. \tag{B.30}$$

Substitute $R_e$ back in Eq. (B.24) and rearrange the terms, we get

$$T_2(x_0 \to x_0+1) - R_e = 2\int_{x_0}^{x_0+1} \frac{e^{A(x)}}{D(x)}\,\mathrm{d}x \int_{-\infty}^{x} e^{-A(y)}\,\mathrm{d}y \int_{y}^{x} \tilde{I}(z)\,\mathrm{d}z\,. \tag{B.31}$$

Then, the first passage time dispersion reads

$$\Delta T_2(x_0 \to x_0+1) = 2\int_{x_0}^{x_0+1} \frac{e^{A(x)}}{D(x)}\,\mathrm{d}x \int_{-\infty}^{x} e^{-A(y)}\,\mathrm{d}y \int_{y}^{x} \tilde{I}(z)\,\mathrm{d}z\,. \tag{B.32}$$

Again, switch the integral in the above equation, but now the integration range is different. The final expression reads

$$\int_{-\infty}^{x} e^{-A(y)}\,\mathrm{d}y \int_{y}^{x} \mathrm{d}z\,\tilde{I}(z) = \int_{-\infty}^{x} \mathrm{d}z \int_{-\infty}^{z} e^{-A(y)}\mathrm{d}y\,\tilde{I}(z)\,. \tag{B.33}$$

Substitute the above expression back into the Eq. (B.32), the resultant equation reads

$$\Delta T_2(x_0 \to x_0+1) = 2\int_{x_0}^{x_0+1} \frac{e^{A(x)}}{D(x)}\,\mathrm{d}x \int_{-\infty}^{x} \mathrm{d}z \int_{-\infty}^{z} e^{-A(y)}\mathrm{d}y\,\tilde{I}(z) \tag{B.34}$$

$$= 2\int_{x_0}^{x_0+1} \frac{e^{A(x)}}{D(x)}\,\mathrm{d}x \int_{-\infty}^{x} \frac{D(z)}{e^{A(z)}}\frac{e^{A(z)}}{D(z)}\,\mathrm{d}z \int_{-\infty}^{z} e^{-A(y)}\mathrm{d}y\,\tilde{I}(z) \tag{B.35}$$

$$= 2\int_{x_0}^{x_0+1} \frac{e^{A(x)}}{D(x)}\,\mathrm{d}x \int_{-\infty}^{x} D(z)\,e^{-A(z)}\,\mathrm{d}z\,\left[\tilde{I}(z)\right]^2\,. \tag{B.36}$$

Since, $A(z)$ and $D(z)$ are periodic functions, we can further simplify the above expression with the use of a geometrical expansion, which is

$$\int_{-\infty}^{x} e^{-A(z)}\mathrm{d}z = \sum_{m=0}^{\infty} \int_{y-1}^{y} e^{-A(z)}\,e^{-fm}\,\mathrm{d}z \tag{B.37}$$

$$= \frac{1}{1-e^{-f}} \int_{y-1}^{y} e^{-A(z)}\mathrm{d}z\,. \tag{B.38}$$

After using the geometric expansion the expression $\tilde{I}(z)$ simplifies into

$$\tilde{I}(z) = \frac{e^{A(z)}}{D(z)} \int_{-\infty}^{z} e^{-A(\tilde{z})}\,\mathrm{d}\tilde{z} \tag{B.39}$$

$$= \frac{1}{1-e^{-f}} \frac{e^{A(z)}}{D(z)} \int_{z-1}^{z} e^{-A(\tilde{z})}\,\mathrm{d}\tilde{z} \tag{B.40}$$

$$= \frac{1}{1-e^{-f}} I(z)\,, \tag{B.41}$$

where

$$I(z) = \frac{e^{A(z)}}{D(z)} \int_{z-1}^{z} e^{-A(\tilde{z})}\,\mathrm{d}\tilde{z}\,. \tag{B.42}$$

With the use of above geometrical expansion and Eq. (B.42), Eq. (B.34) can be simplified in to the form

$$\Delta T_2(x_0 \to x_0+1) = \frac{2}{[1-e^{-f}]^3} \int_{x_0}^{x_0+1} \mathrm{d}x \int_{x-1}^{x} \frac{D(z)}{D(x)}\, e^{A(x)-A(z)}\,\mathrm{d}z\; [I(z)]^2\,. \tag{B.43}$$

Then, the final expression for the effective diffusion coefficient, Eq. (B.19), in term of moments of the first passage time reads

$$D_{\text{eff}} = \frac{\displaystyle\int_{x_0}^{x_0+1} \mathrm{d}x \int_{x-1}^{x} \frac{D(z)}{D(x)}\, e^{[A(x)-A(z)]}\,\mathrm{d}z\; [I(z)]^2}{\displaystyle\left[\int_{x_0}^{x_0+1} \mathrm{d}x\, I(x)\right]^3}\,. \tag{B.44}$$

The simplified form of the average particle current in terms of the first moment of the first passage time reads

$$\langle \dot{x} \rangle = \frac{1-e^{-f}}{\displaystyle\int_{x_0}^{x_0+1} I(x)\mathrm{d}x}\,. \tag{B.45}$$

# Bibliography


[1] A. Einstein, *Über die von der molekularkinetischen Theorie der Wärme geforderte Bewegung von in ruhenden Flüssigkeiten suspendierten Teilchen*, Ann. Phys.(Leipzig) **17**, 549 (1905).

[2] A. Einstein, *Eine neue Bestimmung der Moleküldimensionen*, Ann. Phys.(Leipzig) **19**, 289 (1906).

[3] W. Sutherland, *Dynamical theory of diffusion for non-electrolytes and the molecular mass of albumin*, Phil. Mag. **9**, 781 (1905).

[4] M. Smoluchowski, *Zur kinetischen Theorie der Brownschen Molekularbewegung und der Suspensionen*, Annn. Phys. **21**, 757 (1906).

[5] P. Langevin, *Sur la théories du mouvement brownien*, Competes Rendues Acad. Sci. (Paris), **146**, 530 (1908).

[6] J. Perrin, *Les atomes*, Competes Rendues Acad. Sci. (Paris), **158** 1168, (1914).

[7] B. Hille, *Ion Channels of Excitable Membranes* (Sinauer, Sunderland, 2001).

[8] R.M. Barrer, *Zeolites an Clay Minerals as Sorbents and Molecular Sieves* (Academic Press, London, 1978).

[9] C. Baerlocher, W.M. Meier, and D.H. Oslon, *Atlas of Zeolite Framework Types*, 5th rec.ed. (Elsevier, Amsterdam, 2001).

[10] J.Kärger and D.M. Ruthven, *Diffusion in Zeolites and Other Microporous Solids* (Wiley, New York, 1992).

[11] T. Chou and D. Lohse, *Entropy-Driven Pumping in Zeolites and Biological Channels*, Phys. Rev. Lett. **82**, 3552 (1999).

[12] L. Liu, P. Li, and S.A. Asher, *Entropic trapping of macromolecules by mesoscopic periodic voids in a polymer hydrogel*, Nature **397**, 141 (1999).

[13] Z. Siwy and A. Fulinski, *Fabrication of a Synthetic Nanopore Ion Pump*, Phys. Rev. Lett. **89**, 198103 (2002).

[14] Z. Siwy, I.D. Kosinska, A. Fulinski, and C.R. Martin, *Asymmetric Diffusion through Synthetic Nanopores*, Phys. Rev. Lett. **94**, 048102 (2005).

[15] I. D. Kosinska, I. Goychuk, M. Kostur, G. Schmid, and P. Hänggi, *Rectification in synthetic conical nanopores: a one-dimensional Poisson-Nernst-Planck modeling*, Phys. Rev. E **77**, 031131 (2008).

[16] A.M. Berezhkovskii and S.M. Bezrukov, *Optimizing Transport of Metabolites through Large Channels: Molecular Sieves with and without Binding*, Biophys. J. **88**, L17(2005).

[17] C. Kettner, P. Reimann, P. Hänggi, and F. Müller, *Drift ratchet*, Phys. Rev. E **61**, 312 (2000).

[18] S. Matthias and F. Müller, *Asymmetric pores in a silicon membrane acting as massively parallel brownian ratchets*, Nature **424**, 53 (2003).

[19] F. Müller, A. Birner, J. Schilling, U. Gösele, Ch. Kettner, and P. Hänggi, *Membranes for Micropumps from Macroporous Silicon*, Physica Status Solidi (a) **182**, 585 (2000).

[20] R. Zwanzig, *Diffusion Past an Entropic Barrier*, J. Phys. Chem. **96**, 3926 (1992).

[21] M.H. Jacobs, *Diffusion Processes* (Springer, New York, 1967).

[22] D. Reguera and J.M. Rubi, *Kinetic equations for diffusion in the presence of entropic barriers*, Phys. Rev. E **64**, 061106 (2001).

[23] W.D. Volkmuth and R.H. Austin, *DNA electrophoresis in microlithographic arrays*, Nature **358**, 600 (1992).

[24] G.I. Nixon and G.W. Slater, *Saturation and entropic trapping of monodisperse polymers in porous media*, J. Chem. Phys. **117**, 4042 (2002).

[25] R. Chang and A. Yethiraj, *Dynamics of Chain Molecules in Disordered Materials*, Phys. Rev. Lett. **96**, 107802 (2006).

[26] D. Reguera, G. Schmid, P.S. Burada, J.M. Rubí, P. Reimann, and P. Hänggi, *Entropic Transport: Kinetics, Scaling, and Control Mechanisms*, Phys. Rev. Lett. **96**, 130603 (2006).

[27] P.S. Burada, G. Schmid, D. Reguera, J.M. Rubí, and P. Hänggi, *Biased diffusion in confined media: Test of the Fick-Jacobs approximation and validity criteria*, Phys. Rev. E **75**, 051111 (2007).

[28] P. S. Burada, G. Schmid, P. Talkner, P. Hänggi, D. Reguera, and J. M. Rubi, *Entropic particle transport in periodic channels*, BioSystems **93**, 16, (2008).

[29] P. Hänggi, F. Marchesoni and F. Nori, *Brownian motors*, Ann. Physik (Berlin) **14**, 51 (2005).

[30] P.Reimann, *Brownian motors: noisy transport far from equilibrium*, Physics Reports **361**, 57 (2002).

[31] R.D. Astumian and P. Hänggi, *Brownian motors*, Physics Today **55** (11), 33 (2002).

[32] P. Reimann and P. Hänggi, *Introduction to the Physics of Brownian Motors*, Appl. Physics A **75**, 169 (2002).

[33] I. Derenyi and R.D. Astumian, *ac separation of particles by biased Brownian motion in a two-dimensional sieve*, Phys. Rev. E **58**, 7781 (1998).

[34] T.A.J. Duke and R.H. Austin, *Microfabricated Sieve for the Continuous Sorting of Macromolecules*, Phys. Rev. Lett. **80**, 1552 (1998).

[35] A. Van Oudenaarden and S.G. Boxer, *Brownian Ratchets: Molecular Separations in Lipid Bilayers Supported on Patterned Arrays*, Science **285**, 1046(1999).

[36] M. Kostur and L. Schimansky-Geier, *Numerical study of diffusion induced transport in 2D systems*, Phys. Lett. A **265**, 337 (2000).

[37] C. Keller, F. Marquardt and C. Bruder, *Separation quality of a geometric ratchet*, Phys. Rev. E **65**, 041927 (2002).

[38] J. Han and H.G. Craighead, *Separation of long DNA molecules in a microfabricated entropic trap array*, Science **288**, 1026 (2000).

[39] J. Fu, J. Yoo, and J. Han, *Molecular sieving in periodic free-energy landscapes created by patterned nanofilter arrays*, Phys. Rev. Lett. **97**, 018103 (2006).

[40] M.E. Davis, C. Saldarriaga, C. Montes, J. Garces, and C. Crowder, *A molecular sieve with eighteen-membered rings*, Nature **331**, 698 (1988).

[41] C.C. Freyhardt, M. Tsapatsis, R.F. Lobo, K.J. Balkus, and M.E. Davis, *A high-silica zeolite with a 14-tetrahedral-atom pore opening*, Nature **381**, 295 (1996).

[42] A.Corma and M.E. Davis, *Issues in the Synthesis of Crystalline Molecular Sieves: Towards the Crystallization of Low Framework-Density Structures*, ChemPhysChem **5**, 304 (2004).

[43] M.E. Davis, *Ordered porous materials for emerging applications*, Nature **417**, 813 (2002).

[44] J. B. Heng, C. Ho, T. Kim, R. Timp, A. Aksimentiev, Y. V. Grinkova, S. Sligar, K. Schulten, and G. Timp, *Sizing DNA using a nanometer-diameter pore*, Biophys. J. **87**, 2905 (2004).

[45] A. J. Storm, J. H. Chen, X. S. Ling, H. W. Zandbergen, and C. Dekker, *Fabrication of solid-state nanopores with single-nanometer precision*, Nature Mater. **2**, 537 (2003).

[46] A.J. Storm, C. Storm, J. Chen, H. Zandbergen, J. Joanny, and C. Dekker, *Fast DNA Translocation through a Solid-State Nanopore*, Nano Lett. **5** 1193, (2005).

[47] J. B Heng, A. Aksimentiev, C. Ho, P. Marks, Y. V. Grinkova, S. Sligar, K. Schulten, and G. Timp, *Stretching DNA using an electric field in a synthetic nanopore*, Nano Lett. **5** 1883, (2005).

[48] J. B. Heng, A. Aksimentiev, C. Ho, P. Marks, Y. V. Grinkova, S. Sligar, K. Schulten, and G. Timp, *The electromechanics of DNA in a synthetic nanopore*, Biophys. J. **90**, 1098 (2006).

[49] A. Aksimentiev, B.J. Heng, G. Timp, and K. Schulten, *Microscopic kinetics of DNA tanslocation through synthetic nanopores*, Biophys. J. **87**, 2086 (2004).

[50] L. Brun, M. Pastoriza-Gallego, G. Oukhaled, J. Math, L. Bacri, L. Auvray, and J. Pelta, *Dynamics of Polyelectrolyte Transport through a Protein Channel as a Function of Applied Voltage*, Phys. Rev. Lett. **100**, 158302 (2008).

[51] J.J. Kasianowicz, E. Brandin, D. Branton, and D.W. Deamer, *Characterization of individual polynucleotide molecules using a membrane channel*, Proc. Natl. Acad. Sci. **93**, 13770 (1996).

[52] Y. Choi, A. Mecke, B.G. Orr, M.M. Banaszak Holl, and J.R. Baker (Jr.), *DNA-Directed Synthesis of Generation 7 and 5 PAMAM Dendrimer Nanoclusters*, Nano Lett. **4** 497, (2004).

[53] U. Gerland, R. Bundschuh, and T. Hwa, *Translocation of structured polynucleotides through nanopores*, Phys. Biol. **1**, 19 (2004).

[54] R. Bundschuh and U. Gerland, *Coupled Dynamics of RNA Folding and Nanopore Translocation*, Phys. Rev. Lett. **95**, 208104 (2005).

[55] U.F. Keyser, B.N. Koeleman, S. Van Dorp, D. Krapf, R.M.M. Smeets, S.G. Lemay, N.H. Dekker, and C. Dekker, *Direct force measurements on DNA in a solid-state nanopore*, Nature Physics **2**, 473 (2006).

[56] U.F. Keyser, J. van der Does, C. Dekker, and N.H. Dekker, *Optical tweezers for force measurements on DNA in nanopores*, Rev. Sci. Instrum. **77**, 105105 (2006).

[57] E.M. Purcell, *Life at low Reynolds number*, Am. J. Phys. **45**, 3 (1977).

[58] A. Schüring, S.M. Auerback, S. Fritzsche and R. Haberlandt, *On entropic barriers for diffusion in zeolites: A molecular dynamics study*, J. Chem. Phys.**116**, 10890, 2002.

[59] D. Dubbeldam, R. Beerdsen, T.J.H. Vlugt, and B. Smit, *Molecular simulation of loading-dependent diffusion in nanoporous materials using extended dynamically corrected transition state theory*, J. Chem. Phys. **122**, 224712 (2005).

[60] S. Y. Bhide and S. Yashonath, *n-Pentane and Isopentane in One-Dimensional Channels*, J. Am. Chem. Soc. **125**, 7425 (2003).

[61] B.Q. Ai and L.G. Liu, *Current in a three-dimensional periodic tube with unbiased forces*, Phys. Rev. E, **74**, 051114 (2006).

[62] B.Q. Ai and L.G. Liu, *Transport driven by spatially modulated noise in a periodic tube*, J. Phys.:Condens. Matter, **19**, 266215 (2007).

[63] A. M. Berezhkovskii, M. A. Pustovoit, and S. M. Bezrukov, *Diffusion in a tube of varying cross section: Numerical study of reduction to effective one-dimensional description*, J. Chem. Phys. **126**, 134706 (2007).

[64] A. Barone and G. Peterno, *Physics and Applications of the Josephson Effect* (Wiley, New York, 1982).

[65] Yu. M. Ivanchenko and L. A. Zil'berman, *The Josephson effect on small size tunnel contacts*, Zh.Eksp. Teor. Fiz. **55** 2395 (1968) [Sov. Phys. JETP **28**, 1272 (1969)].

[66] V. Ambegaokar and B. I. Halperin, *Voltage Due to Thermal Noise in the dc Josephson Effect*, Phys. Rev. Lett. **22**, 1364 (1969).

[67] D. Reguera, J.M. Rubí, and A. Pérez-Madrid, *Controlling anomalous stresses in soft field-responsive systems*, Phys. rev. E **62**, 5313 (2000).

[68] J.W.M. Frenken and J. Dawson, *Observation of Surface Melting*, Phys. Rev. Lett. **54** 134 (1985).

[69] F.C. Hoppenstead and E.M. Izhikevich, *Weakly Connected Neural Networks* (Springer, New York, 1974).

[70] R. L. Stratonovich, *Oscillator synchronization in the presence of noise*, Radiotekhnika i elektronika **3** (1958) 497, English translation in Non-linear transformations of stochastic processes, edited by P. I. Kuznetsov, R. L Stratonovich, V. I. Tikhonov, Pergamon press, Oxford 1965.

[71] R. L. Stratonovich, *Topics in the Theory of Random Noise*, Vol. II (Gordon and Breach, New York-London, 1967).

[72] M. Khantha and V. Balakrishnan, *First passage time distributions for finite one-dimensional random walks*, Pramana **21**, 111 (1983).

[73] V. Balakrishnan, C. Van den Broeck, and P. Hänggi, *First Passage Times of Non Markovian Processes: The Case of a Reflecting Boundary*, Phys. Rev. A **38**, 4213 (1988).

[74] P. Hänggi and H. Thomas, *Stochastic processes: Time evolution, symmetries and linear response*, Phys. Rep. **88**, 207 (1982).

[75] P. Hänggi, P. Talkner, and M. Borkovec, *Reaction-rate theory: fifty years after Kramers*, Rev. Mod. Phys. **62**, 251 (1990).

[76] P. Reimann, C. Van den Broeck, H. Linke, P. Hänggi, J. M. Rubi, and A. Perez-Madrid, *Giant Acceleration of Free Diffusion by Use of Tilted Periodic Potentials*, Phys. Rev. Lett. **87**, 010602 (2001).

[77] P. Reimann, C. Van den Broeck, H. Linke, P. Hänggi, J. M. Rubi, and A. Perez-Madrid, *Diffusion in tilted periodic potentials: Enhancement, universality, and scaling*, Phys. Rev. E **65**, 031104 (2002).

[78] B. Lindner, M. Kostur, L. Schimansky-Geier, *Optimal diffusive transport in a tilted periodic potential*, Fluct. Noise Lett. **1**, R25 (2001).

[79] M. Evstigneev, O. Zvyagolskaya, S. Bleil, R. Eichhorn, C. Bechinger, and P. Reimann, *Diffusion of colloidal particles in a tilted periodic potential: Theory versus experiment*, Phys. Rev. E **77**, 041107 (2008).

[80] G. Constantini and F. Marchesoni, *Threshold diffusion in a tilted washboard potential*, Europhys. Lett. **48**, 491 (1999).

[81] Hu Gang, A. Daffertshofer, and H. Haken, *Diffusion of Periodically Forced Brownian Particles Moving in Space-Periodic Potentials*, Phys. Rev. Lett. **76**, 4874 (1996).

[82] H. Kramers, *Brownian motion in a field of force and the diffusion model of chemical reactions*, Physica (Utrecht) **7**, 284 (1940).

[83] S. Lifson and J.L. Jackson, *On the Self-Diffusion of Ions in a Polyelectrolyte Solution*, J. Chem. Phys. **36**, 2410 (1962).

[84] H. Risken, *The Fokker-Planck equation*, 2nd ed. (Springer, Berlin, 1989).

[85] P. Kalinay and J.K. Percus, *Corrections to the Fick-Jacobs equation*, Phys. Rev. E **74**, 041203 (2006).

[86] P. Kalinay and J.K. Percus, *Projection of two-dimensional diffusion in a narrow channel onto the longitudinal dimension*, J. Chem. Phys. **122**, 204701 (2005).

[87] E. Péclet, Ann. Chim. Phys. **3**, 107 (1841).

[88] E. Péclet, *Traité de la Chaleur Considerée dans ses Applications* (Hachette, Paris, 1843).

[89] L.D.Landau and E.M.Lifshitz, *Fluid dynamics*, (pergamon press, Oxford, 1959).

[90] E. Heinsalu, M. Patriarca, I. Goychuk, G. Schmid, and P. Hänggi, *Fractional Fokker-Planck dynamics: Numerical algorithm and simulations*, Phys. Rev. E **73**, 046133 (2006).

[91] M. T. Clarkson, D. Beaglehole, and P. T. Callaghan, *Molecular Diffusion in a Microemulsion*, Phys. Rev. Lett. **54**, 1722 (1985).

[92] J.M. Nitsche and H. Brenner, *Sedimentation and dispersion of Brownian particles in spatially periodic potential fields*, J. Chem. Phys. **89**, 7510 (1988).

[93] R. Pesché and G. Nägele, *Dynamical properties of wall-confined colloids*, Europhys. Lett. **51**, 584 (2000).

[94] A. Gordon, S. Dorfman, and D. Fuks, *Enhancement of diffusion of off-center impurities*, Physica B **328**, 336 (2003).

[95] A. Nag and A.R. Dinner, *Enhancement of Diffusion-Controlled Reaction Rates by Surface-Induced Orientational Restriction*, Biophys. J. **90**, 896 (2006).

[96] E. Yariv and K.D. Dorfman, *Electrophoretic transport through channels of periodically varying cross section*, Phys. Fluids **19**, 037101 (2007).

[97] N. Laachi, M. Kenward, E. Yariv, and K. D. Dorfman, *Force-driven transport through periodic entropy barriers*, Euro. Phys. Lett. **80**, 50009 (2007).

[98] K.D. Dorfman, *Combined electrophoretic and electro-osmotic transport through channels of periodically varying cross section*, Phys. Fluids **20**, 037102 (2008).

[99] H. Bernner and D.A. Edwards, *Macrotransport processes* (Butterworth-Heinemann, Bostan, 1993).

[100] S. Bleil, P. Reimann, and C. Bechinger, *Directing Brownian motion by oscillating barriers*, Phys. Rev. E **75**, 031117 (2007).

[101] B. Ai, and L. Liu, *Facilitated movement of inertial Brownian motors driven by a load under an asymmetric potential*, Phys. Rev. E **75**, 061126 (2007).

[102] B. Ai and L. Liu, *A channel Brownian pump powered by an unbiased external force*, J. Chem. Phys. **128**, 024706 (2008).

[103] H. Kim, C. Kim, E.K. Lee, P. Talkner, and P. Hänggi, *Wall-mediated self-diffusion in slit and cylindrical pores*, Phys. Rev. E **77**, 031202 (2008).

[104] M. Uranagase and T. Munakata, *Statistical mechanics of two hard spheres in a box*, Phys. Rev. E **74**, 066101 (2006).

[105] H. Xie, B. Ai, X. Liu, X. XCheng, L. Liu, and Z. Li, *Particle Transport with Asymmetric Unbiased Forces and Entropic Barrier*, Chinese Phys. Lett. **24**, 3340 (2007).

[106] B.Q. Ai and L.G. Liu, *Phase shift induces currents in a periodic tube*, J. Chem. Phys. **126**, 204706 (2007).

[107] B. Ai, H. Xie, and L. Liu, *Thermal noise can facilitate energy transformation in the presence of entropic barriers*, Phys. Rev. E **75**, 061126 (2007).

[108] G. Schmid, P.S. Burada, P. Talkner, and P. Hänggi, *Rectification through Entropic Barriers* (unpublished).

## Acknowledgments

First and foremost, I want to thank Prof. Dr. Peter Hänggi for introducing me to the fascinating field of Biophysics, giving me the opportunity to work in his group, for his encouragement and constant support. I thank Dr. Eric Lutz for acting as second referee of this thesis.

I am grateful to Dr. Gerhard Schmid for his dedicated support, stimulating discussions, encouragement, and standing by me at all times during my work on this thesis.

I am thankful to Prof. Dr. Miguel Rubí Capaceti and Dr. David Reguera for a great collaboration through out this thesis work.

I would like to thank Prof. Dr. Peter Talkner for his comments, discussions, and collaboration, and Prof. Dr. Fabio Marchesoni for his comments and for careful proofreading of the thesis.

I would also like to express my sincere appreciation to Prof. Dr. Achim Wixforth and Prof. Dr. Ulrich Eckern for being part of the examination board.

I gratefully acknowledge financial support by the Deutsche Forschungsgemeinschaft (DFG) and Nanosystems Initiative Munich (NIM).

For the helpful comments, for providing the style files, and careful proofreading of the thesis I am very thankful to Dr. Roland Doll, K. Thirunavukkuarasu and Georg Reuther.

I would like to thank the former and present members of the group of Theoretical Physics I, and the former colleague of the group of Theoretical Physics II, Dr. Daniela Schneider for providing a pleasant working atmosphere.

Many thanks, especially to Dr. David Zueco, Franz J. Kaiser, Narasimham, Sundar Raj, and Rajnarayana Earla.

Last but not least, I would like to thank my parents for their constant support, and my wife Sravanthi Burada for her encouragement, love and patience.

## Poornachandra Sekhar Burada

---

| | | |
|---|---|---|
| Date of birth | : | 25 May 1980 |
| Nationality | : | Indian |
| Martial status | : | Married to Sravanthi Burada |
| Parents | : | B.A. Rama Rao and B. Anasuyamma |

### Education

| | |
|---|---|
| April 95 | Schooling, A.P, India |
| April 97 | Higher level education, A.P, India<br>(Specialization in Mathematics, Physics, and Chemistry) |
| June 00 | Bachelor's degree, Andhra University, India<br>(Specialization in Mathematics, Physics, and Chemistry) |
| April 03 | Master's degree in Physics,<br>Indian Institute of Technology Madras (IITM), Chennai, India<br>(Thesis advisor: Prof. Dr. G. Markandeyulu) |
| Feb 04 | Visiting student at Harish-Chandra Research Institute, Allahabad, India |
| March 05 | Research Assistant at University of Bonn, Germany |
| Since<br>April 05 | Doctoral studies in Physics, in the group of Prof. Dr. Peter Hänggi,<br>at University of Augsburg, Germany |

### Employment

| | |
|---|---|
| April 05 -<br>March 07 | Wissenschaftlicher Mitarbeiter at University of Augsburg, Germany<br>Funded by the Deutsche Forschungsgemeinschaft (DFG) |
| Since<br>April 07 | Wissenschaftlicher Mitarbeiter at University of Augsburg, Germany<br>Funded by the Excellence cluster "Nanosystems Initiative Munich" (NIM) |